IN SITU MINERAL SEDIMENT CHARACTERIZATION WITH LIGHT SCATTERING AND IMAGE ANALYSIS

by

Michael Ryan MacIver

B.Sc., The University of Western Ontario, 2007

A THESIS SUBMITTED IN PARTIAL FULFILLMENT OF
THE REQUIREMENTS FOR THE DEGREE OF

MASTER OF APPLIED SCIENCE

in

THE FACULTY OF GRADUATE AND POSTDOCTORAL STUDIES

(Mining Engineering)

THE UNIVERSITY OF BRITISH COLUMBIA

(Vancouver)

April 2016

©Michael Ryan MacIver, 2016

ABSTRACT

In this study, optical backscattering (OBS) and *in situ* image analysis are used to measure sediment bed density and aggregate size. A method is described for the measurement and interpretation of OBS height scans to obtain a measurement of aggregate size and solid concentration profiles in sediment beds of flocculated minerals. It was found that when OBS height scans were measured during batch settling and from multiple angles at the end of batch settling, the resulting root-mean-square, F_{rms}, and mean, F_{mean}, signal values can be analysed to quantify the sediment bed solids concentration and aggregate size as a function of height in the sample. A size calibration method was applied which relates the F_{rms} values obtained from model solid ceramic spheres and silica particles to F_{rms} values measured from sediment beds of flocculated kaolin. An iterative fitting method is applied to obtain a calibration function which can be applied to obtain a quantitative description of solid volume as a function of height and time during the batch settling experiment, $\phi_{\mathrm{s}}(h,t)$. Evaluation of the fitted solid volume versus height functions resulted in a reasonable relative error when compared with the measured solid volume in the sample. A brief analysis on a statistical interpretation of image data for various samples of flocculated mineral sediment beds is given. This study suggests that the evaluation of OBS signal values and high magnification image analysis can be applied on the lab scale for determination of aggregate size and sediment bed density and may form the basis of a measurement system that can be applied to larger scale batch settling or pilot thickening equipment to measure rheological properties and mass flux.

PREFACE

Dr. Pawlik conceived the idea to use backscattering height scans to obtain some measure of aggregate size. This was the starting point for the all of the batch settling experiments, which led to algorithms for the interpretation of size and density information from optical backscattering measurement as well as a method for image analysis based on chord lengths. The backscattering laboratory measurements were developed in conjunction with Dr. Pawlik, while the signal interpretation algorithms and computer methods used were developed and implemented by the author of this thesis. A version of Section 7.2 of this thesis, "*In Situ* image analysis," was submitted for publication in the International Mineral Processing Congress 2016 proceedings. The algorithms and implementation used for analysis and manuscript preparation was the work of the author. A version of the size and solid volume profile calibration method described in Sections 4.5.3 and 6.33 is also being prepared for submission to a peer-reviewed journal.

TABLE OF CONTENTS

ABSTRACT ii
PREFACE iii
TABLE OF CONTENTS iv
LIST OF TABLES vi
LIST OF FIGURES vii
LIST OF SYMBOLS x
LIST OF ABBREVIATIONS xi
ACKNOWLEDGEMENTS xii
1 INTRODUCTION 1
1.1 THESIS ORGANIZATION 2
1.2 RELEVANCE OF THIS STUDY 3
1.3 RESEARCH OBJECTIVES 3
2 LITERATURE REVIEW 5
2.1 BATCH SETTLING OF FLOCCULATED SUSPENSIONS 5
2.1.1 SUSPENSION STABILITY AND FLOCCULATION 5
2.1.2 BATCH SETTLING AND SOLID FLUX 7
2.1.3 COMPRESSIVE RHEOLOGY 9
2.2 MEASUREMENT OF FLOCCULATED SYSTEMS 10
2.2.1 OPTICAL METHODS 11
2.2.2 IMAGE-BASED METHODS 15
3 MATERIALS 19
3.1 EQUIPMENT 19
3.1.1 OPTICAL BACKSCATTERING AND TRANSMISSION 19
3.1.2 IMAGE ANALYSIS 19
3.2 FLOCCULATED MINERAL SAMPLES 21
4 OPTICAL BACKSCATTERING METHODS 23
4.1 OBS HEIGHT SCAN OVERVIEW 23
4.2 OBS SIGNAL ANALYSIS OVERVIEW 28
4.2.1 REGION-OF-INTEREST 29
4.2.2 BACKGROUND SIGNAL 30
4.2.3 SIGNAL VALUE CALCULATION 32
4.3 MEASUREMENT OF OBS FROM RIGID SPHERES 33
4.4 CALCULATED OBS FROM SOLID SPHERES 34
4.5 MEASUREMENT OF OBS FROM MINERAL SUSPENSIONS 36
4.5.1 AGGREGATE SIZE 36
4.5.2 RELATIVE AND AVERAGE BED DENSITY 37
4.5.3 CALCULATED SOLID VOLUME PROFILE FUNCTIONS 38
5 IMAGE ANALYSIS METHODS 44
5.1 *IN SITU* IMAGE ANALYSIS OF FLOCCULATED SEDIMENTS 44
6 OPTICAL BACKSCATTERING RESULTS 47

6.1 MEASURED BACKSCATTERING FROM RIGID SPHERES 47
6.2 CALCULATED BACKSCATTERING FROM RIGID SPHERES 48
6.2.1 CALCULATED OBS SIGNAL VALUES 48
6.2.2 SPHERE SIZE-POROSITY RELATIONSHIP 51
6.3 MEASUREMENT OF OBS FROM MINERAL SUSPENSIONS 52
6.3.1 SUSPENSION STABILITY AND SETTLING RATES 52
6.3.2 AGGREGATE SIZE AND BED DENSITY 59
6.3.3 CALCULATED SOLID VOLUME PROFILES 67
7 *IN SITU* IMAGE ANALYSIS RESULTS 74
7.1 THRESHOLD DETERMINATION 74
7.2 WHITE-BLACK RATIO DISTRIBUTIONS 75
7.3 VOID CHORD LENGTH DISTRIBUTIONS 77
7.4 ROTATION SERIES OF IMAGES 78
7.5 STANDARD DEVIATION ANALYSIS 80
8 CONCLUSIONS 82
9 RECOMMENDATIONS 85
REFERENCES 86
APPENDICES 91

LIST OF TABLES

TABLE 6.1 SUMMARY OF HINDERED SETTLING RATES FOR 10 % W/W KAOLIN SUSPENSIONS FLOCCULATED WITH VARYING DOSAGE OF POLYACRYLAMIDE.....57
TABLE 6.2 POWER FIT STATISTICS FOR DATA IN FIGURES 6.16, 6.19 AND 6.21.....66
TABLE 7.1 COMPARISON OF WHITE-TO-BLACK RATIO (FLOC-TO-VOID RATIO) FROM THE ENTIRE IMAGE AND FROM CHORDS 80

LIST OF FIGURES

Figure 2.1 Effect of initial solid concentration on equilibrium floc size for flocculation of kaolin with high MW, 35% anionic PAM, from [6]....6
Figure 2.2 Batch settling schematic showing an initial suspension, left, and the solid volume height relationship, middle, of the suspension diagram shown on the right, from a similar figure in [16]....7
Figure 2.3 Interface settling data for an initially un-networked kaolin sample, $\emptyset 0 = 0.04$, flocculated with 60 g/t high molecular weight, non-ionic polyacrylamide. Data shown is the author's own....8
Figure 2.4 Focused beam reflectance measurement, top, is applied to a moving suspension, adapted from [29]. Optical backscattering height scans, bottom, are measured by moving laser and sensor past a bed of aggregated material....12
Figure 2.5 Analysis of sensor output ac and dc voltage values for turbidity fluctuation measurement in flowing dispersions, after [8]....13
Figure 2.6 Theoretical optical backscattering response of a settling suspension. Larger particles may contribute less to the OBS response on a number basis, while the smaller, more abundant particles may contribute more....15
Figure 2.7 The LubaTube allows characterization of rising aggregates due to pressure differential in the separation vessel and capture column[51]....17
Figure 2.8 Floc window installed to obtain direct images of flocs during thickening installed [53]....17
Figure 3.1 *In situ* high magnification sediment image acquisition apparatus from top and side views....20
Figure 3.2 Sedimentation image acquisition apparatus from top and side views....21
Figure 4.1 OBS height scan of a 10 % w/w kaolin sample flocculated with 60 g/t high molecular weight PAM. The interface between the sediment bed and the supernatant is indicated with a red dashed line....24
Figure 4.2 Optical backscattering height scan (left) and picture of grinding media in a sample cylinder (right)....25
Figure 4.3 Backscattering % versus height for 2.35 and 1 mm diameter ceramic grinding media. In (A) and (C), single OBS height scans of the spheres are given. In (B) and (D) the levelled RMS value is indicated by the dashed line above and below the mean OBS. RMS-OBS for 2.35mm spheres = 9.3282%; for 1mm spheres = 3.15%....26
Figure 4.4 Spheres arranged in a face-centred cubic structure for optical backscattering height scan simulation. The three lines indicate the scan path on the 1mm spheres at the following offsets: 0, 0.33cm and 0.67 cm....27
Figure 4.5 High-level outline of optical backscattering data processing routine....29
Figure 4.6 Region of interested in optical backscattering height scan defined from graphical user input and interface distance calculation....30
Figure 4.7 Region of interested from an OBS height scans with signal background plotted as a dashed line....31
Figure 4.8 Levelled backscattering % signal obtained by subtracting the power fit background from the height scan region of interest....31
Figure 4.9 F_{MEAN}, F_{RMS} and $A_{\text{PK-PK}}$ for a hypothetical, perfectly sinusoidal optical backscattering height scan signal....33
Figure 4.10 Three dimensional model of optical backscattering from rigid spheres....35
Figure 4.11 Calibration of an OBS sensor for particle size and mass concentration using ground silica. From De Visser [61]....39
Figure 4.12 Solid volume profile calibration procedure overview....41
Figure 5.1 Microvideo image and corresponding binary image of a sample of 10% w/w kaolin flocculated with 200 g/t nonionic polyacrylamide....45
Figure 5.2 Chord length measurement for a cross-section of two phase media. Chords are the intersection of lines with the two-phase interface. Adapted from [63]....46
Figure 6.1 Root-mean-square OBS % versus diameter for spheroidal grinding media and silica samples....47
Figure 6.2 Calculated optical backscattering signal values, F_{MEAN} and F_{RMS}, as a function of sphere diameter....49
Figure 6.3 Simulated optical backscattering height scan for randomly close packed 1mm rigid spheres....50
Figure 6.4 Multiple simulated optical backscattering height scan for randomly close packed 1mm rigid spheres....50
Figure 6.5 Measured and calculated RMS-OBS plotted with radial porosity data from Mueller [64]....51

Figure 6.6 Backscattering from 10 %w/w kaolin sample at pH 10.3. Destabilization of the sample occurs slowly as indicated by the decreasing backscattering over the height of the suspension. One scan is taken 24 hours later and the vertical line at 10mm indicates the developing sediment bed. 53
Figure 6.7 Transmission height scans of 10% w/w kaolin at pH 10.3. The lines for all times between 0 and 2 hours overlap. 54
Figure 6.8 Natural pH, 5.3, 10% w/w kaolin sample settling over a two-hour period....55
Figure 6.9 Transmission height scans over two-hour period of 10 % w/w kaolin in deionized water at natural pH, 5.37. 55
Figure 6.10 Bed height from OBS measurements over two hours for PAM-flocculated 10 % w/w kaolin and straight 10% w/w kaolin, Trial A....56
Figure 6.11 Hindered settling rate fit from kaolin batch settling data with 0 and 60 g/t polyacrylamide dosage. 57
Figure 6.12 Transmission % in the top 10 mm of supernatant during a two-hour period for PAM flocculated 10 % w/w kaolin samples. The PAM flocculated lines are above the sample with no polymer added which indicates improved clarification in the sample. 58
Figure 6.13 Magnified images of four 10% w/w kaolin samples after 2 hours with 0, 20, 60 and 160 g/t non-ionic polyacrylamide added....59
Figure 6.14 The F_{MEAN} and F_{RMS} signal values measured after two-hour batch settling 10% w/w kaolin flocculated with nonionic polyacrylamide. 60
Figure 6.15 Levelled F_{RMS} as a function of polymer dosage for polyacrylamide flocculated 10% w/w kaolin for four different trials....61
Figure 6.16 Interpretation of mineral sediment F_{RMS} values with calibration line from solid sphere measurements. 62
Figure 6.17 F_{RMS} values converted to equivalent packing diameter, DF, plotted against sediment bed height after two hours. The anionic polyacrylamide dose, in g/t, is indicated next to the data point. 63
Figure 6.18 Sectional height analysis of the OBS scans of three samples of PAM flocculated kaolin. A second 0 g/t sample is added to confirm the trend of decreasing aggregate size with sample height....64
Figure 6.19 Signal value F_{MEAN} as a function of bed height for a series of 10% w/w kaolin samples flocculated by increasing dosage of polyacrylamide. The numbers next to the data points indicate the dosage on a g/t basis. Fit R^2 = 0.9076 65
Figure 6.20 The F_{DELTA} signal value as a function of solid volume fraction for a series of 10% w/w kaolin samples flocculated by increasing dosage of polyacrylamide. The numbers next to the data points indicate the dosage on a g/t basis. Fit R^2 = 0.9652....66
Figure 6.21 Optical backscattering gain versus particle diameter for fixed suspended sediment concentration of 8 gL^{-1} and 100 gL^{-1}, derived from data in De Visser [61]. The effective diameter range of the aggregates in this study is plotted....68
Figure 6.22 Initial exponential calibration function with upper and lower bounds plotted in black. The remaining lines are the calibration functions output from the optimizer for 12 batch settling trials. The legend symbols can be interpreted as follows, for example: 10k120p-3 indicates a 10 % w/w kaolin sample flocculated by 120 g/t PAM in Trial 3. 69
Figure 6.23 Calculated backscattering versus equivalent aggregate diameter at two different solid volume fractions. 70
Figure 6.24. The $\phi_s(h,\mathrm{T})$ surface from batch settling of a coagulated kaolin suspension, initial ϕ_0 = 0.038. 71
Figure 6.25 Interface settling plot from the $\phi_s(h,\mathrm{T})$ data of batch settling of a coagulated kaolin suspension, with initial solid volume, ϕ_0 = 0.038. 72
Figure 6.26. Solid volume vs height profile from calibrated OBS data....73
Figure 6.27 Solid Volume Height profiles evaluated from multiple scans. 73
Figure 7.1 Microvideo image, binary, and corresponding white-black distribution ratio from a sample of 10% w/w kaolin flocculated with 120 g/t non-ionic polyacrylamide after two hours of batch settling 74
Figure 7.2 Image of PAM flocculated kaolin with four different threshold levels applied....75
Figure 7.3 Impact of threshold level on the final white-black distribution ratios from PAM flocculated kaolin suspensions 75

FIGURE 7.4 WHITE-BLACK DISTRIBUTION RATIO PARAMETERS FOR A TIME SERIES OF IMAGES TAKEN DURING BATCH SETTLING OF A KAOLIN SUSPENSION FLOCCULATED BY VARYING DOSES OF POLYACRYLAMIDE IN TWO TRIALS, (A) AND (B). THE STANDARD DEVIATION OF A SINGLE SAMPLE FROM EACH TRIAL IS PLOTTED IN (C) AND (D). 76
FIGURE 7.5 MEAN OF VOID CHORD DISTRIBUTION AS A FUNCTION OF TIME MEASURED FROM IMAGES OF BATCH SETTLING OF KAOLIN FLOCCULATED BY VARYING DOSAGE OF HIGH MW, NON-IONIC PAM 78
FIGURE 7.6 WHITE-BLACK RATIO DISTRIBUTION MEAN, μ, AND SCALE PARAMETER, s, AS A FUNCTION OF: (A) FINAL BED HEIGHT; AND (B) POLYMER DOSAGE, AT THE END OF THE TWO-HOUR BATCH SETTLING PERIOD FOR THREE DIFFERENT KAOLIN FLOCCULATION TRIALS. 79
FIGURE 7.7 TWO IMAGES WITH A 25% VOID SPACE. THE WHITE-TO-BLACK RATIOS OF THESE IMAGES WOULD BOTH BE 0.75, HOWEVER SUCH A CALCULATION LOSES INFORMATION ABOUT THE SPATIAL ARRANGEMENT OF THE PHASES WITHIN THE MATERIAL. 81

LIST OF SYMBOLS

F_{rms}	[%]	Root-mean-square optical backscattering signal value.
F_{mean}	[%]	Mean optical backscattering signal value.
F_{delta}	[%]	Delta optical backscattering signal value.
$F_{\mathrm{pm\text{-}rms}}$	[-]	Ratio of peak value in region of interest to F_{rms}
ϕ_{s}	[-]	Solid volume fraction.
ϕ_{s}	[-]	Initial solid volume fraction.
ϕ_g	[-]	Gel point.
h_{f}	[mm]	Final sediment bed height.
Q_{s}	[-]	Backscattering efficiency factor.
$A_{\mathrm{pk\text{-}pk}}$	[%]	Peak-to-peak amplitude.
D_{s}	[mm]	Sieve diameter.
D_{F}	[μm]	Equivalent scattering diameter/ scattering diameter.
D_{A}	[μm]	Projected area-based diameter.
A_{p}	[$\mu\mathrm{m}^2$]	Projected aggregate area.
A_{c}	[mm]	Cylinder area
h	[mm]	Height from bottom of sample jar.
t	[s]	Time.
V_{cal}	[cm^3]	Calculated solid volume in the sediment bed.
$\mathcal{S}(h)$	[-]	Height-solid volume function.
E	[W]	Irradiance from incident laser beam.
F	[W]	Optical backscattering light flux.
ρ	[-]	Number particle density
C	[gL^{-1}]	Mass concentration.
ΣRE	[%]	Sum of relative errors
$F_{\mathrm{pm\text{-}rms}}$	[%]	Peak-to-root-mean-square ratio
P_{s}	[Pa]	Effective pressure
L	[mm]	Depth from top of sediment bed.
ε_{m}	[-]	Mean radial porosity.
$p(\mathrm{z})$	[-]	Chord length distribution function.
g	[$\mathrm{m/s}^2$]	Acceleration of gravity.
μ_{s}	[m/s]	Velocity of solid.
μ	[m/s]	Velocity of liquid.
ρ_{s}	[$\mathrm{kg/m}^3$]	Density of solid.
ρ	[$\mathrm{kg/m}^3$]	Density of liquid.

LIST OF ABBREVIATIONS

ABS	Acoustic backscattering
CLD	Chord length distribution
CT	Computed tomography
DLS	Dynamic light scattering
FBMR	Focused beam reflectance measurement
FCC	Face centred cubic packing structure
MW	Molecular weight
OBS	Optical backscattering
PAM	Polyacrylamide
PDA	Photometric dispersion analyser
RCP	Randomly close packed
ROI	Region-of-interest
SALS	Small angle light scattering

ACKNOWLEDGEMENTS

I would like to thank Dr. Marek Pawlik for his supervisor and support throughout this thesis research. His open door policy led to several discussions which were highly important to the outcome of this study. Sally Finora was always helpful and interested in a variety of technical matters of this study. The members of the Pawlik research group are thanked for their discussions on the study of mineral processing and at various times, for technical support on equipment. Special thanks to the support and motivation of Sophie and our new baby Simone.

1 INTRODUCTION

Mineral, chemical, water treatment and agricultural processing generate a variety of fine materials and residues that must be treated, handled, and recycled or disposed. Methods that allow tighter control of variables of solid-liquid separation processes can help to produce slurries which have the desired material properties and are easier to handle [1]. As such, the ability to measure sediment bed properties *in situ*, in real time, is of inherent interest and can contribute to the modelling, design, and operation of solid-liquid separation processes. However few proven instruments exist that can give *in situ*, online information about thickening processes [2].

Batch settling tests have been used for over a century to rapidly estimate design parameters of and the solid flux expected from solid-liquid separation equipment [3]. However, aside from the sediment-supernatant interface, little information is extracted from these tests. Current methods of measuring flocculated sediments typically involve extracting a sample and are rarely carried out *in situ*. This introduces the possibility that pumping or pipetting can introduce shear which may cause irreversible breakage of aggregates into smaller sizes [4]. Focused beam reflectance measurement [5][6] and the turbidity fluctuation method [7] [8], can be used to analyse changes in aggregation state in flowing, flocculated suspensions. Techniques such as XRAY microscopy [9] and cryo-SEM [10] elucidate floc structure but require handling methods that likely distort or destroy floc structure. Acoustic backscattering (ABS) has been applied to the highly concentrated, near-bed region of a thickener [11]. Computed tomography (CT) can provide high spatial resolution 3D density and structural information, but high cost and the requirement that the sample is stationary are two major drawbacks for monitoring batch settling.

Optical backscattering (OBS) and image analysis are two possible candidates for *in situ*, online monitoring of networked beds of solids because they are relatively inexpensive, easy to interpret and give intuitive results. In the present study, OBS height scans and micro-imagery are used to directly measure the flocculated mineral sediment bed during batch settling experiments of polyacrylamide-flocculated kaolin. These methods overcome some of the drawbacks of

established methods which are often limited by solid concentration, particle size range, or require destructive handling methods.

This thesis demonstrates a size calibration method for measuring relative aggregate size and a method of obtaining solid volume-height-time data from *OBS* height scans. An optical backscattering calibration method was developed to determine the solid volume-height relationship in the settling sample as a function of time, $\phi_s(h,t)$. This piece of information may be useful in the application of Kynch's theory [12] to the settling flux of flocculated suspensions, and to the study of compressibility and densification phenomenon in networked sediment beds [13].

High magnification image measurement and analysis of batch settling of kaolin was carried out to apply a statistical-physical feature extraction technique. Two characteristic features of the interaggregate void space are discussed: the void chord length distribution (CLD) and a related measurement, the white-to-black ratio distribution.

1.1 THESIS ORGANIZATION

The main purpose of this thesis was to investigate how to extract meaningful information from optical backscattering (OBS) measured during batch settling tests of flocculated mineral suspensions. A second method, *in situ* image analysis, was also developed and applied during the course of this thesis.

A parallel structure is used in this thesis to emphasize the relationship between the optical backscattering and image analysis methods. A literature review in Section 2 describes the current theory and technology available for measuring and describing flocculated systems. Section 3 describes the materials and equipment used in this study. Sections 4 and 6 contain the OBS method and results, respectively. In Section 4, the relationship between the OBS signal and aggregate size and bed density are examined through the use of model spheres and calculated OBS height scans. In Section 6, the main outcome of the OBS method is studied in detail: two types of calibration methods, one for aggregate size and one for solid volume, are applied to settling suspensions of flocculated material. Section 5 describes the *in situ* image analysis method

used in this study. The relationship between chord length distributions and the relative aggregate size which comprises the sediment bed is developed. In Section 7, the application of the chord length distribution approach is applied to flocculated suspensions of kaolin. Discussion is given throughout this thesis, so the final sections are the conclusions and recommendations of this thesis.

1.2 RELEVANCE OF THIS STUDY

The investigation of *in situ* optical backscattering (OBS) and image analysis methods is of practical industrial and basic scientific interest. The ability to measure aggregate size and structure *in situ* permits a direct apprehension of the material behaviour. Such information could be incorporated into the study of aggregate densification, solid flux, flocculant characterization, and material dewatering behaviour. On the lab scale, the direct practical application of this work is a new method which can be applied to determine the impact of changing chemical-physico conditions on sediment bed density and aggregate size. On a larger scale, the methods developed here could form the basis of new technology for monitoring settling and densification processes in pilot or plant equipment.

1.3 RESEARCH OBJECTIVES

The object of this work was to develop a method for the measurement and interpretation of OBS and high magnification images from sediment beds of aggregated material. The optimization of flocculation or hydrodynamic conditions was not considered. Rather, the focus of this work was the development of signal interpretation methods.

Specific research objectives include:

1. Determine whether useful information on sediment structure can be obtained from optical backscattering (OBS) height scans of flocculated mineral sediments.
2. Apply the OBS technique to a series of polymer flocculated samples.
3. Apply an *in situ* image analysis technique in parallel with the OBS experiments to improve understanding of the OBS signal.

There are two main outcomes from this study. Both are related to the measurement of an optical parameter or property of the flocculated mineral sediments which can be correlated with aggregate size or bed density:

1. An optical backscattering height scan measurement and interpretation model. Two methods were developed under this model:
    a. Direct measurement of the result of flocculation in terms of aggregate size.
    b. Measurement of average bed density and bed density as a function of height and time in a settling sample.
2. The development and demonstration of an *in situ* image analysis technique for sediment bed monitoring during batch settling. This method applies white-black chord length distribution ratios to measure relative bed density as a function of time at a fixed point in a settling suspension.

2 LITERATURE REVIEW

In order to interpret the results of the two methods described in this study, it is necessary to provide background information on the theory and measurement of flocculated mineral systems. There are two main components to this literature review: a description of the phenomenon and theory of batch flocculation and settling; and a description of some of the techniques available for measuring flocculated mineral systems.

2.1 BATCH SETTLING OF FLOCCULATED SUSPENSIONS

In this study, optical backscattering and image analysis are used to study sediment beds produced through the batch settling of flocculated mineral suspensions. Flocculation, batch settling and their respective theories are described here to provide a framework in which the results of this study can be interpreted and applied.

2.1.1 SUSPENSION STABILITY AND FLOCCULATION

An initially homogeneous mineral suspension may undergo aggregation and settling depending on the suspension stability. The factors that affect suspension stability include mineral properties, such as surface charge and particle size [14]; solution properties, such as presence or absence of chemical additives, pH and ionic strength; and the application of mechanical force, such as shear [1]. When the suspension stability is reduced by addition of a high molecular weight (MW) polymer, the resulting aggregation of fine particles into clusters is called flocculation. Suspension destabilization which induces fine particle aggregation by modification of pH or ionic strength is typically referred to as coagulation.

In the present study, suspensions of kaolin particles are flocculated with a high MW non-ionic polyacrylamide (PAM) at the mineral's natural pH, typically about 5.3. Addition of high MW PAM will lead to the substantially larger flocs and a faster settling velocity [15]. Floc size depends on the degree of anionicity and MW of the polymer. Increasing the anionic charge on PAM from 10 to 35 % or increasing MW increases kaolin floc size [16]. The initial solids concentration also has an impact on aggregate growth and equilibrium floc size. Owen et. al. [6] found that the

equilibrium floc size depended on the initial solid concentration of the suspension, as shown in Figure 2.1. In this thesis, the suspensions were typically prepared at about ϕ_s = 0.0395, which corresponds to about 110 g/L.

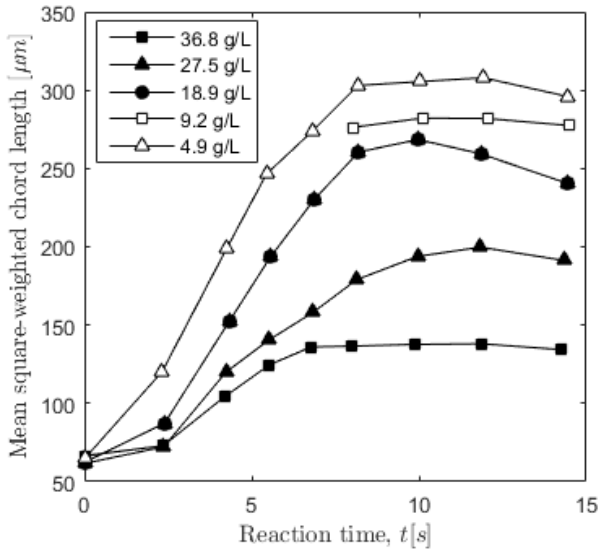

Figure 2.1 Effect of initial solid concentration on equilibrium floc size for flocculation of kaolin with high MW, 35% anionic PAM, from [6].

The expected mechanism of flocculation in the case of a non-ionic polyacrylamide is primarily polymer bridging, which results from aggregation of particles through the adsorbed long, dangling chains [17]. Depending on dosage, PAM is both a suspension stabilizer and destabilizer [18]. At very high dosages, non-ionic PAM will stabilize or disperse kaolin suspensions. A low to intermediate dosage will produce enhanced floc growth and settling velocity.

Several aggregation mechanisms can cause kaolin suspension destabilization [19]. Kaolinite typically occurs as a thin plate-like structure of layered silica and alumina. Tetrahedral silica sheets are bound through oxygen atoms to an octahedral sheet of alumina. As a result, the plates have silica faces while alumina is only exposed on the edges. In suspension, the silica has an almost permanent negative charge, except at very low pH. On the other hand, the alumina is amphoteric, with protonation of exposed hydroxyl groups leading to a positive charge at low pH and deprotonation at high pH resulting in a net negative charge. At high pH, kaolinite suspensions

are more stable because the particles have a net negative charge. Settling is on the order of days and even then residual turbidity may persist. As the pH is decreased, the alumina faces begin to become more positively charged and the suspension will become increasingly unstable due to particle face-edge attraction [20].

2.1.2 BATCH SETTLING AND SOLID FLUX

Batch settling of flocculated suspensions is both a basic solid-liquid separation unit operation and a rheological measurement. For over a century, batch settling tests or jar tests have been used to rapidly estimate design parameters of and the solid flux expected from large scale solid-liquid separation equipment [3].

During a batch settling experiment, a suspension of known initial solids concentration is prepared and allowed to stand. These experiments can be carried out under shear, such as with a rake or paddle, or be allowed to sit undisturbed. Depending on the factors discussed in Section 2.1.1, the solid material in the suspension may begin to aggregate and settle. Over time, a distinct region of higher solids concentration may develop in the lower part of the vessel with a region of lower concentration, or supernatant, above, as shown in Figure 2.2.

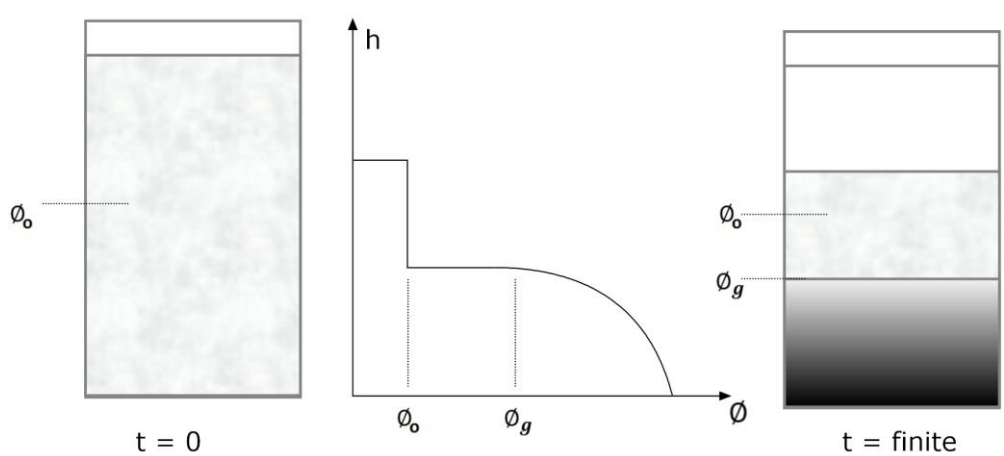

Figure 2.2 Batch settling schematic showing an initial suspension, left, and the solid volume height relationship, middle, of the suspension diagram shown on the right, from a similar figure in [16].

Typically, an interface can be identified between the supernatant and the developing high concentration region. The height of the settling interface can be measured over time and plotted as a so called 'batch settling curve' or 'mudline descent rate', for example refer to Figure 2.3. Initially, when the entire suspension is at ϕ_0, the interface propagates downward linearly, corresponding to free settling of individual particles. This descent results in a clearer phase, or supernatant, above the interface. A region of $\phi_0 < \phi_s < \phi_g$ develops as the material is transported in the downward direction. The solid volume fraction increases to the gel point, ϕ_g, where the particles form a continuous networked structure and free settling is prevented by particles lower in the network.

In this thesis, the kaolin suspensions prepared had an initial solid volume, $\phi_0 < \phi_g$, so the suspensions were initially un-networked. As such, the description of batch settling behaviour will be related to suspensions that are initially un-networked. At solid volume fractions above the gel point, a network pressure develops. When the pressure is stronger than the aggregate network strength, the network collapses and the solid volume fraction continues to increase.

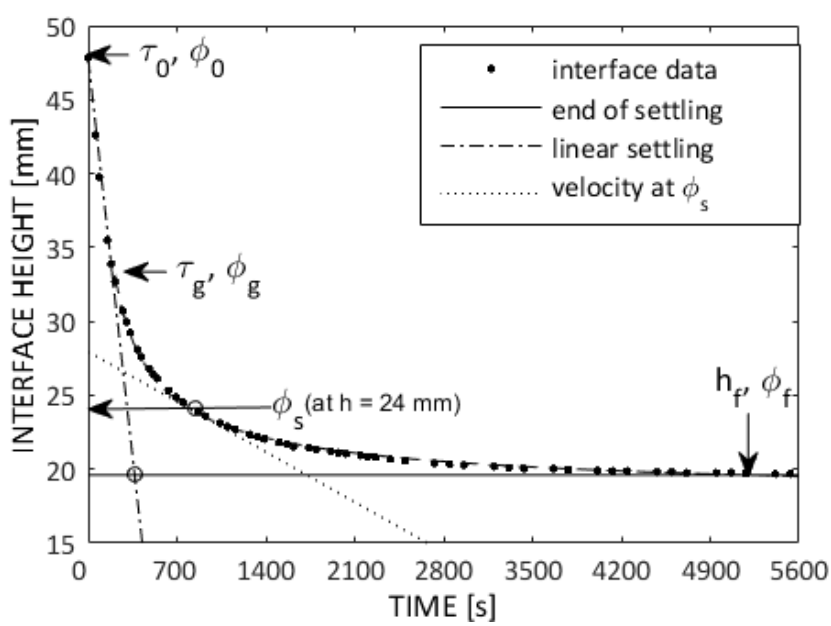

Figure 2.3 Interface settling data for an initially un-networked kaolin sample, $\emptyset_0 = 0.04$, flocculated with 60 g/t high molecular weight, non-ionic polyacrylamide. Data shown is the author's own.

Kynch proposed a theory in 1952 to describe solid flux that made the scientific analysis of batch settling and thickener sizing possible. The solid flux function, Equation (2.1), is used with the mass balance, Equation (2.2), to determine the solid flux over the entire concentration range [12],

$$f(\phi) = \phi \cdot u(\phi), \tag{2.1}$$

where $u(\phi)$is the settling velocity as a function of solid concentration.

$$\frac{\partial \phi}{\partial h} dh + u(\phi) \frac{\partial \phi}{\partial h} \partial h = 0 \tag{2.2}$$

The Talmage and Fitch method for thickener sizing, based on a graphical interpretation of Kynch's method [21] was used well into the 1990s [3]. In this method, a line is drawn tangent to the batch settling curve to obtain the settling velocity and a horizontal line is drawn to the y-axis, such that the solid volume fraction can be calculated if the settling vessel dimensions are known. For example, in Figure 2.3, the velocity of the suspension when the interface height is 24 mm can be found by making a line tangent to the height versus time plot at that point.

While Kynch theory, and methods based on it, apply to ideal, incompressible suspensions it does not adequately describe the behaviour of flocculated suspensions [1]. Flocculated suspensions are compressible and thus the suspension properties, and most importantly the solid volume fraction, are not uniform over the height of the settling vessel.

2.1.3 COMPRESSIVE RHEOLOGY

To account for compressibility of flocculated suspensions, modern compressive rheology theory incorporates additional tests to measure the compressional behaviour of the networked bed [22]. Two theories exist which use different terminology for equivalent physical parameters: the dynamic sedimentation-consolidation model and an applied compressional rheological model. The first theory incorporates pore pressure and effective solid stress to model the curved iso-concentration lines that arise in suspensions of flocculated material [23]. The second applies the

theory of compressive rheology to flocculated suspensions to model solid-liquid separation processes with the compressional yield stress and hindered settling factors as parameters [1].

Application of these theories requires measurement of macroscopic mechanical and transport properties such as compressive or shear yield stress and fluidization upflow [22]. The compressive yield stress can be measured on the macroscopic level, by filtration [24] or on the microscopic level, with atomic force microscopy [25].

Despite the increased sophistication of sedimentation theory, the best way to measure the parameters important to modelling solid-liquid separation processes, such as the solid flux density and the solid effective stress, is still considered an open problem [26]. According to Concha the theories described above "ignore the individuality and physical structure of particles and fluids, and considers the solid and the fluid as continuous media. [27]" Nonetheless, recent refinements of the compressional rheology model have incorporated a "scaled aggregate diameter" to account for aggregate restructuring as a result of applied shear during thickening [28]. However, this correction factor is based on an evaluation of fluidisation data and the improved mass transport obtained during a sheared batch settling test versus a standard, unsheared test. No direct material size or structure measurement is made. Perhaps one way to improve these models is the inclusion of parameters based on the *in situ* measurement of aggregate size and bed density. For instance, a more detailed *in situ* representation of solid concentration and aggregate size would be useful, such as the definition of $\phi_s(h,t)$ and effective diameter proposed in this thesis.

2.2 MEASUREMENT OF FLOCCULATED SYSTEMS

In the present study, optical backscattering and image acquisition are used to measure the sediment bed that results from flocculating mineral suspensions. The solid concentration is high, $\phi_s > \phi_g$, and the particles form a networked structure. In this section, some of the advantages and disadvantages of existing methods are discussed as they apply to current system under study. The methods discussed here are by no means an exhaustive list. Direct

measurement of such a system with existing techniques is inherently difficult, due to limitations such as particle size, solid concentration range, and the requirement of potentially destructive dilution and handling methods.

Measurement methods can be roughly divided into optical and non-optical methods. Optical methods may be further sub-divided into imaging, such as photography or confocal laser microscopy, and non-imaging techniques, such as those based on laser backscattering. Non-optical methods include acoustic scattering and rheology based measurements. A detailed review of many of these methods is given by Gregory [29] and more recently by Liang et. al. [30]. Combined methods which use of video for larger particles and laser diffraction for smaller particles have also been used [31].

An important distinction is made between *in situ* measurement techniques and those that require removal of material for measurement. Pumping or pipetting can introduce shear which may cause irreversible breakage of aggregates into smaller sizes [4]. Electron microscopy, such as scanning electron microscopy (SEM) or tunnelling electron microscopy (TEM), can provide nanoscale resolution, but require the sample material to be extracted and dried on a sample plate for measurement. Cryo-SEM may better preserve floc structure [10], but the impact of the freezing process has not been well described. Traditional microscopy can be carried out at a higher moisture content, but still requires removal, dilution and mounting of the sample on a slide. Although these methods provide detailed material information on the nano- and micro-scale, the handling required may distort or completely destroy the aggregates.

2.2.1 OPTICAL METHODS

2.2.1.1 LASER-BASED METHODS

A variety of laser based methods, including focused beam reflectance measurement (FBRM), small angle light scattering (SALS), dynamic light scattering (DLS), turbidity fluctuation (PDA), and optical backscattering (OBS) exist. Here, FBMR, PDA and OBS are discussed. The other two, SALS and DLS, are highly limited by the operational concentration range. Use of these techniques requires significant dilution and pumping to obtain suspensions in a measureable range.

Additionally, the application of SALS to flocculated particles is based on the assumption of uniform refractive index which may not be valid at low density [29].

FBMR uses a laser beam to scan particles, on-line and *in situ*, with a laser probe connected to a pipe or vessel that contains a flowing suspension [32]. As the particles pass the focused and rapidly rotating laser beam, they reflect light back to the sensor, as shown in Figure 2.4. This can result in the measurement of thousands of chords per second, at up to 20 % solids concentration, and over a large aggregate size range, from 1 µm to 1000 mm [29]. The disadvantage is that agitation is required, which makes it difficult to apply, without serious modification, to stationary sediment beds of flocculated material.

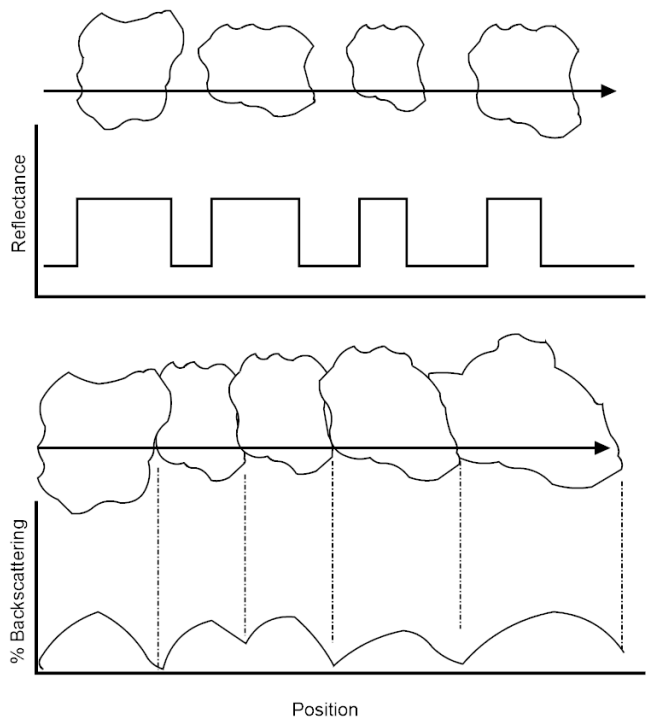

Figure 2.4 Focused beam reflectance measurement, top, is applied to a moving suspension, adapted from [29]. Optical backscattering height scans, bottom, are measured by moving laser and sensor past a bed of aggregated material.

Typically, FBRM is used as an indicator of aggregation rather than an absolute measure of particle size. For example, mean chord length from FBRM has been used to determine the state of maximum aggregation during experiments with changing dosage [5] and shear [6].

Determination of particle size is possible through inversion of the chord length distribution to a particle distribution. This requires additional information about the aggregate shape, because inversion may result in non-unique solution unless some starting parameters are known [33] [34].

The turbidity fluctuation method [8], the basis of the commercial Photometric Dispersion Analyser [7], can be used to analyse changes in aggregation state in flowing, flocculated suspensions. This method is based on the observation that the root-mean-square turbidity fluctuation, “ac” voltage, and measured turbidity, “dc” voltage, are correlated with changes in aggregate size, as presented in Figure 2.5.

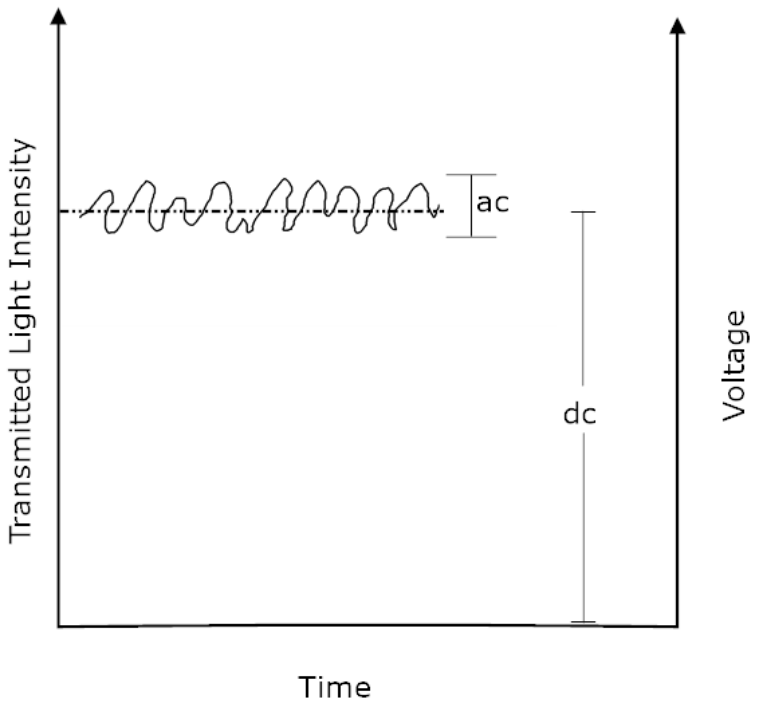

Figure 2.5 Analysis of sensor output ac and dc voltage values for turbidity fluctuation measurement in flowing dispersions, after [8].

For ideal, monodisperse particles, Gregory developed quantitative relationships between particle size, number concentration and voltage-turbidity fluctuation measurement. However, Gregory concluded that these relationships do not apply to hetero-disperse assemblages at high solid volume fractions [8]. Nonetheless, relative measurements can be made to identify trends in

flocculation. This can be applied to aggregates to determine a flocculation factor or flocculation efficiency, a relative value to allow determination of trends in aggregate growth or destruction during conditioning or the application of shear [26].

Optical backscattering instruments (OBS) are used in a variety of scientific and engineering fields and are all based on the same basic principle [35]. A light source is projected through a suspension and the reflectance is measured with a photodetector at a specific angle. The OBS measurement is typically used for relative measurement of suspended solids, although a detailed analysis of the size and quantity of suspended matter is possible with calibration [36].

Calibration of OBS sensors is necessary because particle shape, surface roughness, degree of flocculation, and refractive index all impact the optical backscatter response [37]. The radiant flux, F, scattered by a suspension as a function of particle size, mass concentration and scattering efficiency, according to Mie theory [38][39] is,

$$F = \frac{3}{2}\frac{VCEQ_s}{\rho D} \tag{2.3}$$

Equation 2.3 indicates that the larger particles contribute less to overall scattering than the smaller particles. For example, in Figure 2.6, As the larger particles fall out of the suspension, there is not a consequent drop in the total OBS signal. It is necessary to calibrate sensors to correct for these differences in size in order to obtain a meaningful measurement.

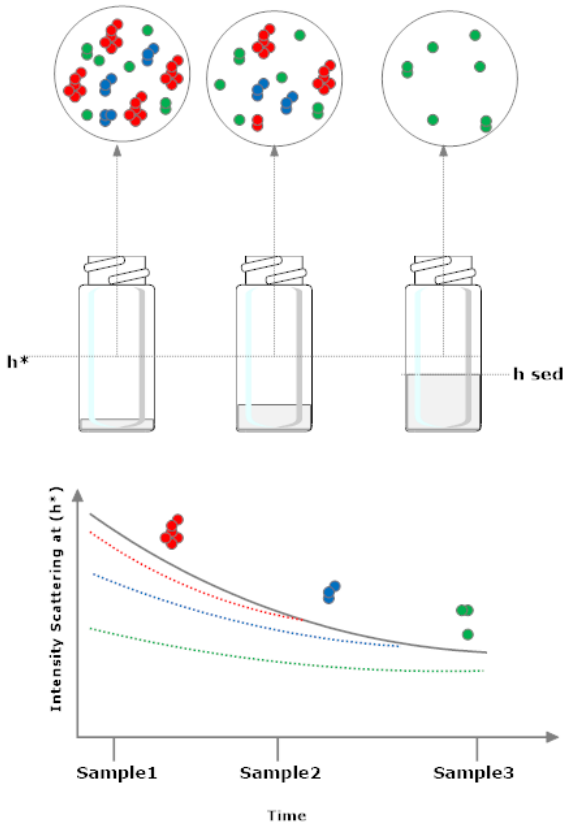

Figure 2.6 Theoretical optical backscattering response of a settling suspension. Larger particles may contribute less to the OBS response on a number basis, while the smaller, more abundant particles may contribute more

2.2.2 IMAGE-BASED METHODS

Image analysis is one of the oldest particle characterization techniques. It remains highly useful because of the rich morphological information it can provide [40]. Image-based techniques for flocculated systems can be divided into three stages: image acquisition, pre-processing, and image analysis. Techniques exist for laboratory measurement as well as for use in on-line measurement on the industrial scale.

Typically, the central objective of image analysis is to extract a feature, or set of features, from the image. The three main categories of features are physical, statistical and dynamic [41]. In flotation monitoring, physical features includes aggregate size and bubble size [42]. Statistical approaches seek to extract a more complete set of features from images. Examples include higher order textural feature analysis methods such as gray level co-occurrence matrices,

wavelets, steerable pyramids and textons [43]. In studies of flocculation, aggregation, and thickening, feature extraction has been mostly restricted to the physical domain. A recent exception to the typical physical feature extraction approach was a study on the image analysis of floc blanket concentration gradients with calibrated light attenuation [44].

Physical methods rely on segmentation to identify features related to the physical structure of the material in the image. Applications include particle size and shape analysis applications of free settling flocs [45] and measurement of aggregation rate and particle size in stirred vessels [46]. For the measurement of flocs, an image analysis setup must acquire a large number of good quality images and a computer processing algorithm is required, which can efficiently analyse and highlight 'in-focus' flocs. Several methods are described for removing out-of-focus flocs and experimental setups for improving the number of in-focus-flocs [47] [45] [48] [31]. The projection of a narrow slit of light exactly through the focal plane only illuminates in-focus flocs [48]. Methods that use frontal lighting, which produce white flocs [49], and rear projection of lighting, which produce dark flocs [47], have been used. Such setups can be used to determine density of aggregates from settling velocity if quiescent conditions are obtained through careful design [50]. After image acquisition and pre-processing it is possible to use the images to calculate a variety of properties such as effective diameters, fractal dimensions or capacity, and number or volume based size distributions.

On the industrial scale, there are several examples of in situ image analysis applications. The LubaTube, Figure 2.7, reported by Malysa et al. [51] has been used in the evaluation of heavy oil sands separation.

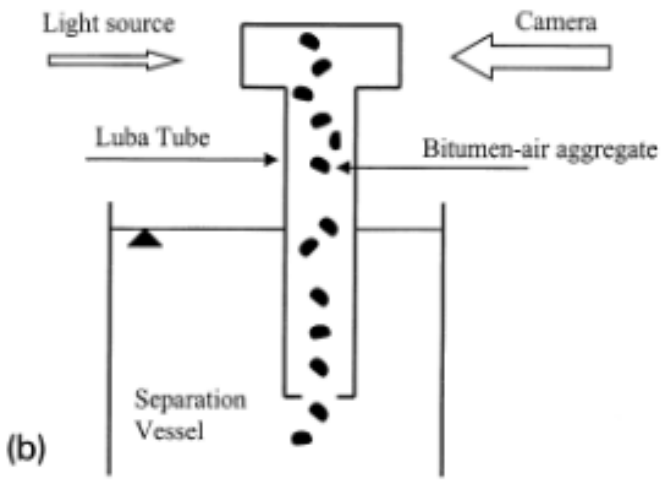

Figure 2.7 The LubaTube allows characterization of rising aggregates due to pressure differential in the separation vessel and capture column[51]

Aggregates are forced to rise into the image capture chamber by the pressure differential between the submersed tube and separation vessel. A similar technique, aerated floc characterization, has been reported by Rubio et al, [52]. Concha and Segovia installed a 'floc window' on a thickener as part of a project to study instrumentation and control strategies for optimising thickeners [53]. A video camera is attached to the 'floc window' to monitor the flocculation process. The only reference to this installation stated that a 'statistical technique' was applied to interpret the results, with no further details given.

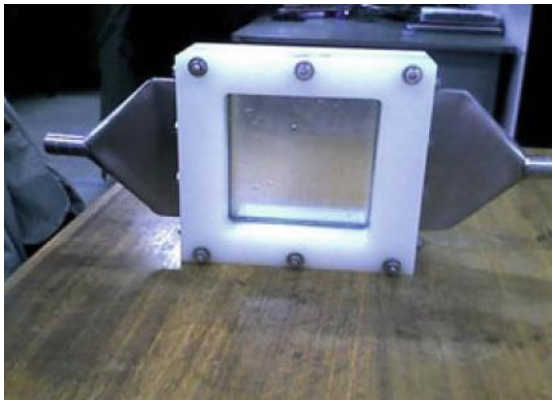

Figure 2.8 Floc window installed to obtain direct images of flocs during thickening installed [53]

In this thesis, a statistical-physical feature extraction method is applied to *in situ* images of flocculated kaolin acquired during batch settling. Two characteristic features of the interaggregate void space are discussed: the void chord length distribution (CLD) and a related measurement, the white-to-black ratio distribution.

2.2.3 NON-OPTICAL METHODS

2.2.3.1 ACOUSTING SCATTERING

Typically, the application of acoustic backscattering (ABS) has been limited to the study of sediment flux in marine environments [54]. Hunter et. al. recently reported the application of ABS measurement to the measurement of the highly concentrated, near-bed region of a thickener as a function of height and time [11]. The technique is based on determining the correlation between ABS penetration and attenuation measured with an acoustic probe and changes in the underlying solid concentration. Hunter et. al. found that the acoustic signal decayed earlier for suspensions that had undergone greater densification at a higher rake speed, and the signal decayed later for the less dense suspension. From this initial study, it appears that this could be a promising technology for the *in situ* measurement of sediment bed concentration as a function of height and time.

2.2.3.2 SLURRY RESISTANCE

Slurry resistance measurements seek to correlate solids concentration and porosity distribution to changes in the signal from multiple conductivity probe pairs. The basis of this measurement is the detection of voltage variations across electrode pairs to indicate differences in resistance of the slurry. By using a high scan rate and small spacing between sets of probes, small variations in solids concentration can be detected. It was suggested, with an improved understanding of the signal, that conductivity probe pair measurements may permit measurement of the porosity distribution in the compact sediment region of thickeners [55].

3 MATERIALS

3.1 EQUIPMENT

3.1.1 OPTICAL BACKSCATTERING AND TRANSMISSION

A TURBISCAN MA 2000, an optical analyser with two modes of operation, transmission and backscattering, was used to measure optical backscattering height scans from flocculated mineral sediments, solid ceramic spheres, and silica particles. The instrument contains a moving platen with a near-infrared LED laser light source, operating at a wavelength λ = 850 nm, a transmission photodiode, and a backscattering photodiode at 135°. The platen moves upward in 40 µm increments to produce transmission % and backscattering % graphs as a function of sample height. The instrument is typically used to measure chemico-physical phenomena occurring in concentrated liquid dispersions, such as creaming, coalescence, and cluster formation [56]. Optical backscattering and transmission data were recorded by collecting scans of the flocculated mineral sediment samples according to a set schedule over a two-hour period. At the end of the two-hour period, 10 scans were collected from various angles by rotating the cylindrical sample cell.

3.1.2 IMAGE ANALYSIS

Different image acquisition configurations were used for *in situ* sediment bed measurement and sedimentation size distribution measurements, as shown in Figure 3.1 and Figure 3.2, respectively. The method and results of the sedimentation image analysis is given APPENDIX G.

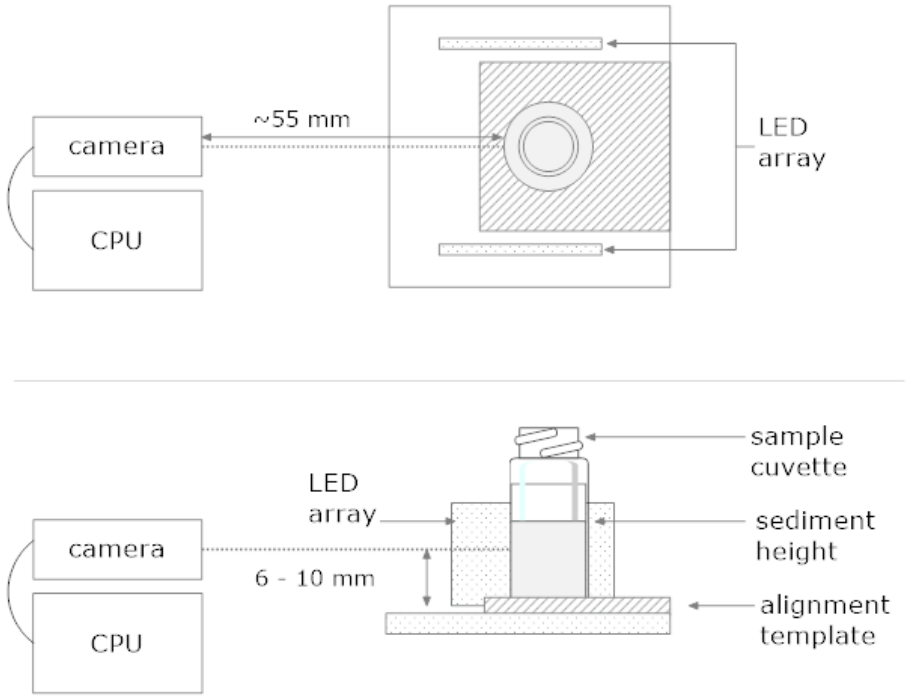

Figure 3.1 *In situ* high magnification sediment image acquisition apparatus from top and side views.

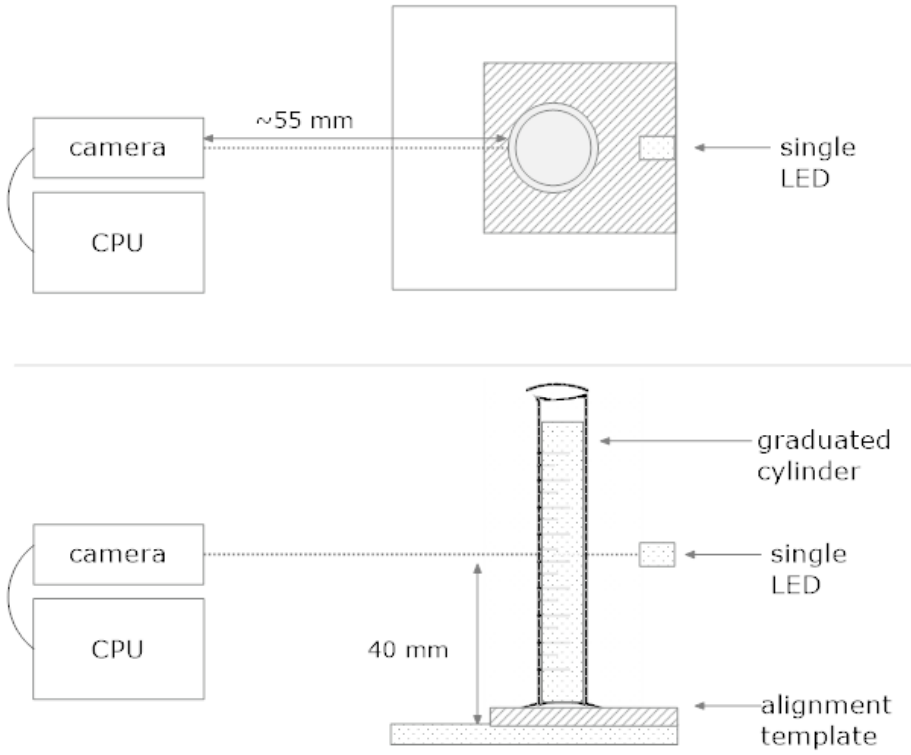

Figure 3.2 Sedimentation image acquisition apparatus from top and side views.

The two setups used a microvideo camera connected to a computer. A NAVITAR USB video microscope setup with 6x zoom, 7mm-1mm field-of-view (FOV), and 15 FPS at 640x480 resolution was used. For the *in situ* image analysis setup, a 3 X 5 array of 12V, cool white LEDs was placed on either side of the sample to create uniform lighting conditions. A box was placed over the entire apparatus to limit the impact of ambient light on the images. For the sedimentation image analysis of particle size, a single LED was used to illuminate the field-of-view. An image of a calibrated microscope slide accurately positioned at the focal distance was used to convert pixel size to metric measurement.

3.2 FLOCCULATED MINERAL SAMPLES

Batch flocculation and settling of kaolin was carried out in 30 mL sample cells. Varying dosages of a non-ionic polyacrylamide (PAM) were used to flocculate 10 w/w % kaolin suspensions, in distilled water at the mineral's natural pH, 5.3. The volume average kaolin particle size distribution was 8.86 μm, determined using a Malvern Mastersizer 2000.

A 1 g/L PAM stock solution was prepared by adding 0.4 g of 2-propenamide homopolymer (PAM), (Polysciences), with MW 5 – 6 MDa to 400 mL of distilled water and stirring at room temperature at 375 rpm for four hours. Polymer solution preparation was carried out starting 12-15 hours before the experiment. A kaolin suspension at 10 % w/w solids, was prepared by adding 2.5g kaolin (J.T Baker "Kaolin, Technical", powder washed and ignited, hydrated aluminosilicate, Lot No. 39,535, $\rho_s = 2.7$ g/cm^3) to 22.5 mL of distilled water. The samples were left at natural pH, 5.3 and shaken vigorously for 30 seconds to disperse the mineral. It is noted that some natural aggregates may still exist within suspension, and that the individual kaolin particles are probably not perfectly dispersed under these conditions.

Polymer dosage was made on a gram per ton [g/t] basis by transferring the required volume of stock solution, typically between 0.1 and 1 mL of solution, to the sample cell containing the kaolin suspension. The cell was then gently inverted 10 times to distribute the polymer within the

sample and induce floc growth. After preparation, the sample was transferred immediately to the Turbiscan or to the microvideo apparatus for data acquisition.

It should be noted that the above flocculation procedure was used only to produce flocs for testing, and no attempt was made to optimize the polymer dosage or the hydrodynamic conditions for maximum settling rates or lowest turbidity of the supernatant.

4 OPTICAL BACKSCATTERING METHODS

This section describes the optical backscattering (OBS) methods used in this thesis:

1. Measurement of OBS from solid spheres;
2. Calculation of OBS from solid spheres;
3. Measurement of OBS from batch settling of mineral suspensions;

The first two methods are important to analysing the signals measured in the third method. Simple relationships between derived OBS signal values and the underlying material structure are used to interpret the OBS signal measured from suspensions of mineral sediments. Two calibration methods, one for size and one for solid volume, are developed in this section. Before describing the methods used in this thesis, an overview of OBS height scan measurement is given.

4.1 OBS HEIGHT SCAN OVERVIEW

This section gives an overview of how optical backscattering height scans are measured and interpreted for the purpose of this thesis. First, the concept of OBS height scans and their key features are discussed by examining the OBS signal from rigid ceramic spheres. Then, the signal analysis method is described and applied to model and mineral sediment samples.

The Turbiscan takes optical backscattering (OBS) and transmission measurements every 40 µm over the height the cylinder in the sample compartment. In this thesis, this process is referred to as a 'scan.' In Figure 4.1, a sample OBS and transmission % scan are shown.

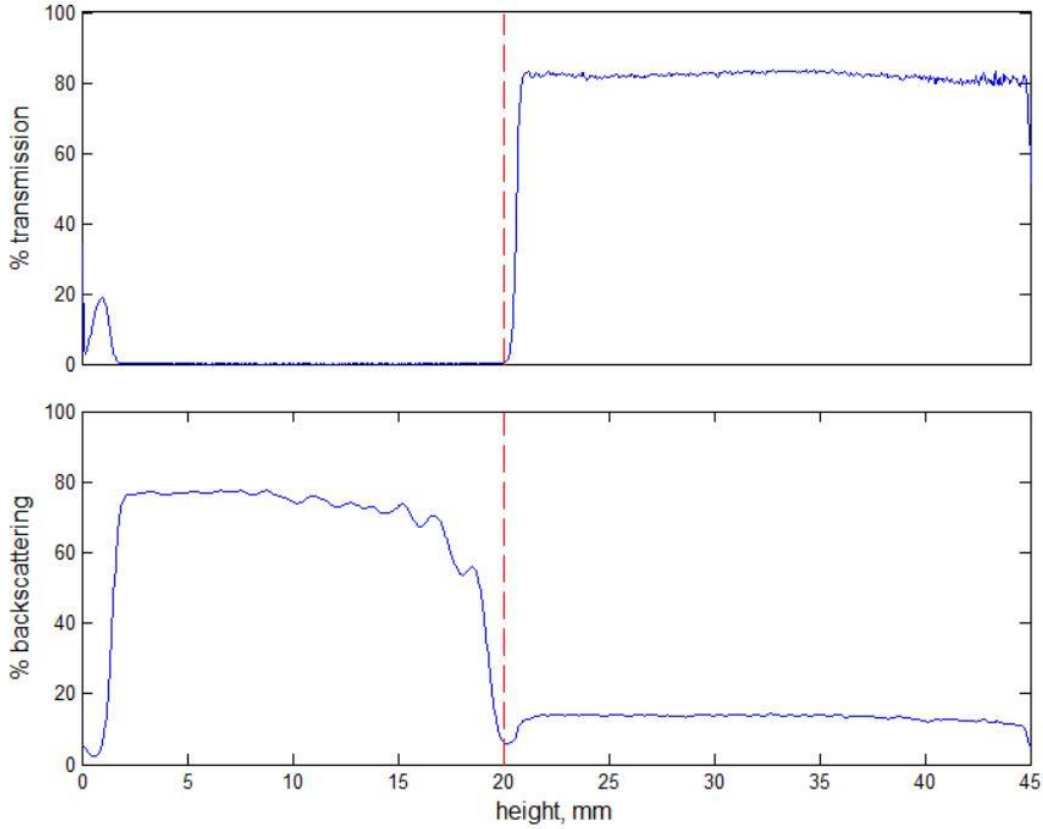

Figure 4.1 OBS height scan of a 10 % w/w kaolin sample flocculated with 60 g/t high molecular weight PAM. The interface between the sediment bed and the supernatant is indicated with a red dashed line.

In Figure 4.1, the sample height is along the horizontal axis. The abrupt decrease in transmission % and increase in backscattering % around 20 mm indicates the sediment-supernatant interface. The decrease in backscattering % around 1-2 mm is due to the bottom of the sample cylinder. In Figure 4.2, an OBS height scan is given beside the corresponding sample of ceramic spheres from which it was measured.

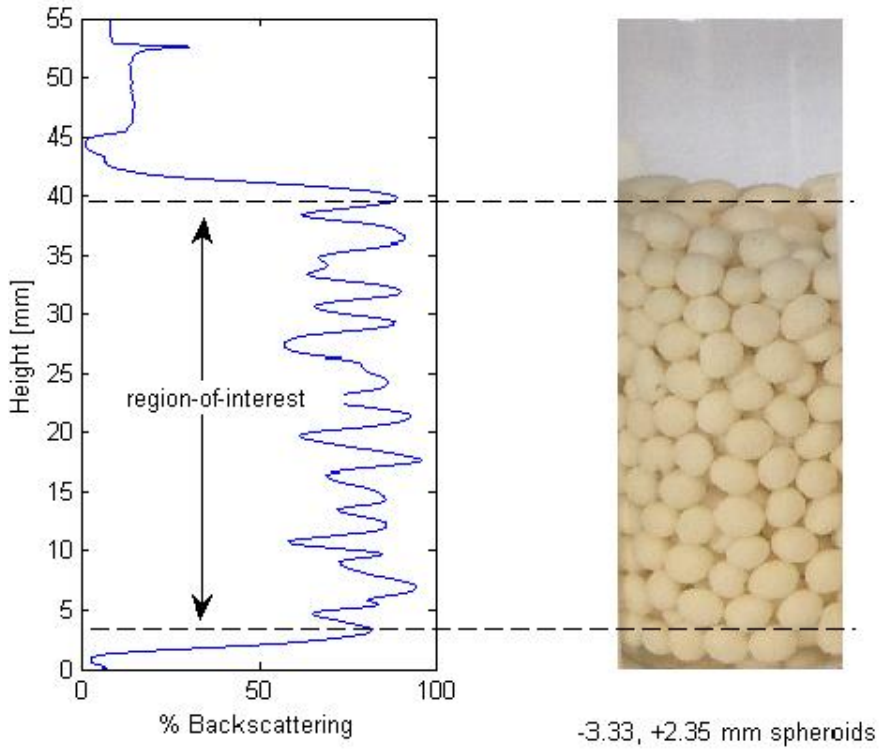

Figure 4.2 Optical backscattering height scan (left) and picture of grinding media in a sample cylinder (right).

In Figure 4.2, the signal rises rapidly from the bottom of the sample, takes on a periodic pattern over the height of the occupied portion of the sample tube, then falls to zero again. From visual inspection, it appears that the peak widths and locations are related to sphere size and position.

Rotating the cylinder and rescanning the sample from a different angle produces a different OBS height scan. After many rotations and OBS height scans, the resulting signal measurements typically fall within a characteristic intensity band, or amplitude. Refer to Figure 4.3, where the OBS height scans of 1 mm and 2.35 mm diameter ceramic spheres are compared. Note that height is presented on the x-axis in this figure. In Figure 4.3 (A) and (C), a single scan is given, while in (B) and (D), multiple scans are overlaid to demonstrate that multiple scans of a single sample will tend to fall within a characteristic % backscattering band.

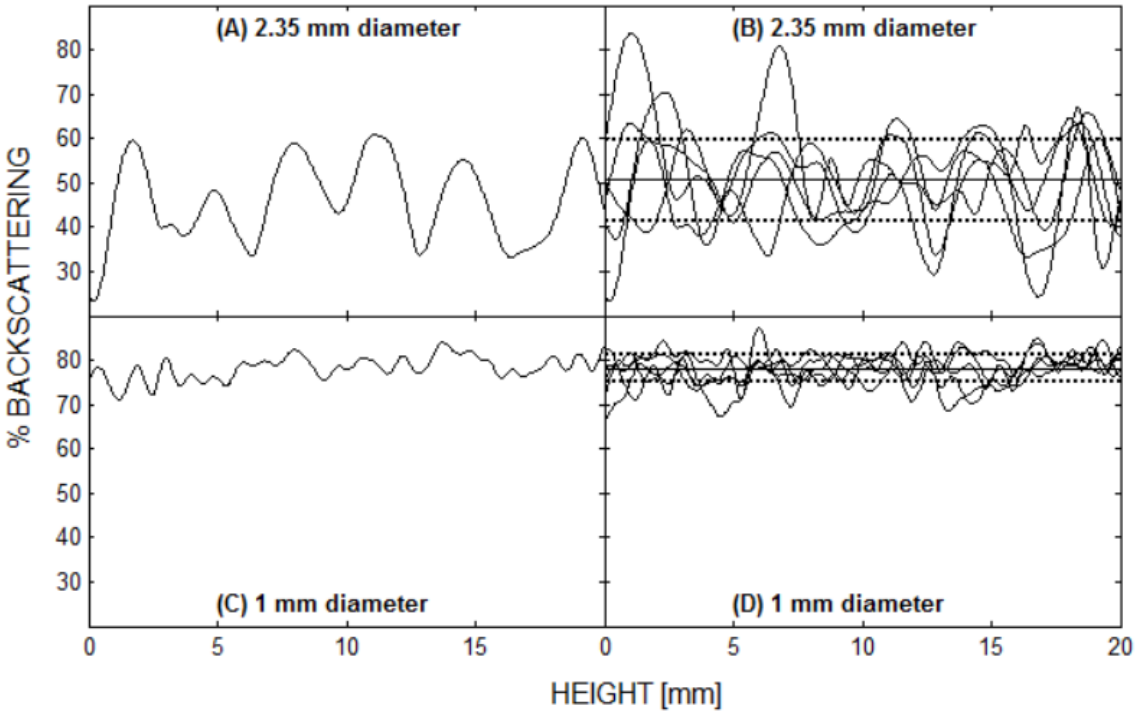

Figure 4.3 Backscattering % versus height for 2.35 and 1 mm diameter ceramic grinding media. In (A) and (C), single OBS height scans of the spheres are given. In (B) and (D) the levelled RMS value is indicated by the dashed line above and below the mean OBS. RMS-OBS for 2.35mm spheres = 9.3282%; for 1mm spheres = 3.15%.

In Figure 4.3, the mean OBS value is higher for smaller spheres and the larger spheres have a lower mean OBS value. Conversely, the oscillating signal amplitude for larger spheres is greater than the signal amplitude range of the smaller spheres.

The correspondence between the OBS height scan signal and the underlying sphere packing structure can be confirmed with simulated OBS height scans. Using a simple rendering technique, outlined in Section 4.4, simulated OBS height scans of ideal spheres can be generated. Refer to Figure 4.4, where a face-centred cubic packing structure and the corresponding simulated OBS height scans are shown.

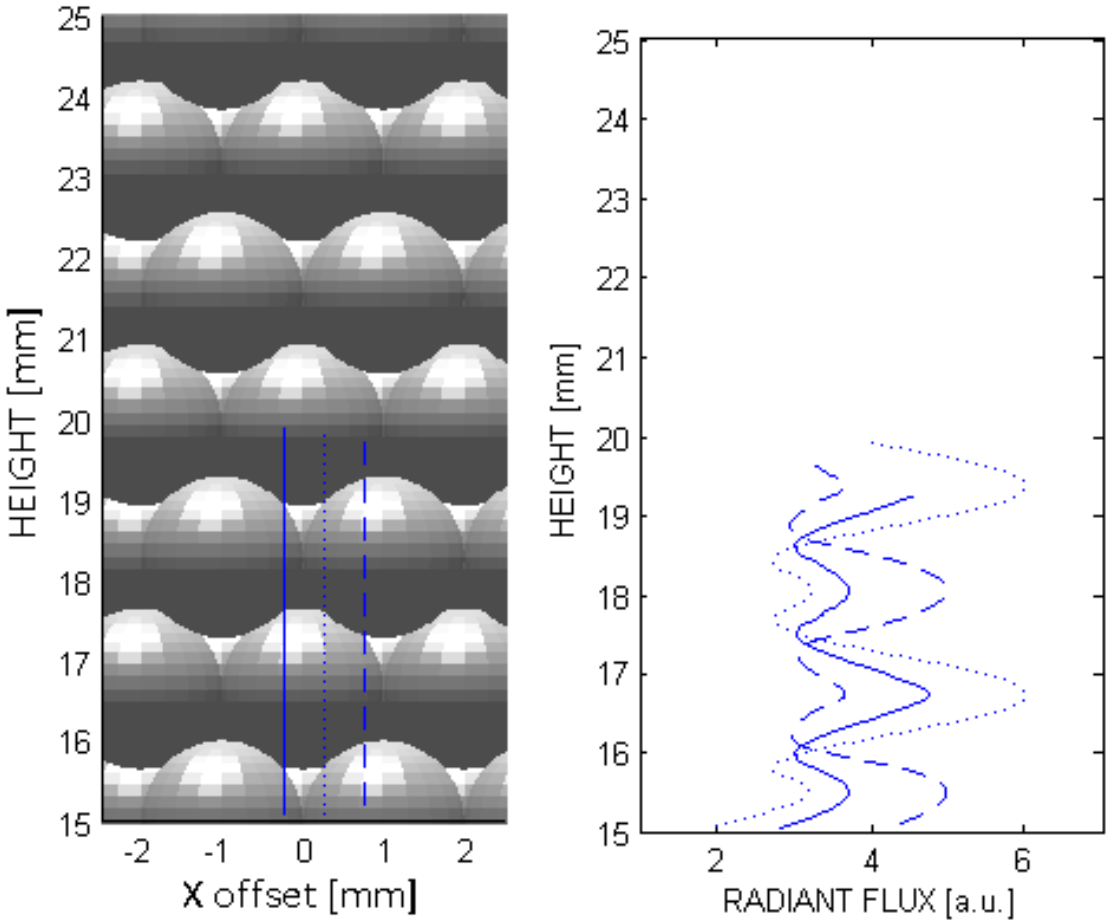

Figure 4.4 Spheres arranged in a face-centred cubic structure for optical backscattering height scan simulation. The three lines indicate the scan path on the 1mm spheres at the following offsets: 0, 0.33cm and 0.67 cm.

For each vertical OBS scan line of a solid structure, the resulting OBS signal is sort of 1D 'image' of the packing structure. In the height direction, each measurement, taken at 40 μm intervals, is a pixel in the 1D 'image'. The intensity of each pixel is a measurement of the local backscattering intensity.

The reflectance at any given position in the scan is a function of the refractive index, surface roughness, and angle between the light source and sensorFor a finite beam and sensor size, Lambertian reflectance can provide a reasonable description of the signal response. The simplified version of Lambert's cosine law is

$$F_D = \cos(\theta)\, CE \tag{4.1}$$

where: F is the reflected light, θ is the angle between the light source and the observer, C is colour of the material, and E is the incident light [57]. Note that the symbols have been changes from the source referenced to be consistent with the symbols used elsewhere in this thesis. As the light source and sensor 'scans' a spherical feature the angle between the light source and sensor changes so the intensity will vary between bright at cos(0) =1, and no reflectance at cos(2π) = 0. In reality, the sensor and beam size are not finite and the features typically scanned are not spherical. The angle between observer and light source needs to be calculated for each photon, which will be emitted from a different part of the light and interact with a different part of the material. This produces a signal value which can be loosely considered as the sum of the underlying local reflectance values. In turn, these reflectance values are a function of the material properties, such as refractive index and surface roughness, as well as the angle between the observer and light source. So, a local 'peak' will be expected where the angle is smallest, whereas a 'trough' will be expected with large angles between light source and observer.

The peak width is also indicative of the feature scanned. As the light source and sensor scan a small sphere, the signal will start at a minimum, pass through a maximum, then return to a minimum over the height of the sphere. A larger sphere will require a larger sample height, so the resulting intensity peak width will be larger. As discussed above, due to the non-finite beam width and sensor size, it is the total local reflectance at a specific backscattering angle that is measured.

4.2 OBS SIGNAL ANALYSIS OVERVIEW

It is proposed in this thesis that the OBS signal from aggregated mineral sediments can be processed to obtain information about relative aggregate size and sediment bed density. A block diagram overview of the algorithm used to process OBS data is given in Figure 4.5.

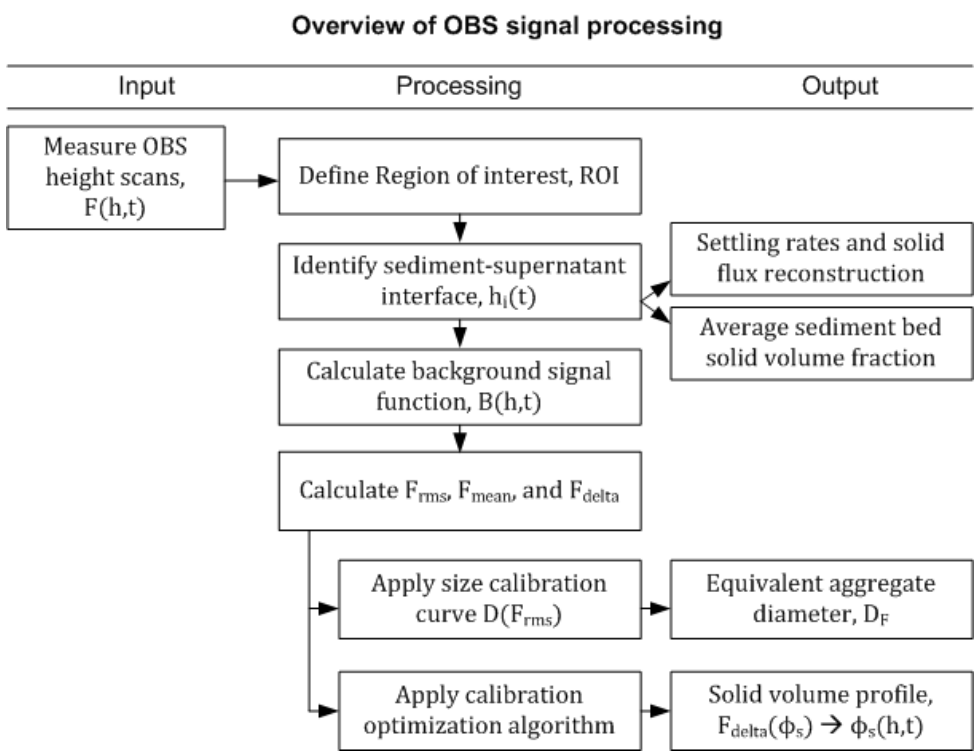

Figure 4.5 High-level outline of optical backscattering data processing routine.

4.2.1 REGION-OF-INTEREST

The first step to processing the OBS height scan signal is to determine a 'region-of-interest' (ROI), as shown in Figure 4.6. It is not possible to use the entire OBS height scan of spheres or mineral sediments because there are 'edge effects' in the signal. The OBS signal at the bottom of the height scan contains the bottom edge of the glass sample cylinder, for about 1.5mm, then a region where the signal level rapidly rises. The signal decays back to zero at the top of the scan, which indicates the solid-supernatant interface. To make a proper analysis of the signal, these 'edge effects' must be removed so that only the signal which corresponds to variations in the solid material itself is considered.

For solid spheres, the user is prompted to select the top and bottom of the ROI. Refer to Figure 4.2, which indicates a region of interest in the OBS height scan of a packed cylinder of solid spheres. In the case of flocculated mineral samples, the OBS signal values change over the height of the sample as a result of changes in aggregate size and bed density. This requires the analysis

of sub-regions within the ROI. Moving windows of 1.2 mm, overlapped by 0.8 mm, were used in the calculation of the OBS signal values. The user graphically selects the lower bound of the ROI and inputs a distance from the interface for the upper bound of the ROI. The interface is then identified by the script using an approximate derivative method which calculates the difference between adjacent points. This approach ensures consistent treatment of the data rather than introducing user bias.

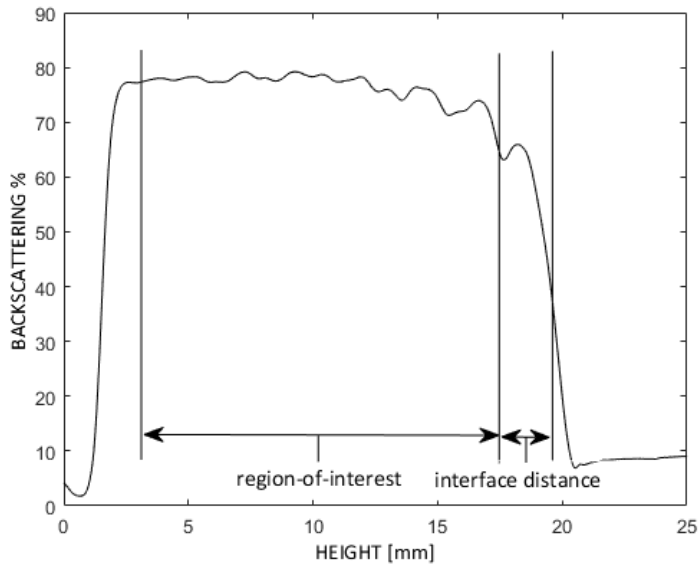

Figure 4.6 Region of interested in optical backscattering height scan defined from graphical user input and interface distance calculation.

4.2.2 BACKGROUND SIGNAL

Next, the background signal value is calculated. In the case of solid spheres, the signal average across the height of the sample will be linear. For sediment beds with a non-uniform bed density, shown in Figure 4.7, the background signal as a function of height, $B(h)$, is obtained by fitting a piece-wise cubic function. The levelled OBS signal can then be calculated by subtracting the fit result, (h), given by the dashed line from the OBS signal vector, as shown in Figure 4.8.

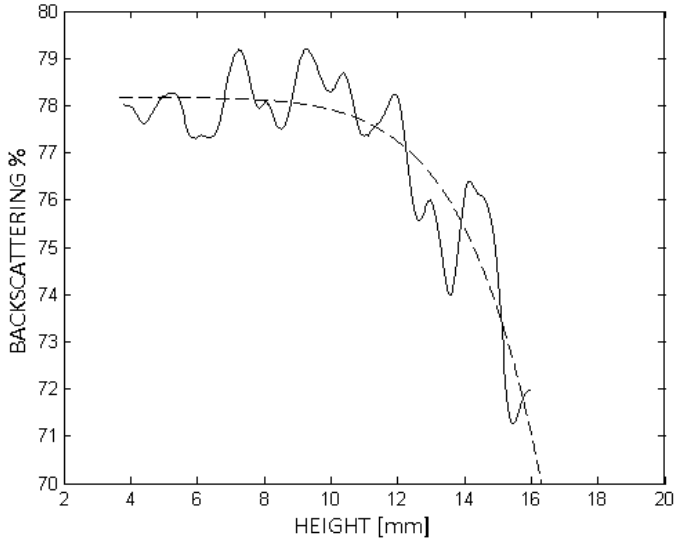

Figure 4.7 Region of interested from an OBS height scans with signal background plotted as a dashed line.

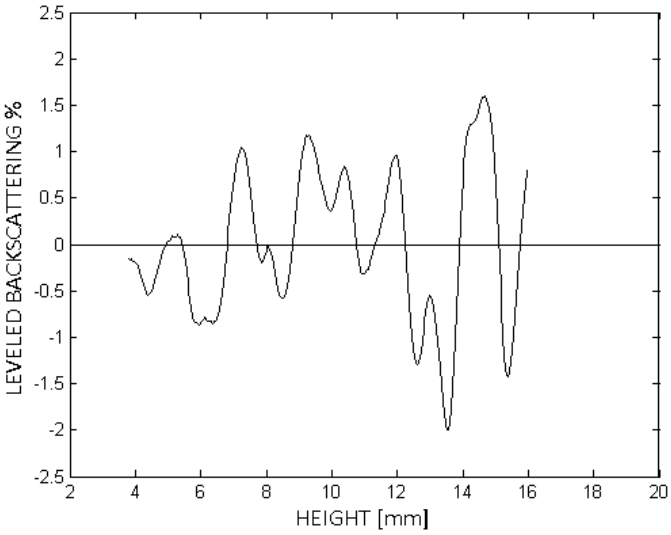

Figure 4.8 Levelled backscattering % signal obtained by subtracting the power fit background from the height scan region of interest.

4.2.3 SIGNAL VALUE CALCULATION

The optical backscattering % values, F, are converted to a signal value, F_{delta}, for further analysis. The procedure for obtaining F_{delta} is described in detail here and is used in place of raw OBS % values to obtain an improved correlation with solid volume fraction.

The ROI is divided into N windows and $F_{\text{delta}}(h)$ is obtained by calculating $F_{\text{delta,i}}$ for each window i. The levelled root-mean-square of the OBS signal, F_{rms}, is calculated for the mid-point of the ROI window i, at height k, according to

$$F_{rms,i} = \sqrt{\frac{1}{k} * \sum_{h=j}^{H} |F(h) - B(h)|^2} \tag{4.2}$$

where h is the height index, j is the first height value in the ROI sub-region, and H = j + k is the upper index of the ROI sub-region. In this study, k is set to 30, which represents a height of 1.2 mm. The mean value of window i is

$$F_{mean,i} = \frac{1}{k} * \sum_{h=j}^{H} B(h) \tag{4.3}$$

and the peak-to-peak amplitude, $A_{\text{pk-pk},i}$ is

$$A_{pk-pk,i} = 2 \cdot F_{rms,i} \cdot F_{pm-rms,i} \tag{4.4}$$

where $F_{\text{pm-rms},i}$ is the peak-to-mean root-mean-square ratio or "crest factor", which is a ratio of the largest % backscattering absolute value to $F_{\text{rms},i}$ in window i. For a perfectly sinusoidal signal, Equation (4.4) is equal to $2\sqrt{2}F_{\text{rms}}$. Figure 4.9 shows the relation between F_{rms}, F_{mean} and $A_{\text{pk-pk}}$ for a sinusoidal signal. While the application of this peak-peak amplitude approach is not clearly defined for cases where the underlying signal is not perfectly sinusoidal, it may provide a meaningful approximation of the signal amplitude.

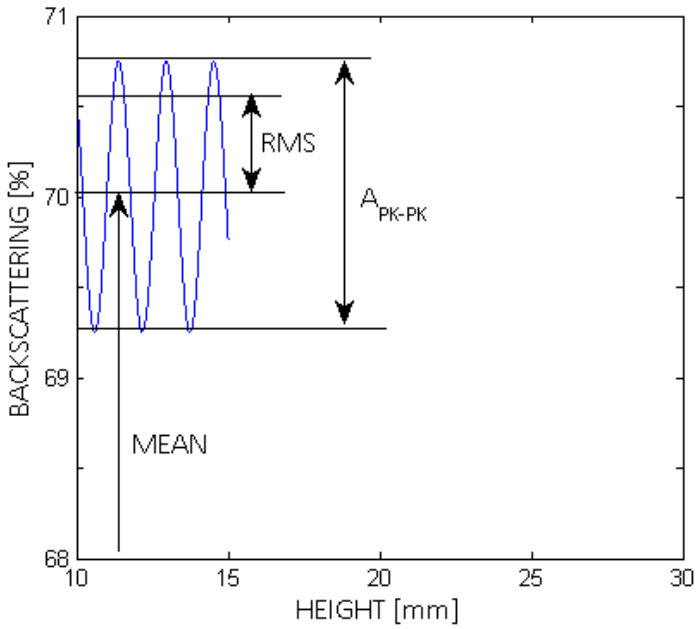

Figure 4.9 F_{mean}, F_{rms} and $A_{\text{pk-pk}}$ for a hypothetical, perfectly sinusoidal optical backscattering height scan signal.

The F_{delta} value of window i is calculated by combining the mean and peak-peak amplitude

$$F_{delta,i} = F_{mean,i} - A_{pk-pk,i} \tag{4.5}$$

Calculation of F_{delta} values for the series of moving windows in the ROI produces the dataset $F_{\text{delta}}(h)$. Application of this procedure to the time series of height scans produces $F_{\text{delta}}(h, t)$.

4.3 MEASUREMENT OF OBS FROM RIGID SPHERES

OBS height scans of ceramic grinding media spheres ranging in size from 1 mm to 4.76 mm and silica samples, ranging from 300 µm to 1000 µm, were used to generate a calibration plot. The grinding media size was verified by dry sieving and four silica samples were obtained by wet sieving. Height scans were recorded from multiple angles by opening the instrument lid, rotating the sample cylinder, and measuring another OBS height scan. In this study, 10 scans were collected from each sample and are referred to as the 'rotation series' of scans. As shown in Figure 4.3, this approach can be used to obtain an improved correlation between the derived

signal and the underlying material size. A picture of the samples used and the F_{rms} results, calculated according to Section 4.2.3, are given in APPENDIX C. The resulting F_{rms} versus diameter data were fitted with Equation (4.6),

$$F_{\mathrm{rms}}(D_F) = \mathrm{a}{D_F}^{b} \tag{4.6}$$

where a and b are fit parameters, and D_F is the sphere diameter that produces the measured F_{rms} value.

4.4 CALCULATED OBS FROM SOLID SPHERES

Optical backscattering height scans are calculated using a 3D modelling software and a MATLAB processing algorithm. A brief description of the method is given in this section, but the full details are presented in APPENDIX D. The method used was inspired by the CCD method used by Talanta et. al. to calculate the light flux in the backscattered sensor of the Turbiscan [56]. In the present work, rather than using a camera to measure the actual light backscattered in the Turbiscan, a computer model of the solid spheres is made and software rendered images are used to calculate the backscattered light flux. The results of this method are reported to support the F_{rms} and F_{mean} signal values described in Section 4.2.3.

To calculate OBS height scans, the coordinates of packing structures of face-centred-cubic (FCC) and randomly close packed (RCP) spheres are generated in MATLAB then imported to BLENDER, a 3D modelling software [58]. A light source and sensor are setup to resemble the optical arrangement in the Turbiscan, as shown in Figure 4.10 for a RCP structure.

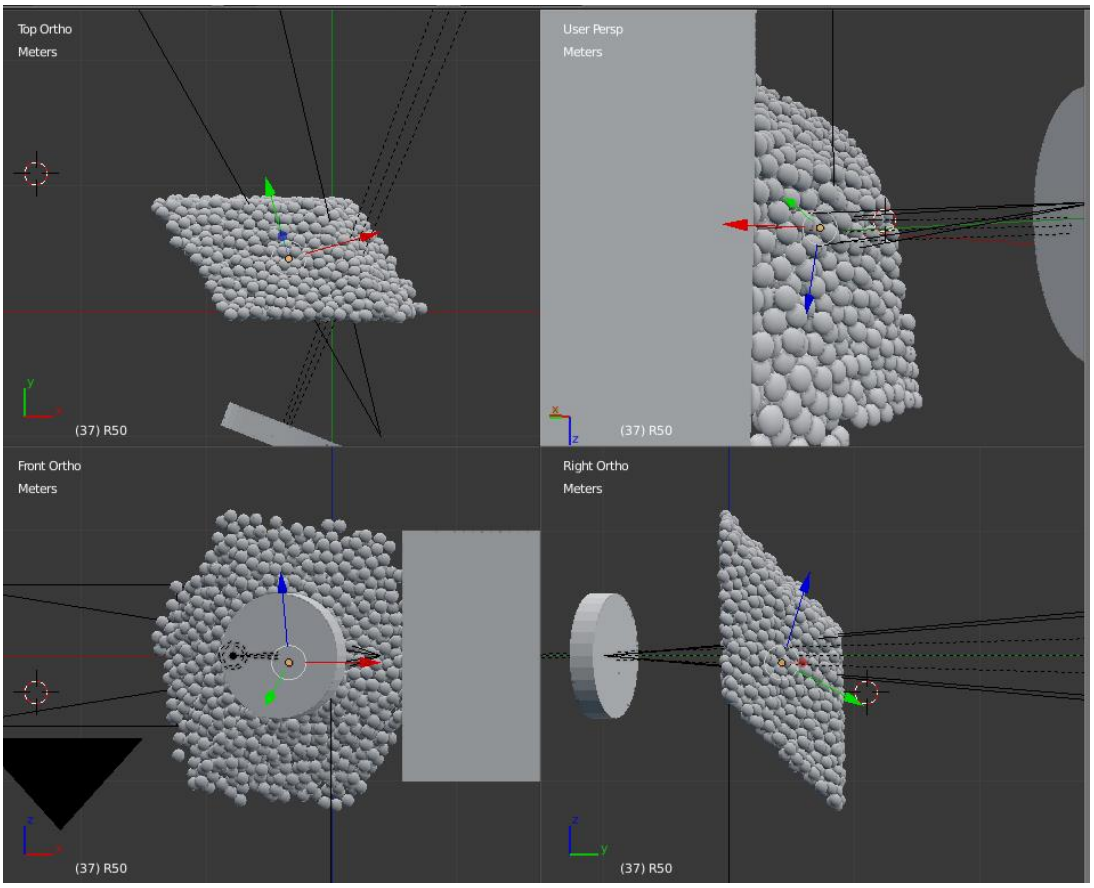

Figure 4.10 Three dimensional model of optical backscattering from rigid spheres.

Images of the packing structure are rendered at 40 µm intervals using BLENDER's built-in physically based light transport algorithms, then imported to MATLAB for further processing. The images are imported to MATLAB and integrated to get a calculated light flux for each image. The raw counts are arbitrary units that are sensitive to distance of the light from the spheres, light intensity, image resolution, and many other parameters. The resulting intensity for each image is then plotted against the height at which the image was captured. This results in a 1D image of the sphere packing structure. The F_{mean} and F_{rms} signal values, in arbitrary units, are then calculated from this 1D intensity versus height data.

4.5 MEASUREMENT OF OBS FROM MINERAL SUSPENSIONS

This section contains a description of the methods used to obtain aggregate size, bed density, and solid volume fraction height versus time profiles, $\phi_s(h,t)$, from a series of optical backscattering height scans.

OBS height scans were measured for a period of two hours during the batch settling of PAM flocculated kaolin. Directly after sample preparation, the sample was transferred to the Turbiscan to record OBS height scans during batch settling. Early in the experiment, when the sample is settling rapidly, scans are measured every 30 seconds; while later in the experiment, when the sample is settling slowly, measurements are taken every five minutes. Each scan takes approximately 30 seconds to complete. The scans collected in the two-hour period are referred to in this thesis as the 'time series' of scans.

At the end of a two-hour period, height scans were recorded from multiple angles. The sample cuvette was rotated so that a new section of the sample could be scanned. The measurement of multiple OBS height scans is carried out by simply opening the instrument lid, rotating the sample cylinder, and measuring another OBS height scan. In this study, 10 scans were collected from each sample and are referred to as the 'rotation series' of scans in this thesis. The purpose of this approach is to check the statistical validity of individual scans. For solid spheres, the measurements can be taken directly after putting the spheres in the jars. It is assumed they settle immediately.

4.5.1 AGGREGATE SIZE

As demonstrated in Figure 4.3, the F_{rms} signal values calculated from OBS height scans of solid spheres is related to sphere diameter. It is proposed in this thesis that measurement of OBS from solid spheres can be used as a calibration to determine a measure of aggregate size called "equivalent scattering diameter." Such an approach directly relates the F_{rms} value obtained from packed cylinders of solid spheres to sedimented mineral aggregates.

The fit parameters from the calibration plot obtained with Equation (4.6) are used to calculate the "equivalent scattering diameter", D_F, of mineral sediment bed F_{rms} value using Equation (4.7).

$$D_F = \exp\left(\frac{1}{b} * log\left(\frac{F_{rms}}{a}\right)\right) \tag{4.7}$$

where D_F is the equivalent scattering diameter; and the calibration parameters are $a = 3.4289$ and $b = 0.82$. Similar to the analysis of bed density by section, the D_F value can be calculated from the average F_{rms} value over the entire ROI, or it can be calculated from sub-sections of the ROI height.

4.5.2 RELATIVE AND AVERAGE BED DENSITY

Changes in the F_{rms} and F_{mean} values can be compared to relative and quantitative changes in bed density. Relative bed density can be examined by comparing the final sediment bed height to the F_{rms}, F_{mean} and F_{delta} values. Measurement of the bed height is carried out for each OBS height scan using an approximate derivative method to locate the region of rapidly changing OBS % near the top of the sediment bed, which indicates the sediment-supernatant interface.

The average bed density can be measured by carrying out a height-volume calibration to determine the volume which the sediment bed occupies. A height-volume calibration, with water, allows conversion of height to solid volume fraction. Known masses of water were added to the Turbiscan sample vial and the height of the water-air interface was measured using the approximate derivate method discussed above. The temperature of the water was automatically maintained at 25°C by the Turbiscan and the mass is converted to volume by the density of water at this temperature, 997.0479 kg/m^3. The detailed results are given in APPENDIX C. Using Equation (4.8), a measured sediment height can now be converted to solid volume fraction if the initial mass in the suspension is known.

$$\phi_s = \frac{\frac{m_k}{\rho_k}}{A_c h_f + w} \tag{4.8}$$

where ϕ_s is solid volume fraction; h_f is the final sediment bed height; A_c and w are the height-volume linear fit parameters, 0.4993 and -0.4173, respectively; m_k is the initial mass of kaolin; and σ_k , is the density of dry kaolin, 2700 kg/m^3.

4.5.3 CALCULATED SOLID VOLUME PROFILE FUNCTIONS

The object of the method described in this section is to obtain a function $F_{delta}(\phi_s)$ which can be used to convert the backscattering flux as a function of height and time, $F\ (h,t)$, which is directly measured by the OBS instrument, to solid volume fraction profiles as a function of height and time, $\phi_s(h,t)$.

4.5.3.1 CALIBRATION OVERVIEW

Calibration is necessary because particle size, shape and concentration all have an impact on the OBS signal. The radiant flux, F, scattered by a suspension as a function of particle size, mass concentration and scattering efficiency, according to Mie theory [38][39] is,

$$F = \frac{3}{2}\frac{VCEQ_s}{\rho D} \tag{4.9}$$

where V is the scattering volume [cm^3], C is the mass concentration [gL^{-1}], E is the OBS irradiance [W], Q_s is the scattering efficiency, ρ is particle density [gcm^{-3}], and D is the particle diameter [μm]. Equation (4.9) predicts that a constant mass concentration containing homogenous spherical particles will have an inverse relationship between particle radius and scattered light intensity [38]. For the height scan method applied in this thesis, it means that the OBS response at a given height is proportional to the local mass concentration C, and scattering efficiency Q_s, but inversely proportional to particle diameter, D, and density, ρ.

While Mie theory is not expected to give accurate results for non-spherical particles, it does give a first-order description of changes expected from size dispersion changes [59]. For example, Gibbs and Wolanski found that changes in floc size can have the same impact as changing the concentration up to 2.5 times [60].

De Visser et. al. carried out an OBS sensor calibration, shown in Figure 4.11, for particle size and suspended sediment concentration using ground silica [61]. De Visser found that an inverse power law was the best fit to the OBS gain, F_m, as a function of particle size,

$$F_m = \frac{A}{D^B} \tag{4.10}$$

where A and B are empirical fit parameters. When B is equal to 1, Equation (4.10) becomes the regression according to Mie theory given in Equation (4.9).

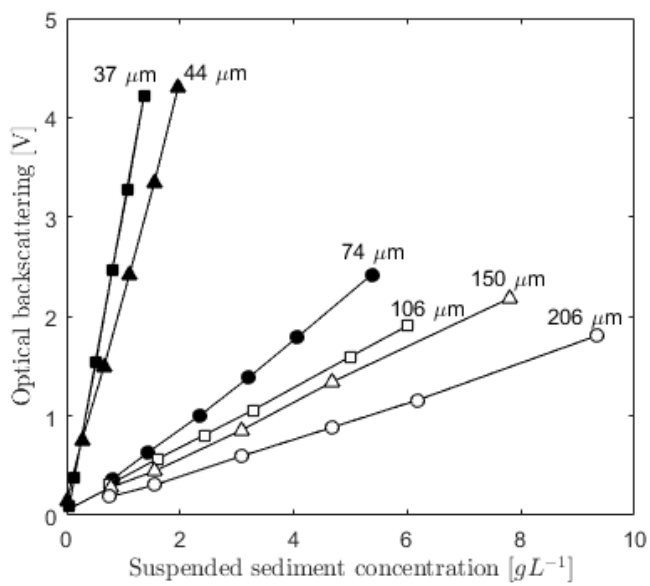

Figure 4.11 Calibration of an OBS sensor for particle size and mass concentration using ground silica. From De Visser [61].

In this thesis, values of F_{delta} are used in place of the raw % backscattering data, F, as described in Section 2.2. Here, F_{delta} is considered as a function of local solid volume. For this purpose,

Equation (4.9) is written by substitution of $\phi_s = C/(1000\rho)$ to obtain Equation (4.11), which is now expresses the radiant flux as a function of solid volume, ϕ_s.

$$F_{\text{delta}}(\phi_s) = \frac{3}{2}\frac{V\phi_s E Q_s}{D}10^{-3} \tag{4.11}$$

During the batch settling experiment, the scattering volume, V, and irradiance, E, are constant, so the calibration function $F_{\text{delta}}(\phi_s)$ determines the impact of changes in the scattering efficiency to diameter ratio, Q_s/D due to particle size and shape.

4.5.3.2 CALIBRATION ALGORITHM

The calibration procedure in this thesis produces a function, $F(\phi_s)$, which can be used to convert $F(h,t)$ data to $\phi_s(h,t)$. An 'internal', iterative calibration algorithm was used. It is 'internal' because all of the data required for the calibration can be obtained from a single batch settling experiment. The method is iterative because a simulated annealing solver is used to optimize the parameters of the calibration function.

The basis of this algorithm is the assumption that the total solid volume in the suspension remains constant throughout the experiment. As the suspension settles, it passes through a series of states with a solid concentration that varies in height and time, $\phi_s(h,t)$. The instrument measures the backscattering as a function of height and time, $F(h,t)$, which corresponds to $\phi_s(h,t)$. The algorithm described here produces a calibration function $F(\phi_s)$ by estimating the fit parameter set β that will minimize the error between the known and calculated total solid volume. An overview of the calibration algorithm used is shown in Figure 4.12.

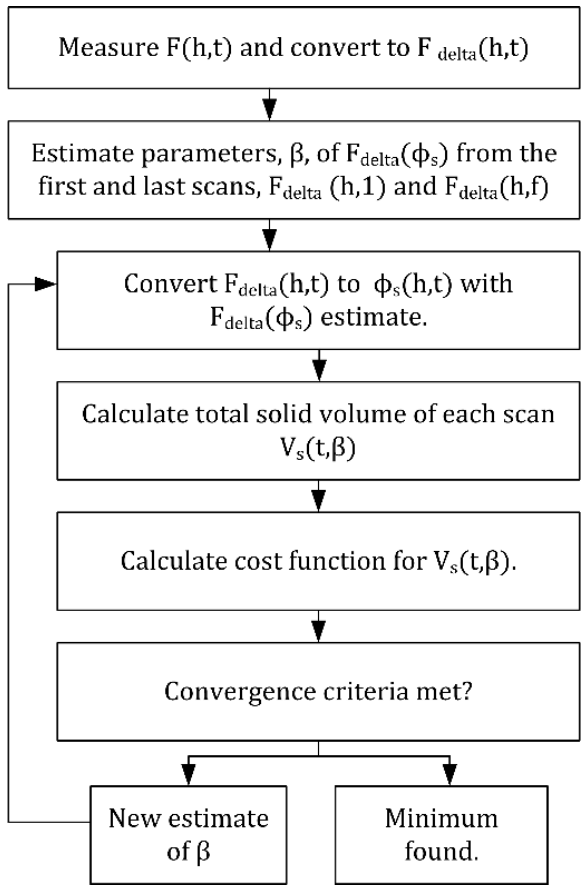

Figure 4.12 Solid volume profile calibration procedure overview.

The total solid volumes of the sample can be calculated from any of the OBS height scans with the calibration as follows. The estimated calibration function $F_{\text{delta}}(\phi_s)$ is applied to convert $F_{\text{delta}}(h)$ to $\phi_s(h)$. The volume of solids per unit area in the suspension, ω_c, for a given height scan at time t can be calculated [62]

$$\omega_{c,t} = \int_0^L \phi_s(h)dh \tag{4.12}$$

where L is the sediment-supernatant interface height. The total volume of solid, V_s, in the sample can be obtained by multiplying Equation (4.12) by the cross sectional area, A_c, of the cylinder

$$V_{s,t} = A_c \int_0^L \phi_s(h)dh \tag{4.13}$$

If the fit parameter set β are correct, then the total solid volume, $V_{s,t}$, calculated for each of the OBS height scans in the time series will be equal to the initial solid volume, V_i, in the sample. The objective of the calibration procedure is to find the parameter set that reduces the error in the calculated, $V_{s,t}$, and known total solid volume, V_i.

Several functional forms could be used as the basis of the calibration algorithm. Here, a three parameter power fit is applied to model the optical backscattering as a function of local solid volume concentration,

$$F_{delta}(\phi_s) = \beta_0 F_{delta}{}^{\beta_1} + \beta_2 \tag{4.14}$$

where the parameter set is

$$\beta = \begin{pmatrix} \beta_0 \\ \beta_1 \\ \beta_2 \end{pmatrix}$$

This model was selected to be flexible enough to accurately model the rapid increase in optical backscattering at lower concentrations and slower increase in scattering at higher solids concentration.

A global, constrained, nonlinear optimization algorithm was used to find the calibration parameter set β. The function was chosen to meet two objectives: minimize the total relative error of all the scans and to minimize the maximum absolute error of the set of scans. The cost function used in the optimization is

$$min\left[a_s\left(max\ \frac{|V_s(t) - V_i|}{V_i}\right) + b_s \sum_{t=1}^{T} \frac{|V_s(t) - V_i|}{V_i}\right] \tag{4.15}$$

where a_s and b_s are weighting constants, 1.25 and 0.1, respectively. These weighting constants were chosen after a few trials of the fitting algorithm to strike a balance between minimizing the total relative error and the absolute error of any given measurement. A global, constrained optimization algorithm was used because Equation (4.15) has many local minima. The simulated annealing solver from the MATLAB 'Global Optimization Toolbox' was used to find the global minimum of the problem.

In the optimization, the parameters of $F_{\mathrm{delta}}(\phi_s)$ are continuously updated and the cost function Equation (4.15) is re-calculated until a minimum is found. This approach is based on mass conservation: the total solid volume in the sample must remain the same despite the changes in local solid volume fraction across the height of the sample as a result of settling. Changes to the OBS signal values reflect mass flux as the concentration gradient develops and transitions between the initial and final states. This method applies when complete flocculation has occurred and all of the initially suspended mass is below the settling interface. To validate this assumption in the present study, the optical transmission % data from the height scans was analyzed to approximate the total suspended solids.

5 IMAGE ANALYSIS METHODS

Two image analysis methods were used in this thesis:

1. *In situ* image analysis of batch settling.
2. Sedimentation image analysis;

In situ image analysis was applied to measure changes in batch settling behaviour as function of polymer dosage. Sedimentation image analysis was used to measure aggregate size by taking images of aggregates as they fall through suspension. That method and its results are described in APPENDIX G.

5.1 *IN SITU* IMAGE ANALYSIS OF FLOCCULATED SEDIMENTS

In this section, an experimental approach to analysing void space within flocculated mineral sediments using chord length distributions is described. The chord length distribution has been described as a fundamental descriptor of random heterogeneous material [63] and is a specific case of the general N-point correlation function which can be used to describe material structure and transport properties based on 2D and 3D images [63]. This technique allows a comparison of the apparent void space in samples flocculated by varying dosages of a polymer.

Kaolin suspensions were prepared as described in Section 3.2. Immediately after preparation, the sample tube was transferred to the microvideo apparatus for image acquisition. Images were then acquired over a two-hour period. At the end of two hours, several images are taken of different parts of the sample, at the same height, by rotating the sample jar. This allows a determination of the statistical validity of the field of view size to be made, and is referred to as the “rotation series” of images. The sediment bed height is also accurately measured using the Turbiscan.

Several custom MATLAB scripts were used to process the images and perform feature extraction. Image processing included a threshold step, using Otsu’s method, and a morphological closing step, which is a dilation followed by erosion. In this study, a simple visual

inspection was carried out to ensure that the thresholding value could be uniformly applied. A script which displayed an array of images from each sample at various times was used to ensure uniform performance of the threshold value across the data set. A sample image and its' corresponding binary image is shown in Figure 5.1.

The resulting binary image is a two phase representation of the material as depicted in Figure 5.1 and Figure 5.2. Here, the void space is black, and labelled "Phase 2"; while the space occupied by kaolin is white, and labelled "Phase 1." The two features extracted from the time series of binary images are the void chord length distribution and a white-black ratio distribution.

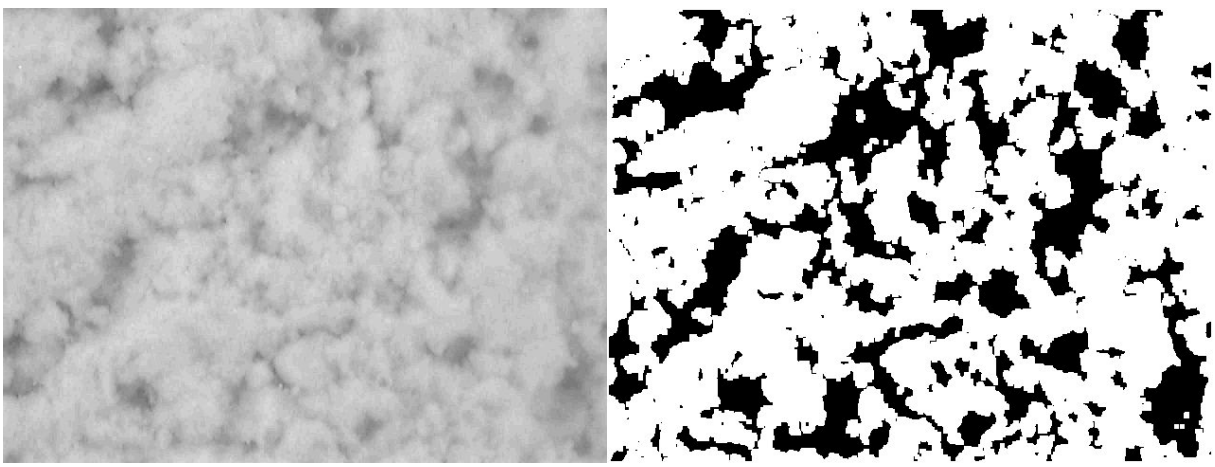

Figure 5.1 Microvideo image and corresponding binary image of a sample of 10% w/w kaolin flocculated with 200 g/t nonionic polyacrylamide.

The probability density function of the void chord lengths, $p_v(z)$, for "Phase 2", is obtained by laying random lines over the binary image and determining where the lines intersect each of the two phases, as shown in Figure 5.2. In this thesis, the line segments that overlap "Phase 1" are called "floc chords" and the segments that overlap "Phase 2" are called "void chords." A more detailed description of how chord lengths are obtained from the images is given in APPENDIX A.

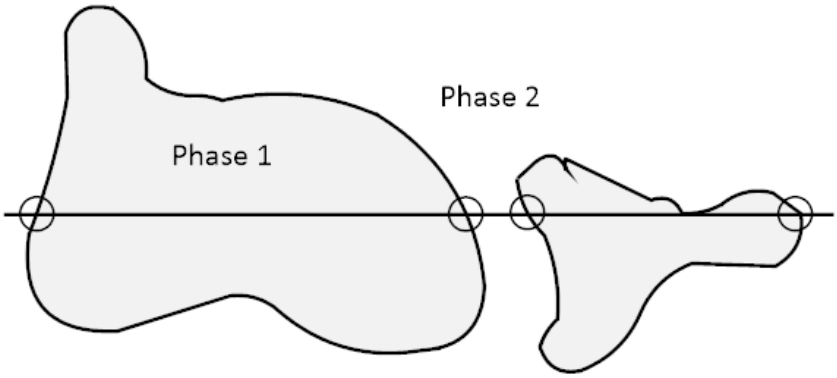

Figure 5.2 Chord length measurement for a cross-section of two phase media. Chords are the intersection of lines with the two-phase interface. Adapted from [63]

The probability density function of the voids takes an exponential form, from which a mean value, μ_v, can be calculated. The $p_v(z)$ distributions are fitted to the void chords extracted from each image from the two-hour batch settling experiment and to the rotation series of images obtained at the end of batch settling.

A white-to-black chord ratio distribution, $p_w(r)$, is obtained by calculating the white-to black pixel ratio for each chord used to sample the chord length distribution. After a sufficient number of chord samples, the white-to-black ratio will converge on the pixel-based white to black balance of the image. The pixel-based white-black ratio is obtained by counting the white pixels and dividing by the total number of pixels. A logistic distribution was found to be the best model for $p_w(r)$ by trial and error with various distribution models. The logistic distribution has two parameters, shape, μ_r, and scale, s, and is similar to the normal distribution but has longer tails and a higher kurtosis. The shape parameter of the logistic distribution, μ_r, is equivalent to the mean, while the scale parameter, s, is related to the standard deviation, σ, by $s = (\sqrt{3}/\pi)\ \sigma$. Interpretation of trends in the distribution parameters as a function of time permits an analysis of the ratio of occupied-to-unoccupied space in the suspensions during batch settling.

6 OPTICAL BACKSCATTERING RESULTS

6.1 MEASURED BACKSCATTERING FROM RIGID SPHERES

The results of measuring OBS from rigid spheres and silica samples is given in Figure 6.1. The root-mean-square backscattering, F_{rms}, is plotted against particle diameter to obtain an F_{rms} versus diameter calibration.

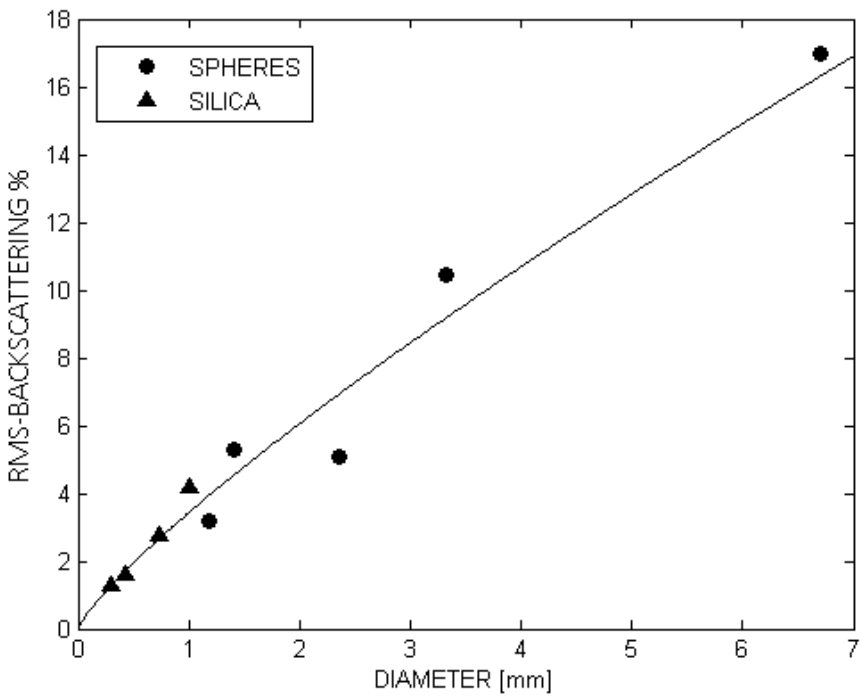

Figure 6.1 Root-mean-square OBS % versus diameter for spheroidal grinding media and silica samples.

The line-of-best fit in Figure 6.1 is the result of fitting Equation (6.1), with a coefficient of correlation, $R^2 = 0.969$.

$$f(d) = \mathrm{a}D_s{}^b \tag{6.1}$$

where D_s is the sphere diameter; and a = 3.4289 and b = 0.82 are fit parameters.

A discussion of the relationship between sphere size and bed porosity is given in APPENDIX C.

6.2 CALCULATED BACKSCATTERING FROM RIGID SPHERES

Calculated optical backscattering (OBS) height scans were generated with a combination of 3D modelling software and MATLAB, as discussed in Section 4.4. Face-centred cubic (FCC) and randomly close packed (RCP) structures were scanned to permit calculation of the F_{mean} and F_{rms} optical backscattering values. The relationship between sphere size and bed porosity is considered as it relates to the study of porosity in beds of flocculated mineral sediments.

6.2.1 CALCULATED OBS SIGNAL VALUES

The FCC model scans were calculated at three representative positions in the packing structure. As indicated in Figure 4.4, there is good correspondence between the location of OBS height scan peaks and troughs and the underlying packing structure. The calculated OBS height scans display a characteristic amplitude and periodicity observed in the OBS scans of solid spheres and mineral sediments. In Figure 6.2, F_{rms} and F_{mean} values are given for height scans of varying diameter FCC packing structures. The FCC scan results demonstrate the OBS signal trends observed in the measured OBS height scans. While F_{mean} decreases as sphere size increases, F_{rms} increases.

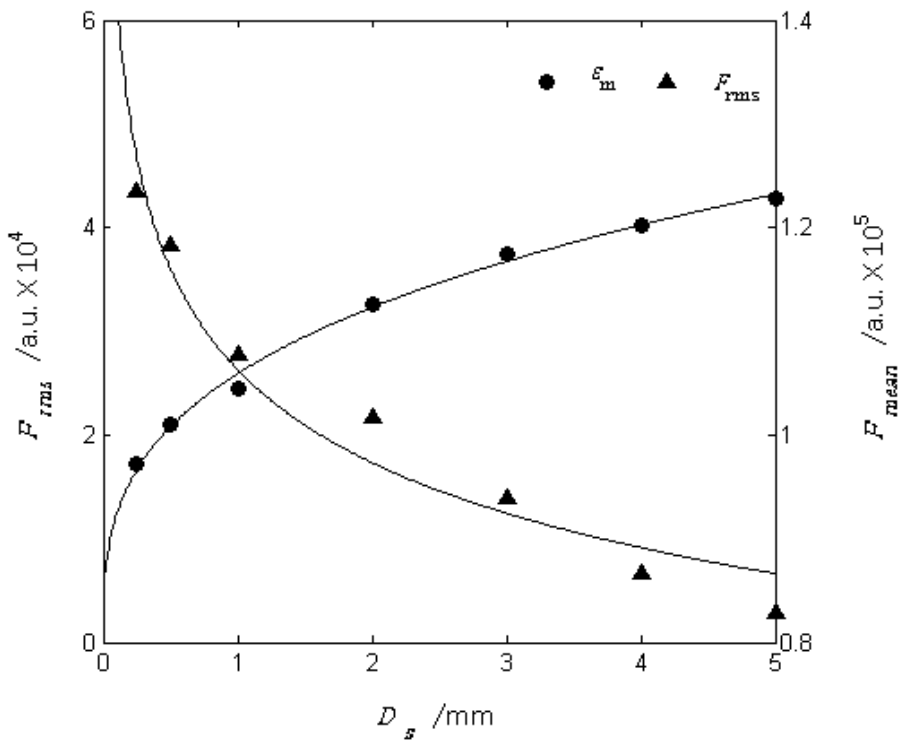

Figure 6.2 Calculated optical backscattering signal values, F_{mean} and F_{rms}, as a function of sphere diameter

The randomly close packed sphere structure in Figure 4.10 was 'scanned' and the results are plotted in Figure 6.3, with a single scan, and Figure 6.4, with multiple scans are overlaid.

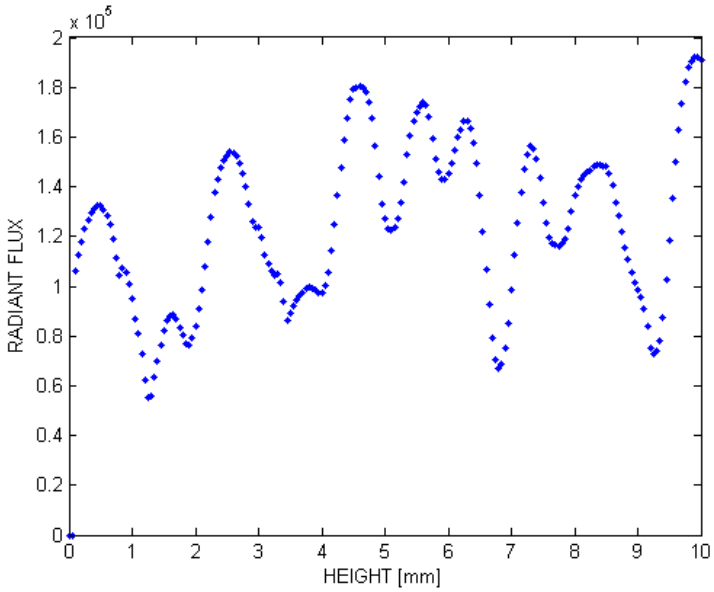

Figure 6.3 Simulated optical backscattering height scan for randomly close packed 1mm rigid spheres

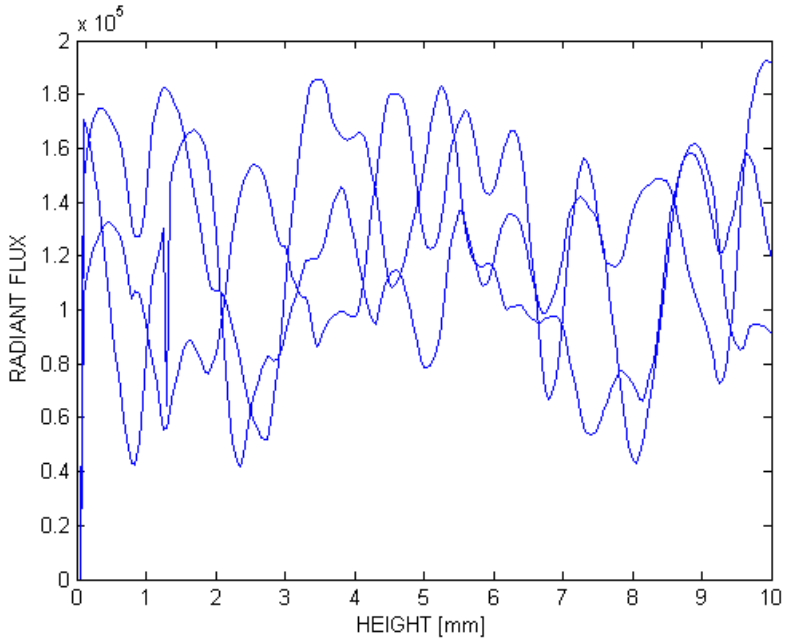

Figure 6.4 Multiple simulated optical backscattering height scan for randomly close packed 1mm rigid spheres

6.2.2 SPHERE SIZE-POROSITY RELATIONSHIP

In this section, F_{rms} measurements from packed beds of rigid spheres are compared to literature values of mean porosity, ε_{m}. If a cylinder of fixed diameter, D_{c}, is filled with spheres of diameter, D_{s}, then the mean axial and radial porosity, ε_{m}, will vary according to the cylinder-to-sphere diameter. Mueller [64] gives modelled mean porosity values on the basis of $D_{\text{c}}/D_{\text{s}}$, which are converted here by multiplying the $D_{\text{c}}/D_{\text{s}}$ ratio by the sample cylinder diameter, i.e., 20 mm. InFigure 6.5, the resulting ε_{m} and F_{rms} values are plotted as a function of sphere diameter. This comparison indicates that F_{rms} values can be used as an indicator of porosity in beds of packed spheres based on the good linear correspondence between ε_{m} and F_{rms} values.

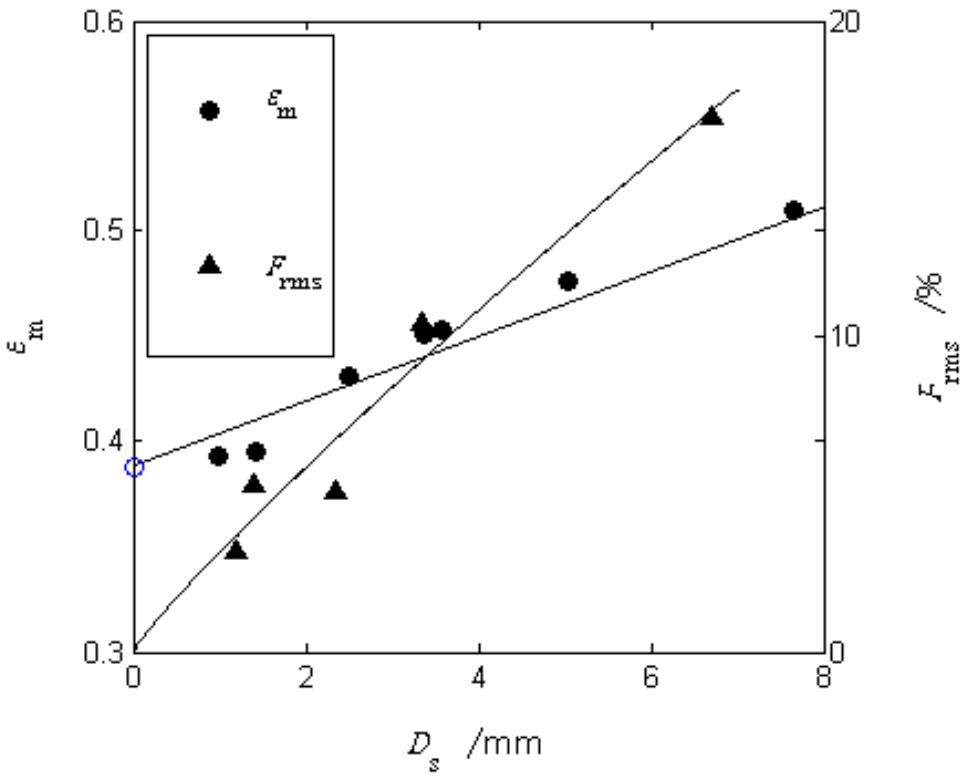

Figure 6.5 Measured and calculated RMS-OBS plotted with radial porosity data from Mueller [64].

For a packed bed of solid spheres, the mean radial porosity is a measure of the ratio of occupied versus unoccupied space. In Figure 6.5 the linear fit parameters for ε_{m} in this diameter range are

m = 0.0154 and b = 0.371. The intercept, then, is at ε_m = 0.388, which corresponds to a packing fraction, 1 - ε_m, of 0.612. As the sphere diameter decreases relative to the cylinder diameter, the mean radial porosity approaches the maximum packing fraction for poured random packing, between 0.609 to 0.625 [65]. In sediment beds of flocculated fine mineral particles there are many other factors to consider. Flocs are highly porous structures, with water representing 90 % or more of their particle volume [62]. Packing efficiency is also dependent on particle shape. Flocculated aggregate is known to exhibit fractal scaling, or least, power law scaling [66]. This means that aggregates are denser while larger flocs are extended structures with densities approaching that of the surrounding liquid [67]. Compressibility of the sediment bed depends on the network strength and bed height, whereas incompressible spheres will not exhibit such behaviour. For a packed bed of spheres, ε_m increases marginally from 0.405 to just over 0.42 for a diameter increase from about 50 to 300 μm. However, for beds of flocculated mineral sediments, this dependence may be significantly different due to their non-spherical, extended structure which leads to significantly lower packing efficiency.

6.3 MEASUREMENT OF OBS FROM MINERAL SUSPENSIONS

This section analyses optical backscattering data to obtain aggregate size and sediment bed density information. First, an overview of the range of suspension stability and settling observed in this thesis is discussed.

6.3.1 SUSPENSION STABILITY AND SETTLING RATES

In this section, the optical backscattering and transmission profiles of coagulated kaolin samples, at two different pH values, and a polyacrylamide flocculated kaolin sample are compared. A higher pH will stabilize the suspension, while addition of polymer typically destabilizes the suspension. At high pH, the kaolin suspension is more stable and takes on the order of one day to develop a discernible sediment bed. Figure 6.6 and Figure 6.7 show a time series of backscattering and transmission height scans, respectively, from a coagulated 10 % w/w kaolin sample undergoing settling at pH 10.3.

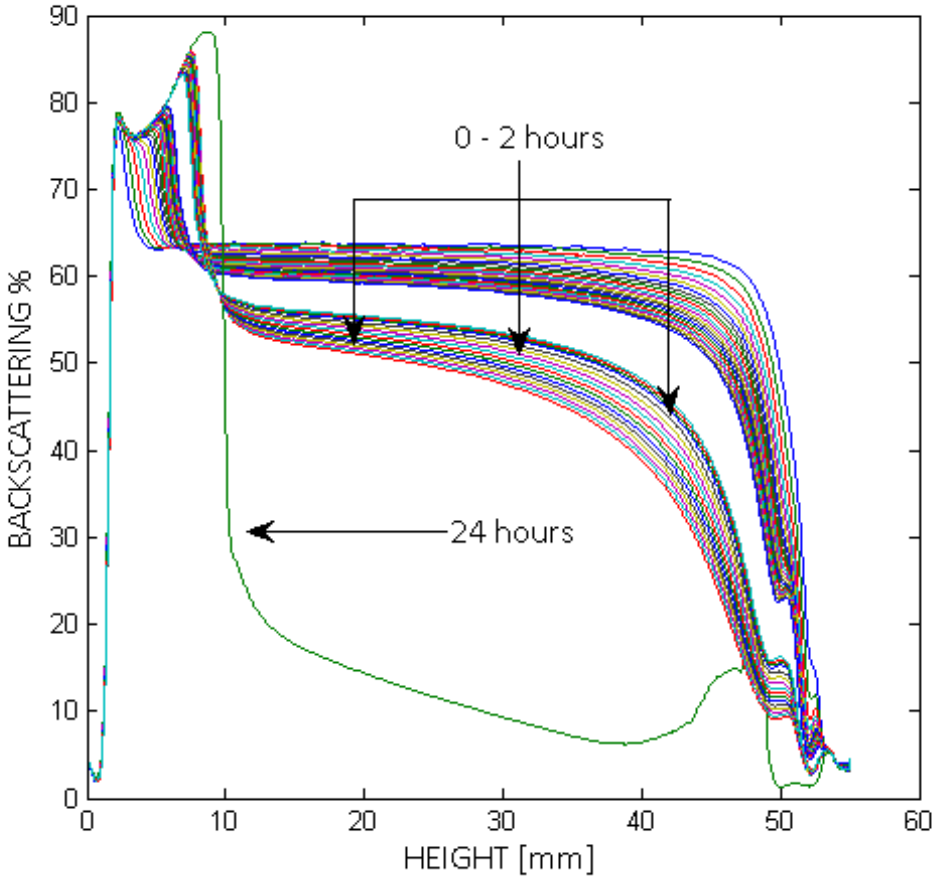

Figure 6.6 Backscattering from 10 %w/w kaolin sample at pH 10.3. Destabilization of the sample occurs slowly as indicated by the decreasing backscattering over the height of the suspension. One scan is taken 24 hours later and the vertical line at 10mm indicates the developing sediment bed.

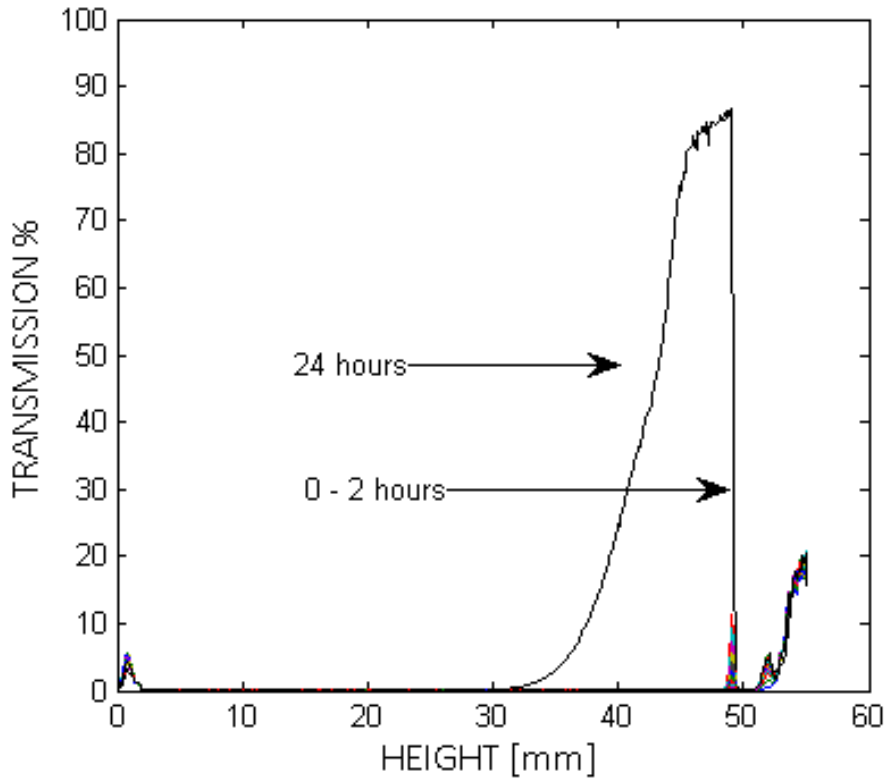

Figure 6.7 Transmission height scans of 10% w/w kaolin at pH 10.3. The lines for all times between 0 and 2 hours overlap.

While the sediment bed reached 10mm in height after 24 hours, the supernatant remained quite turbid. In the first 2 hours, there is hardly an observable change in the transmission data. After 24 hours, the top 10 mm has started to clarify, but the remainder of the suspension remains highly turbid. At lower pH, the suspension is far less stable and begins to coagulate immediately. In Figure 6.8 and Figure 6.9, the backscattering and transmission height scans, respectively, are given for a 10% w/w kaolin sample undergoing settling over a two-hour period.

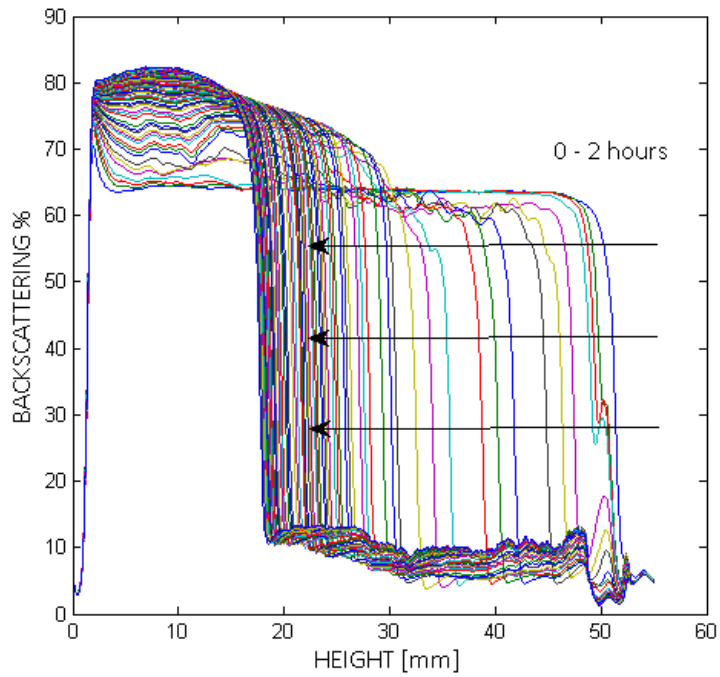

Figure 6.8 Natural pH, 5.3, 10% w/w kaolin sample settling over a two-hour period.

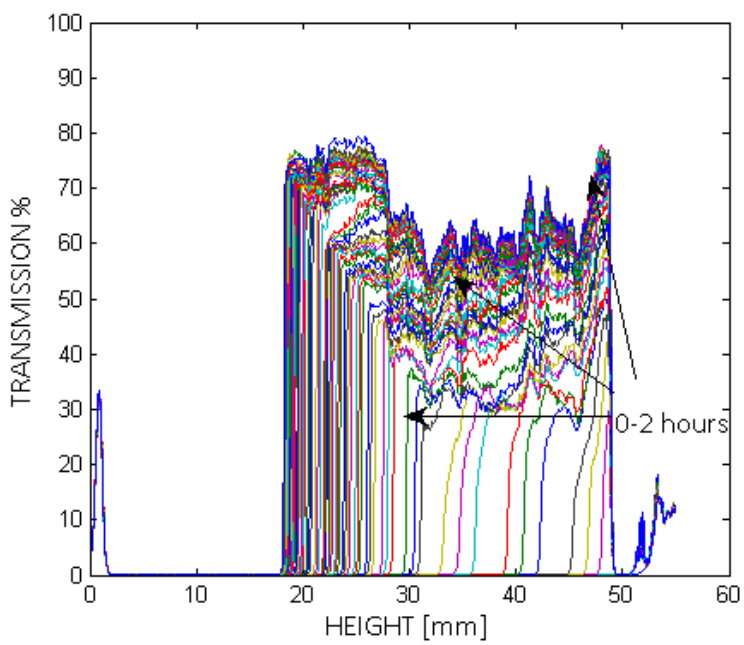

Figure 6.9 Transmission height scans over two-hour period of 10 % w/w kaolin in deionized water at natural pH, 5.37.

The stability is further reduced by addition of polyacrylamide. To obtain a clearer picture of how flocculation improves settling and clarification of kaolin suspensions, the impact of polyacrylamide on the interface settling data is given in Figure 6.10 and the supernatant transmission in Figure 6.12.

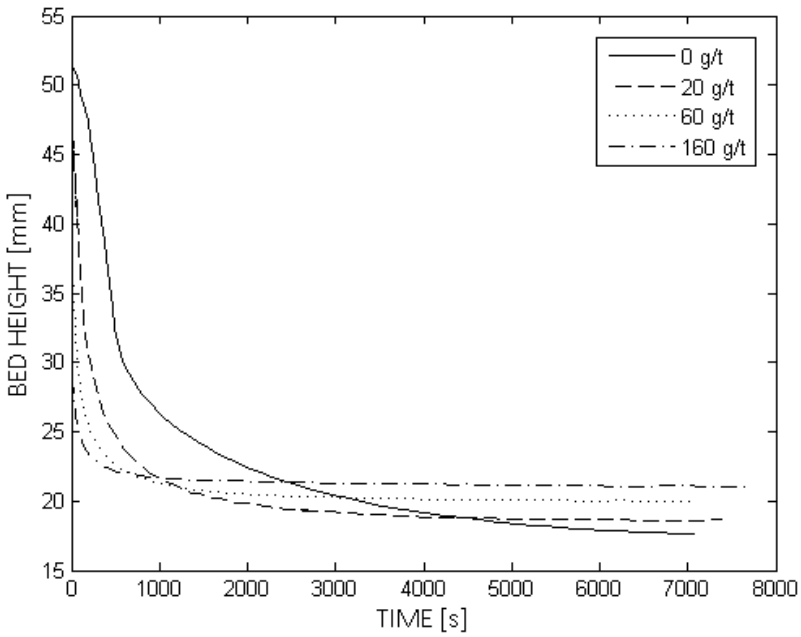

Figure 6.10 Bed height from OBS measurements over two hours for PAM-flocculated 10 % w/w kaolin and straight 10% w/w kaolin, Trial A.

The interface velocity, or settling rate, increases as polyacrylamide is added. This indicates the formation of larger aggregates which sediment and clarify the suspension faster. The hindered settling velocity can be approximated as the velocity of the linear portion of the settling data, as shown in Figure 6.11 for two sets of interface settling data. The results of two different trials are summarized in Table 6.1.

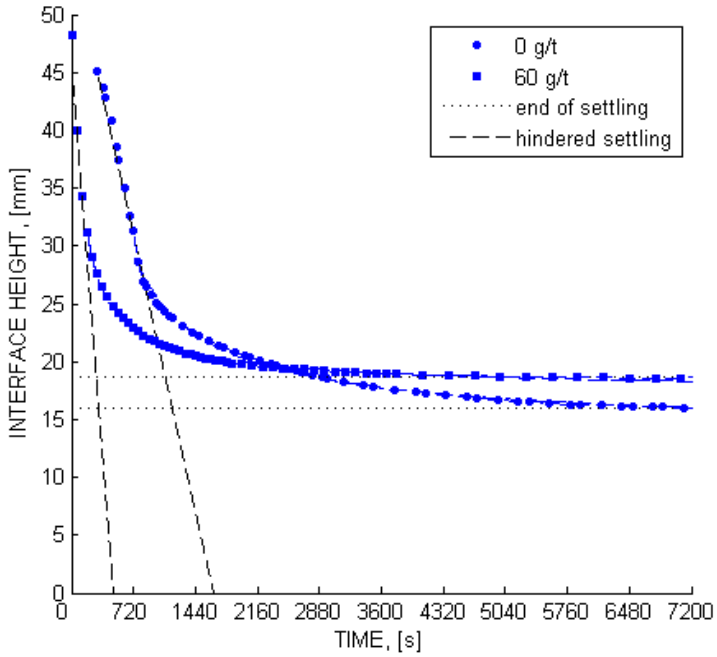

Figure 6.11 Hindered settling rate fit from kaolin batch settling data with 0 and 60 g/t polyacrylamide dosage.

Table 6.1 Summary of hindered settling rates for 10 % w/w kaolin suspensions flocculated with varying dosage of polyacrylamide

$Trial$	$Dose\ [g/t]$	$Settling\ rate\ [cm/hr]$
A	0	12.23
A	20	26.94
A	60	37.63
A	160	43.20
B	0	11.29
B	10	17.82
B	20	26.96
B	100	57.22

The transmission and backscattering data indicated that the kaolin suspensions settle and clarify quicker as the polymer dose is increased. The rapidly falling sediment interface in the samples at high PAM dosage indicate highly effective flocculation resulting in large aggregates of kaolin particles.

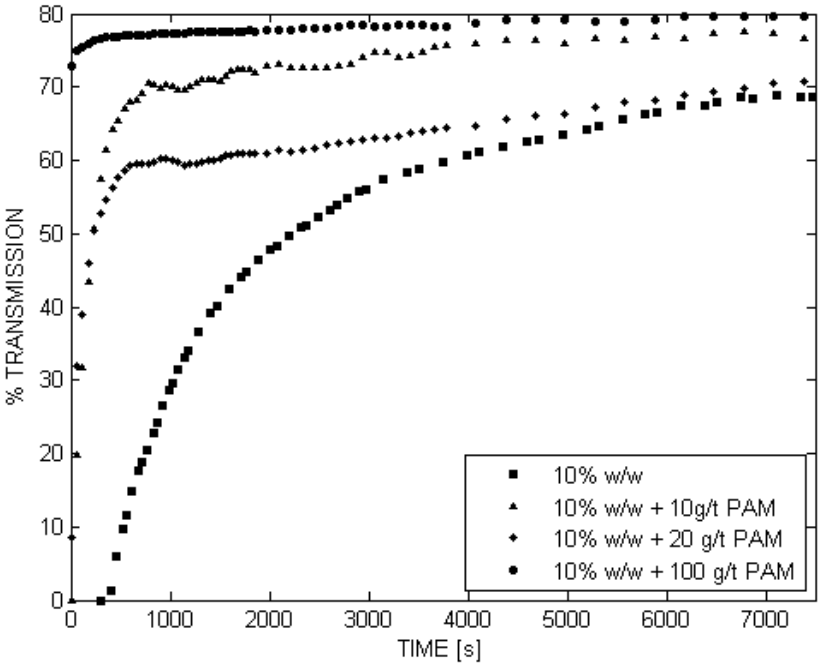

Figure 6.12 Transmission % in the top 10 mm of supernatant during a two-hour period for PAM flocculated 10 % w/w kaolin samples. The PAM flocculated lines are above the sample with no polymer added which indicates improved clarification in the sample.

The transmission % in the top portion of the suspensions clarifies much quicker when polyacrylamide is added. At the end of the two-hour period, the upper region of the samples was at approximately 70% or above, which indicates a relatively clear supernatant.

The final sediment bed varies depending on the chemical conditions. Coagulation leads to a lower bed height: after 24 hours, at pH 10.3, the bed height reaches 10 mm. Based on the transmission and backscattering data, this sample has not completely clarified so the final bed height may be higher than 10 mm. After 24 hours, at pH 5.2, coagulation of a 10 % w/w kaolin suspension produced a bed height of 14.45 mm. Flocculation leads to a range of final sediment bed heights, with 15.76 mm measured for a 20 g/t PAM dose and 17.55 mm measured for a 160 g/t PAM dose. This indicates that the flocculation mechanism has an impact on floc size and the subsequent bed density. Stable suspensions are composed of small aggregates that settle slowly, but they result

in a tighter networked sediment bed. Decreasing stability results in faster suspension settling and clarification, but a less dense sediment bed develops.

6.3.2 AGGREGATE SIZE AND BED DENSITY

In this section, the signal analysis method and interpretation described in Section 4.2.3 and 4.5 are applied to batch settling trials of PAM flocculated kaolin suspensions.

A series of 10 % w/w kaolin samples were flocculated by varying doses of polyacrylamide and OBS height scans were measured from multiple angles after two hours of settling. The general trend, as indicated in Figure 6.13, is that increased aggregate size results from increased polymer dosage. The F_{rms} and F_{mean} measured from these samples are shown in Figure 6.14.

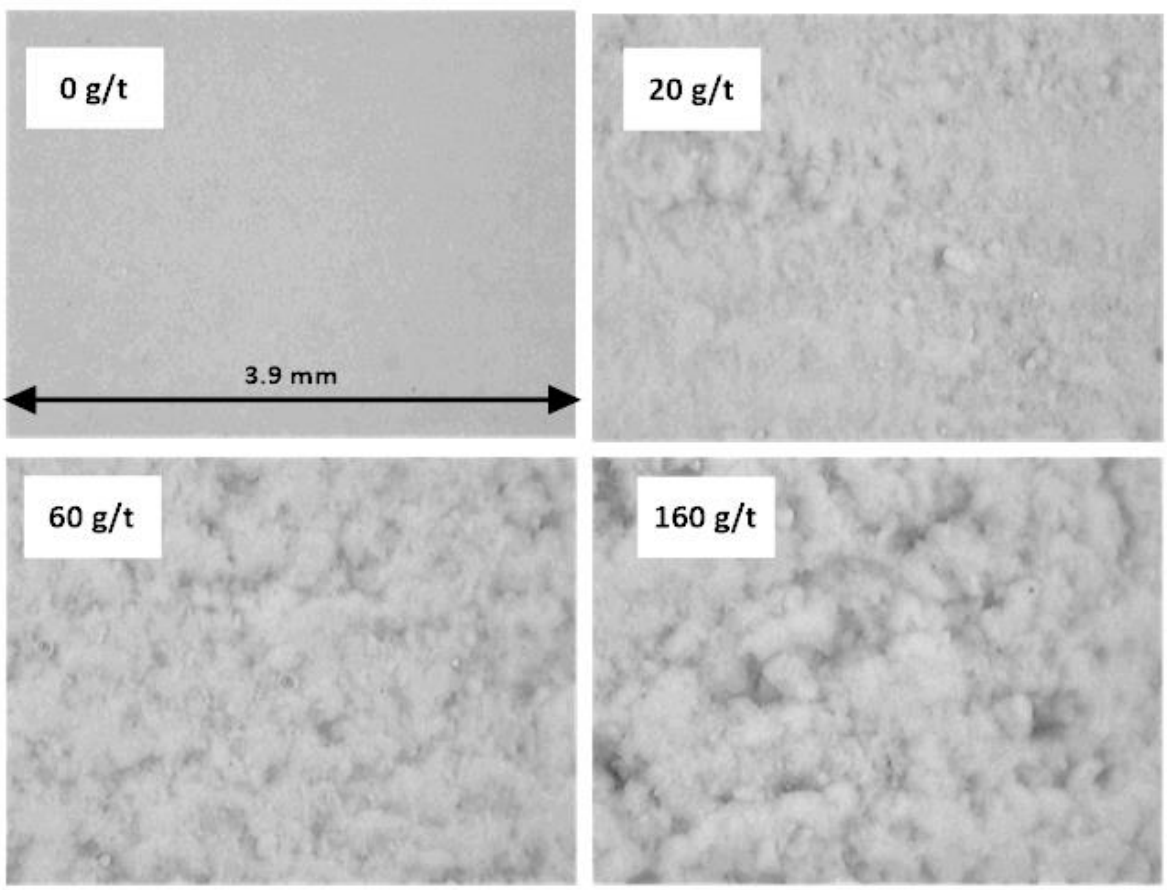

Figure 6.13 Magnified images of four 10% w/w kaolin samples after 2 hours with 0, 20, 60 and 160 g/t non-ionic polyacrylamide added.

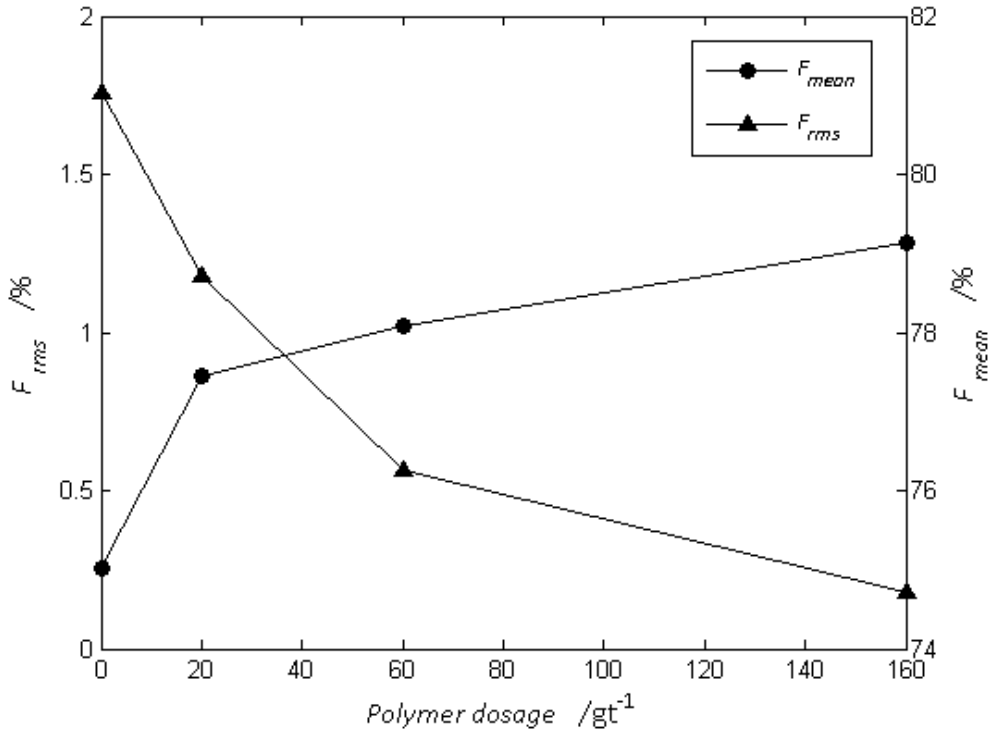

Figure 6.14 The F_{mean} and F_{rms} signal values measured after two-hour batch settling 10% w/w kaolin flocculated with nonionic polyacrylamide.

The F_{rms} and F_{mean} values exhibit trends similar to those in the measured and simulated OBS height scans of solid spheres, shown in Figure 6.2. Increased F_{mean} indicates a more densely packed sediment bed, while decreased F_{rms} indicates the sediment bed is comprised of smaller aggregates. While these size and density trends are typically observed with increasing PAM dosage, there is not always a direct relationship between polymer dose and floc size. In the present experimental setup, flocculation is induced by inverting the sample cells by hand. Although the flocculation results were not always reproducible, resulting in flocs of different sizes at a given polymer dosage, the measured optical properties of the sediments gave well defined trends when plotted as a function of floc/feature size, as described below. The hydrodynamic conditions used to generate the flocs in this study is of secondary importance.

The F_{rms} values of Trial 1, in Figure 6.15, indicate that even a 20 g/t dose led to a sediment bed composed of flocs larger than at any other dosage in Trials 2 to 4. The reproducibility of batch

settling trials was studied by Farrow and Swift by using the settling rate, or mudline descent rate, as a metric of aggregation [68]. The standard mean error of the settling rate resulting from 10 measurements by three different operators was between 12.3 and 26.2 %. It appears from the results in Figure 6.15 that flocculation, especially in small batch jars used in this thesis, is highly sensitive to solid and polymer distribution and applied shear.

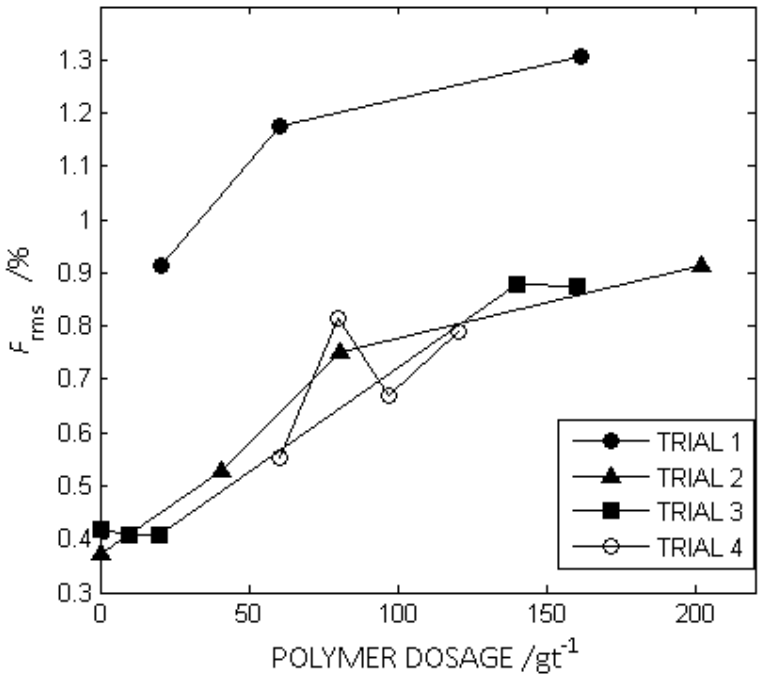

Figure 6.15 Levelled F_{rms} as a function of polymer dosage for polyacrylamide flocculated 10% w/w kaolin for four different trials.

Despite the inconsistent flocculation results, the signal interpretation method applied here is independent of the method used to induce flocculation. This observation means that this OBS approach gives results that are independent of the hydrodynamic conditions of the experiment, and the measured quantities are only a function of sediment properties. The way in which the sediment is produced is of secondary importance. As described in the following sections, the signal values investigated show a strong correlation with the result of flocculation and can be used as an indicator of aggregate size and bed density.

6.3.2.1 AGGREGATE SIZE

The F_{rms} calibration curve developed in Section 4.3 is applied to the F_{rms} results from height scans of beds of flocculated mineral sediments. The range of the F_{rms} signal values measured from flocculated mineral sediment beds is indicated in Figure 6.16 to gain an impression of the range of sizes obtained, the F_{rms} values obtained from every sample measured is converted to equivalent packing diameter and shown in Figure 6.17.

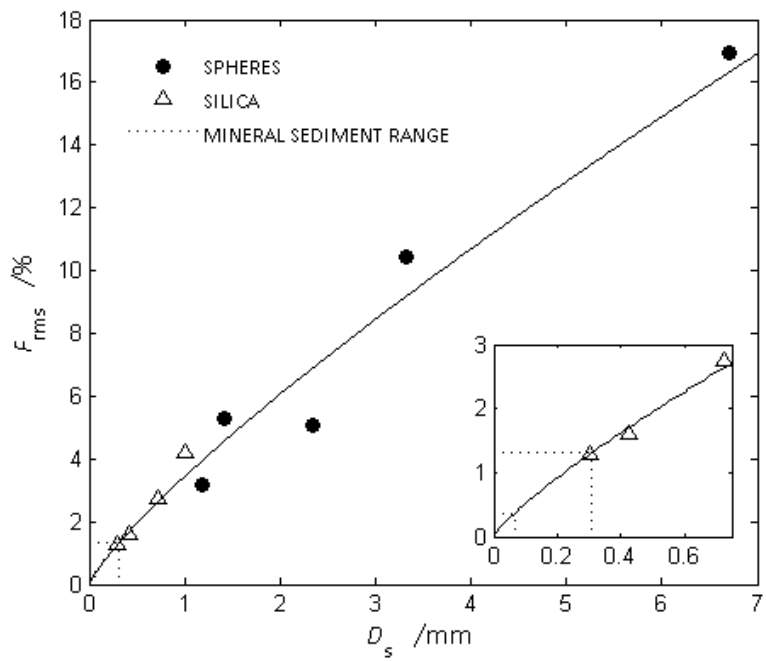

Figure 6.16 Interpretation of mineral sediment F_{rms} values with calibration line from solid sphere measurements.

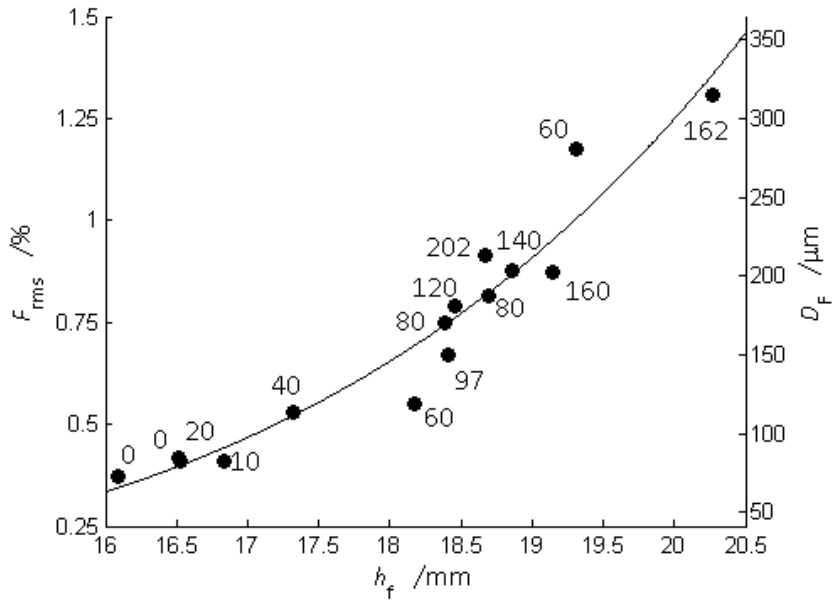

Figure 6.17 F_{rms} values converted to equivalent packing diameter, D_F, plotted against sediment bed height after two hours. The anionic polyacrylamide dose, in g/t, is indicated next to the data point.

The results in Figure 6.17 indicate that the sediment beds in this study were composed of aggregates that had an equivalent OBS diameter, D_F, in the range 66 to 309 µm. The increased aggregate diameter is strongly correlated with increased final bed height, which indicates that the lower density beds are composed of larger aggregates with a lower packing efficiency. A more detailed analysis is made by applying the calibration plot to the results of sub-sections of the ROI, as shown in Figure 6.18.

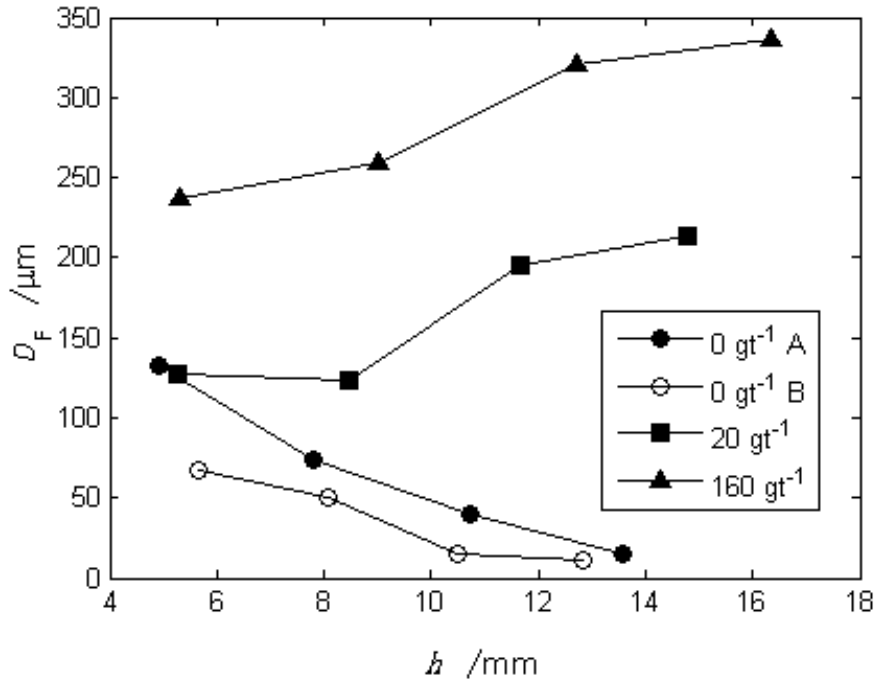

Figure 6.18 Sectional height analysis of the OBS scans of three samples of PAM flocculated kaolin. A second 0 g/t sample is added to confirm the trend of decreasing aggregate size with sample height.

The data in Figure 6.18 indicate that, for PAM flocculated samples, the aggregate diameter is increasing from the sample bottom to top. For the coagulated samples, the effective diameter is decreasing from the sample vessel bottom to the top. These trends are the result of settling behaviour, in the case of coagulated samples, and compression, in the case of flocculated samples. As shown in Section 6.3.1, the coagulated samples are much more stable, which is likely the result of a higher surface charge and interparticle repulsive force. This will lead to a more typical Stokes' Law settling behaviour, where larger aggregates will settle quicker and the smaller aggregates settle at a slower rate. In the flocculated samples, the flocs lower in the sample experience compression as a result of the mass of flocs above. As a result, the effective diameter of these flocs becomes compressed. Conversely, the flocs at the top of the sample do not experience the same compression and have a larger effective diameter

6.3.2.2 AVERAGE BED DENSITY

The final sediment bed height can be used as an indicator of relative bed density. Microscopic properties such as particle shape, particle size, and degree of flocculation are important contributors to the final sediment volume [62]. The initial mass was the same for all samples, so changes in the volume of space occupied by the sediment bed indicates a change in bed density. The signal values F_{rms} and F_{mean} which are used to derive F_{delta} also show a good correlation with bed height and are shown in Figure 6.18 and Figure 6.19. In Figure 6.20, the bed height is converted to solid volume fraction, ϕ_s by applying Equation (4.8).

The increase in F_{rms} with increased bed height in Figure 6.17 indicates that larger aggregates are produced from increased polymer dosage. A decrease in F_{mean} with increased bed height in Figure 6.19 indicates that the sediment bed is less dense.

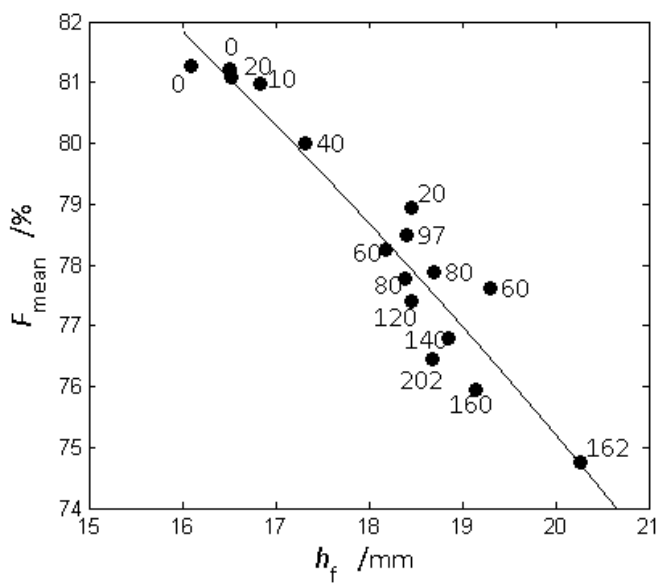

Figure 6.19 Signal value F_{mean} as a function of bed height for a series of 10% w/w kaolin samples flocculated by increasing dosage of polyacrylamide. The numbers next to the data points indicate the dosage on a g/t basis. Fit R^2 = 0.9076

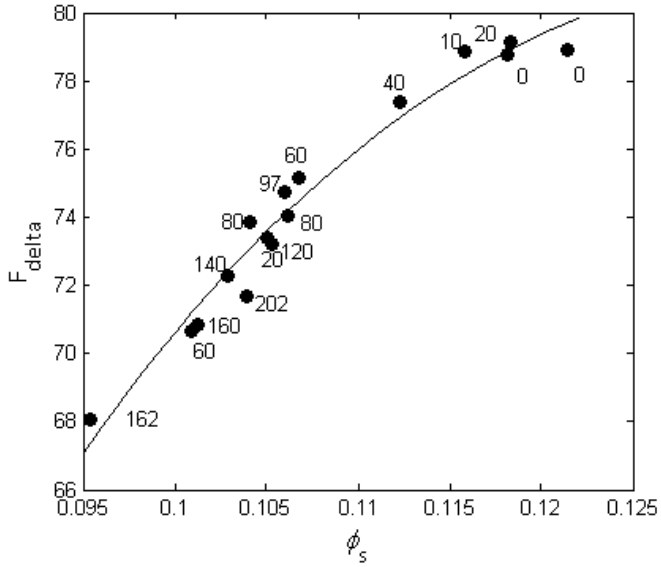

Figure 6.20 The F_{delta} signal value as a function of solid volume fraction for a series of 10% w/w kaolin samples flocculated by increasing dosage of polyacrylamide. The numbers next to the data points indicate the dosage on a g/t basis. Fit R^2 = 0.9652.

The trend lines in Figure 6.18, Figure 6.19, and Figure 6.20 are obtained by fitting an exponential function, Equation (6.2), to the data. The result of fitting Equation (6.2) to various signal value and physical property combinations is reported in Table 6.2.

$$f(x) = a \cdot \exp(bx) + c \cdot \exp(dx) \tag{6.2}$$

Table 6.2 Power fit statistics for data in Figures 6.16, 6.19 and 6.21

OBS signal value	R^2	$RMSE$
F_{rms} vs h_{f}	0.9148	0.0909
F_{mean} vs h_{f}	0.9075	0.6580
F_{delta} vs h_{f}	0.9614	0.7455
F_{delta} vs ϕ_{avg}	0.9652	0.7079

The F_{rms} and F_{mean} values have a good correlation with increased bed height with R^2 = 0.9148 and 0.9075 respectively; furthermore, conversion to the F_{delta} value gives an improved result, to R^2 = 0.9614 and rescaling the data into solid volume fraction incrementally improves the fit to R^2 = 0.9652. The conversion to solid volume fraction is based on the assumption that all of the initially suspended kaolin, 2.5 g, is deposited in the sediment bed after two hours. To validate this

assumption, the transmission % for all samples was measured and found to be > 80 % in the top 15 mm after two hours. This is a good indication that the samples were relatively free of residual suspended kaolin.

6.3.3 CALCULATED SOLID VOLUME PROFILES

The backscattering height scan data from twelve batch settling trials on kaolin flocculated by varying dosage of PAM, was used to estimate the $\phi_s(h,t)$ profiles using the iterative calibration function procedure described in Section 4.5.3. The result was used to analyse the particle scattering efficiency, plot 3D figures of the solid volume height profiles, and to calculate the effective pressure as a function of bed depth.

6.3.3.1 AGGREGATE DIAMETER EFFECTS

The purpose of this section is to explore the relationship between aggregate size and scattering efficiency predicted by Mie theory observed by De Visser [61]. Equation (4.9) predicts that larger particles have a lower scattering efficiency and smaller particles have a larger scattering efficiency. In the present study, any trend size-scattering should be observable in the calibration parameters obtained from the solid volume fitting algorithm.

De Visser calibrated an OBS sensor for particle size and suspended mass concentration. The sensor gain values were written in the expression as a function of particle diameter. OBS response in De Visser's work can be replotted in terms of particle diameter by converting the data in Figure 4.11 to an isoconcentration OBS gain versus particle diameter plot, shown in Figure 6.21.

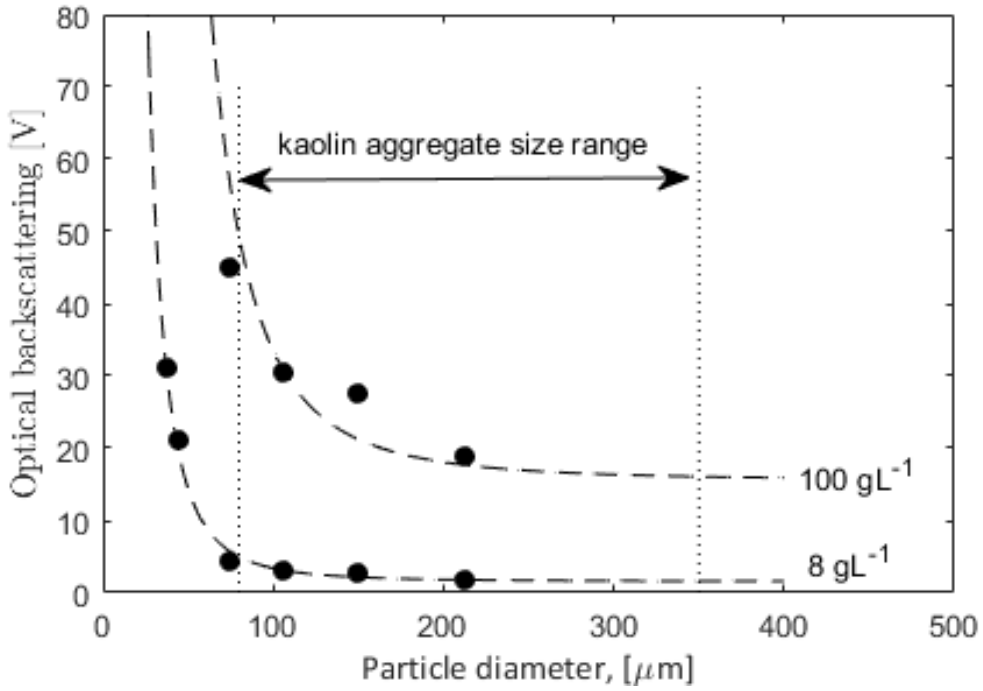

Figure 6.21 Optical backscattering gain versus particle diameter for fixed suspended sediment concentration of 8 $gL^{-1}$and 100 gL^{-1}, derived from data in De Visser [61]. The effective diameter range of the aggregates in this study is plotted.

In the batch settling experiments conducted for this thesis, aggregate diameter is not explicitly known. The impact of solid volume and aggregate size are both included in the calibration curves obtained from the calibration algorithm. In Figure 6.22 the calibration curves determined for each of the batch settling trials is shown. The increasing trend of backscattering with solid volume is observable for the entire family of curves. However, it is difficult to visually discern any trend with respect to polymer dosage. To analyse the impact of aggregate size and scattering efficiency, an isoconcentration plot was generated, shown in Figure 6.23.

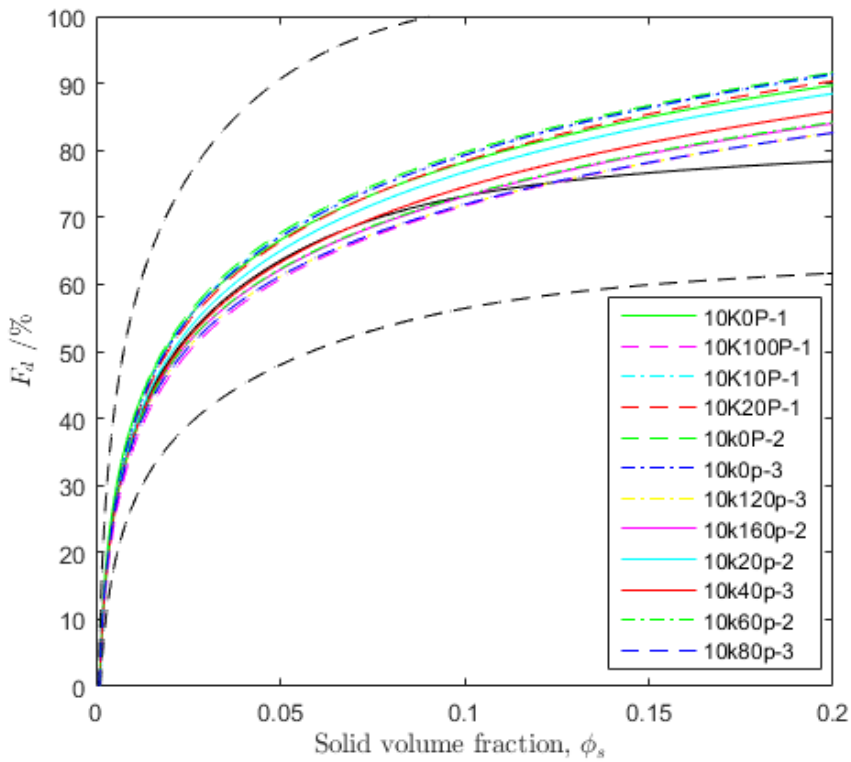

Figure 6.22 Initial exponential calibration function with upper and lower bounds plotted in black. The remaining lines are the calibration functions output from the optimizer for 12 batch settling trials. The legend symbols can be interpreted as follows, for example: 10k120p-3 indicates a 10 % w/w kaolin sample flocculated by 120 g/t PAM in Trial 3.

Each calibration curves in Figure 6.22 is evaluated at two solid volume fractions, ϕ_s = 0.04 and ϕ_s = 0.125, which are the approximate solid volume limits observed in this thesis. The final bed height for the settling experiment is used to calculate the equivalent aggregate diameter as described in Section 6.3.2.1. The isoconcentration lines, at two solid volume fractions, were then drawn on a plot of backscattering versus equivalent aggregate diameter, shown in Figure 6.23.

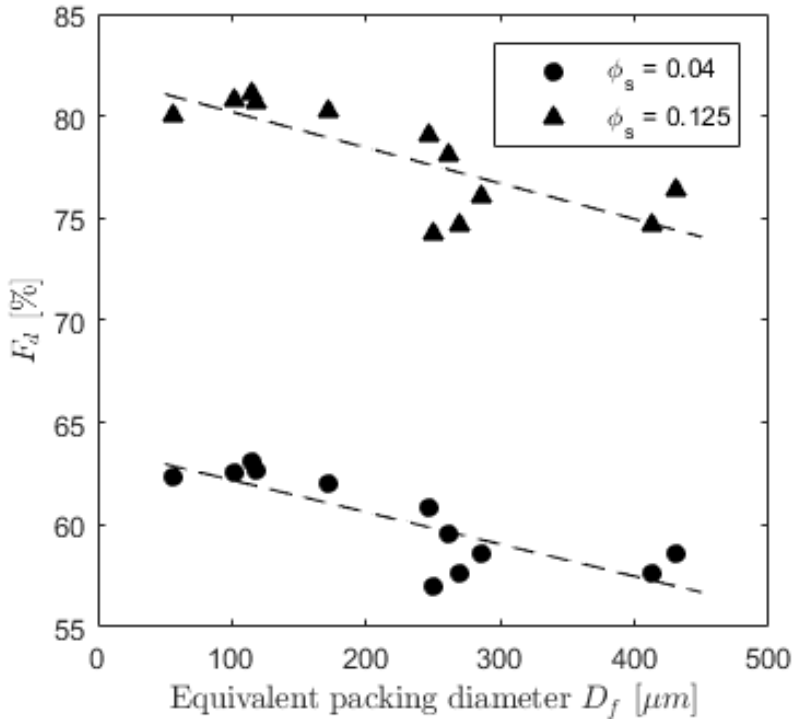

Figure 6.23 Calculated backscattering versus equivalent aggregate diameter at two different solid volume fractions.

This plot shows the effect of varying concentration and aggregate diameter on optical backscatter response in the present batch settling trials. Doubling the aggregate size from 200 to 400 μm causes a 4.5% increase in OBS, while tripling the solid volume from 0.04 to 0.125 produces an 18 % increase in OBS. This result is consistent with the observation of other researchers that, after concentration, particle size has a large impact on the OBS signal [35] [39]. Further comparison of these trends with the work of De Visser and others would be possible if the OBS % versus voltage slope used by the Turbiscan was known.

6.3.3.2 SETTLING SURFACES

In Figure 6.24, the $\phi_s(h,t)$ surface is plotted for the batch settling of a coagulated kaolin suspension, with initial solid volume, of ϕ_0 = 0.038. The top view of the surface, in the h versus t plane, is shown in Figure 6.25. This plane is simply the interface settling curve, which is typically used for analysis of batch settling experiments. The data behind these images are a potentially rich source of information about the mechanics of sediment transport in settling suspensions.

Rather than calculating the average solid concentration from the interface, it is possible to use this data to know the solid volume at any point in position or time during the settling experiment. Further work which uses this approach to interpreting OBS height scans of settling suspensions may provide a novel way to evaluate existing models of sedimentation or to estimate the parameters used in the determination of solid flux, such as the hindered settling function.

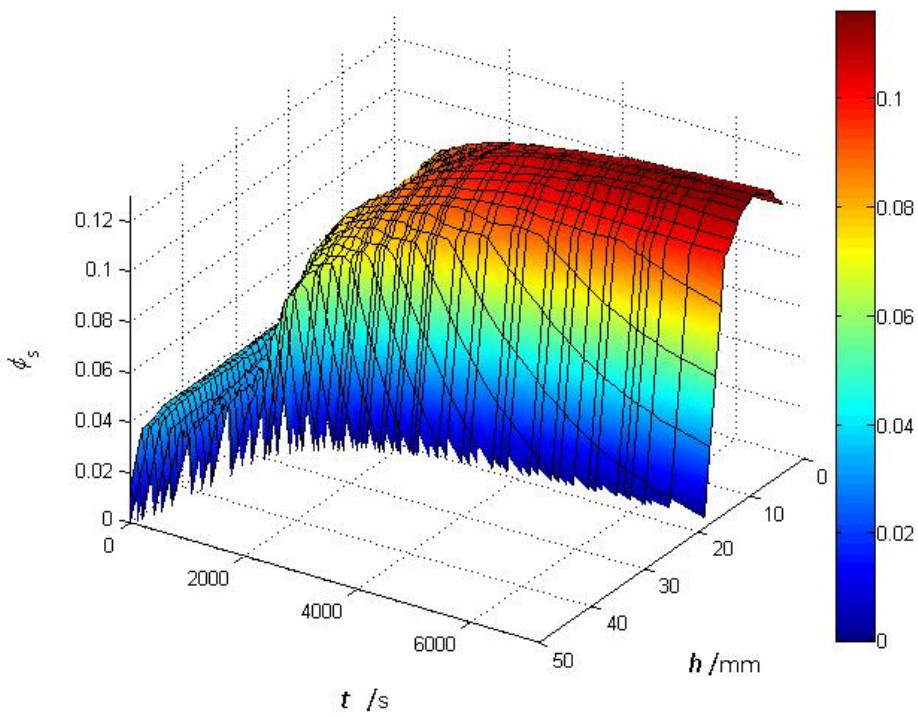

Figure 6.24. The $\phi_s(h,t)$ surface from batch settling of a coagulated kaolin suspension, initial ϕ_0 = 0.038.

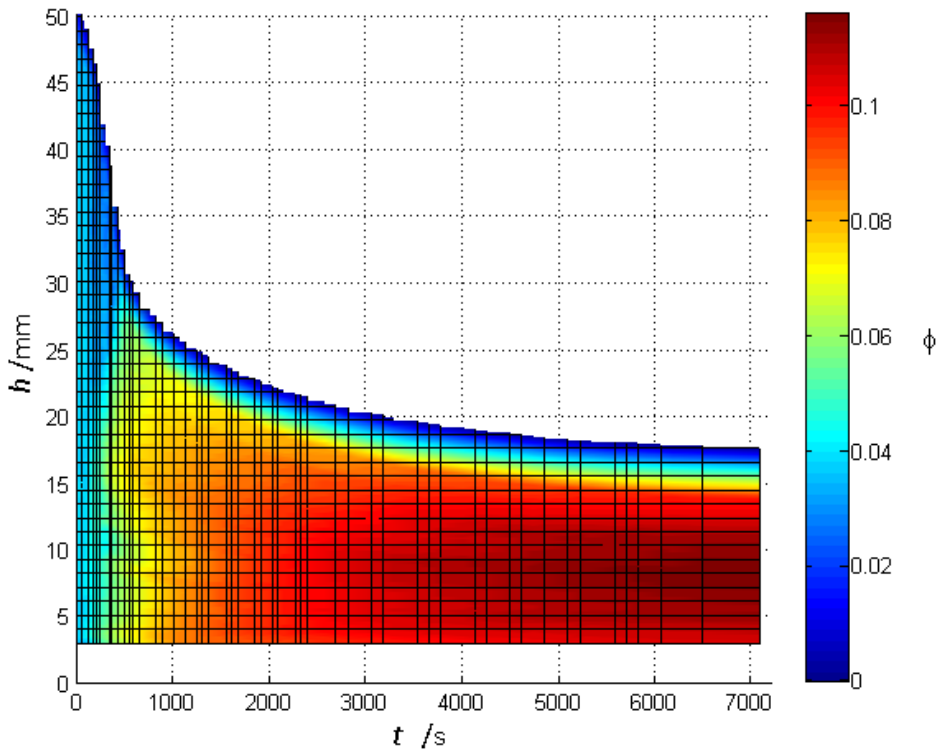

Figure 6.25 Interface settling plot from the $\phi_s(h,t)$ data of batch settling of a coagulated kaolin suspension, with initial solid volume, ϕ_0 = 0.038.

6.3.3.3 DENSITY PROFILE AT THE END OF BATCH SETTLING

The sediment bed height-density profiles of different samples, at the end of batch settling are compared. It was found that multiple scans, from different angles, were necessary to adequately observe the height-density profiles in the samples. In Figure 6.26 the sediment bed solid volume versus height profiles for one series of samples are plotted. The trend is not completely clear, although it appears that generally a lower dosage of polymer results in a higher bed density and a higher dosage results in a lower bed density. However, if multiple scans are compiled and analysed, as shown in Figure 6.27, an improvement in the height-solid volume trends are observable.

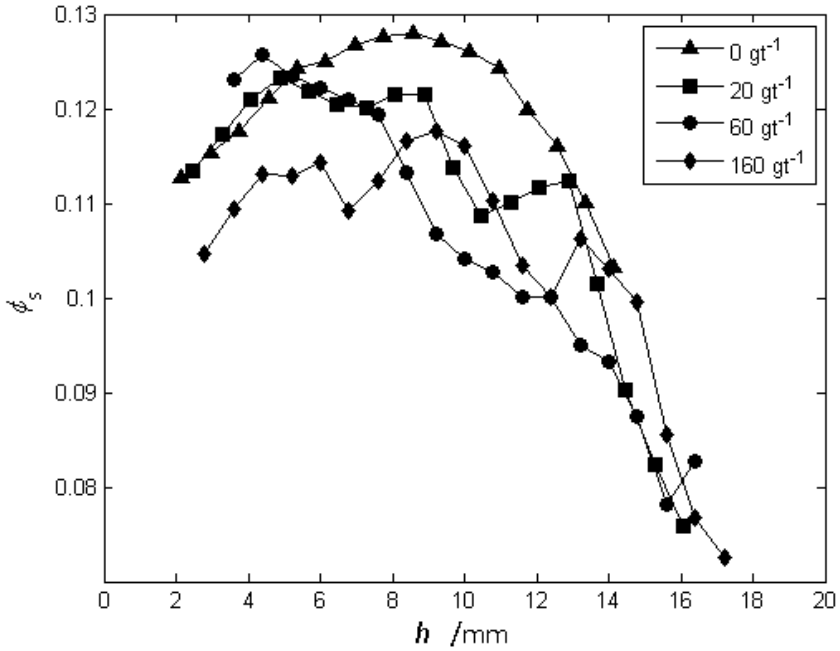

Figure 6.26. Solid volume vs height profile from calibrated OBS data.

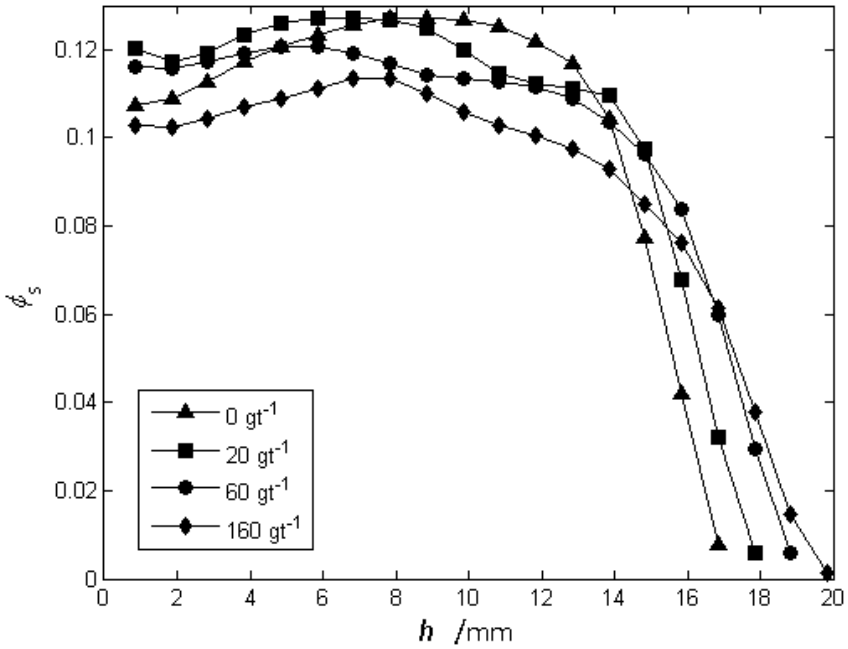

Figure 6.27 Solid Volume Height profiles evaluated from multiple scans.

7 *IN SITU* IMAGE ANALYSIS RESULTS

A series of batch settling trials of PAM flocculated kaolin were carried out and images were acquired. With reference to Figure 6.13, it is possible to visually observe trends in changing aggregate size and void space as a result of increased polymer dosage in kaolin suspensions. The objective of the *in situ* image analysis technique described here is to directly quantify these observed trends.

Figure 7.1 shows a sample image, the corresponding binary, and the white-black ratio distribution, $p_{\mathrm{w}}(r)$, of a 10 % w/w kaolin suspension flocculated with 120 g/t PAM after two hours of batch settling.

Figure 7.1 Microvideo image, binary, and corresponding white-black distribution ratio from a sample of 10% w/w kaolin flocculated with 120 g/t non-ionic polyacrylamide after two hours of batch settling

7.1 THRESHOLD DETERMINATION

The threshold level was determined according to the method discussed above and fixed at 0.675 for all images in this study. Figure 7.2 shows part of the array used to choose the threshold value. Small changes in the threshold can produce binary images which appear to overestimate or underestimate the amount of void space in the 2D plane presented to the camera. For this reason, it was important to visually inspect the effect of the threshold on the image.

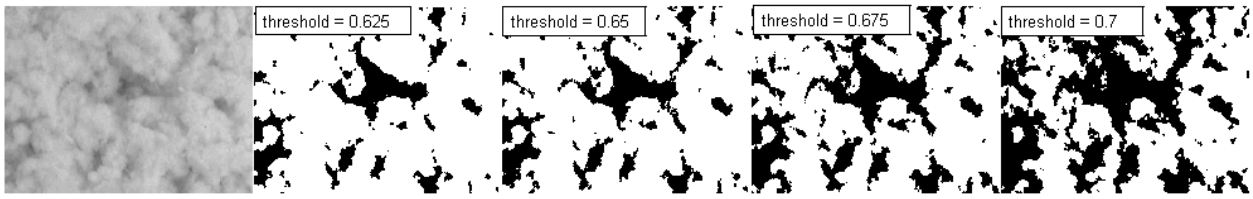

Figure 7.2 Image of PAM flocculated kaolin with four different threshold levels applied

In Figure 7.3 (B), when a threshold value of 0.725 is used, the mean of the distribution of the sample flocculated by 60 g/t is lower than the mean of the 20 g/t sample. However, this does not agree with visual inspection, which suggests that the 60 g/t flocculated sample has a looser packing and thus should have a lower white-black distribution ratio mean. In Figure 7.3 (A), the order expected from the sediment bed height measurements, 160 g/t > 60 g/t > 20 g/t > 0 g/t, is obtained. This is a useful check to perform during calibration and parameter selection to ensure the results are physically realistic.

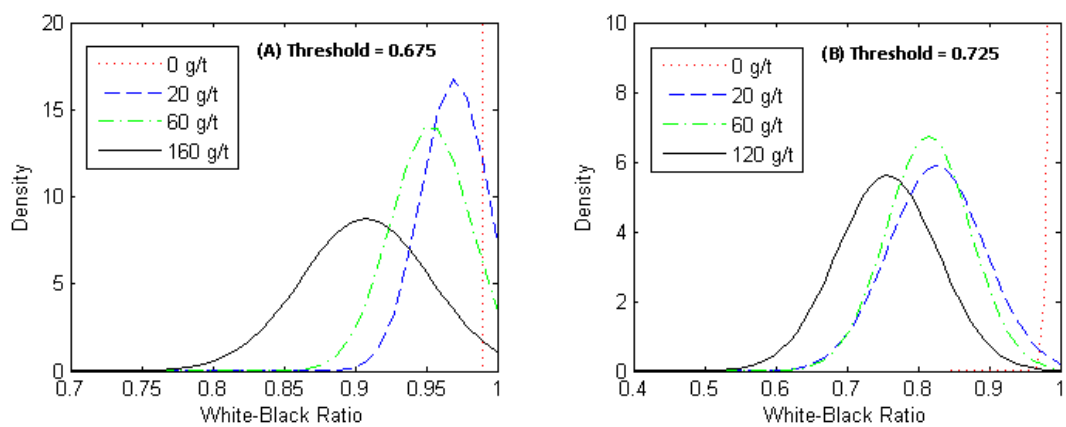

Figure 7.3 Impact of threshold level on the final white-black distribution ratios from PAM flocculated kaolin suspensions

7.2 WHITE-BLACK RATIO DISTRIBUTIONS

In Figure 7.4 (A) and (C), the mean of the white-black ratio distribution, $p_w(r)$, is given over a two-hour period for two different batch settling trials. In this study 500 chords were used to sample $p_w(r)$. After this many samples, the $p_w(r)$ mean and the pixel-based white-black ratio are approximately the same. For example, in Trial 2, shown in Figure 7.4 (C) and (D), the relative

difference between the distribution and pixel-counting values across the time series was 0.663 +/- 0.537% on a 95% confidence interval. Because the $p_w(r)$ and the pixel-based ratio are the same, the added value in the chord length ratio method is the standard deviation value. As shown in Figure 7.4 (B) and (D), the mean and standard deviation values typically counterpose one another.

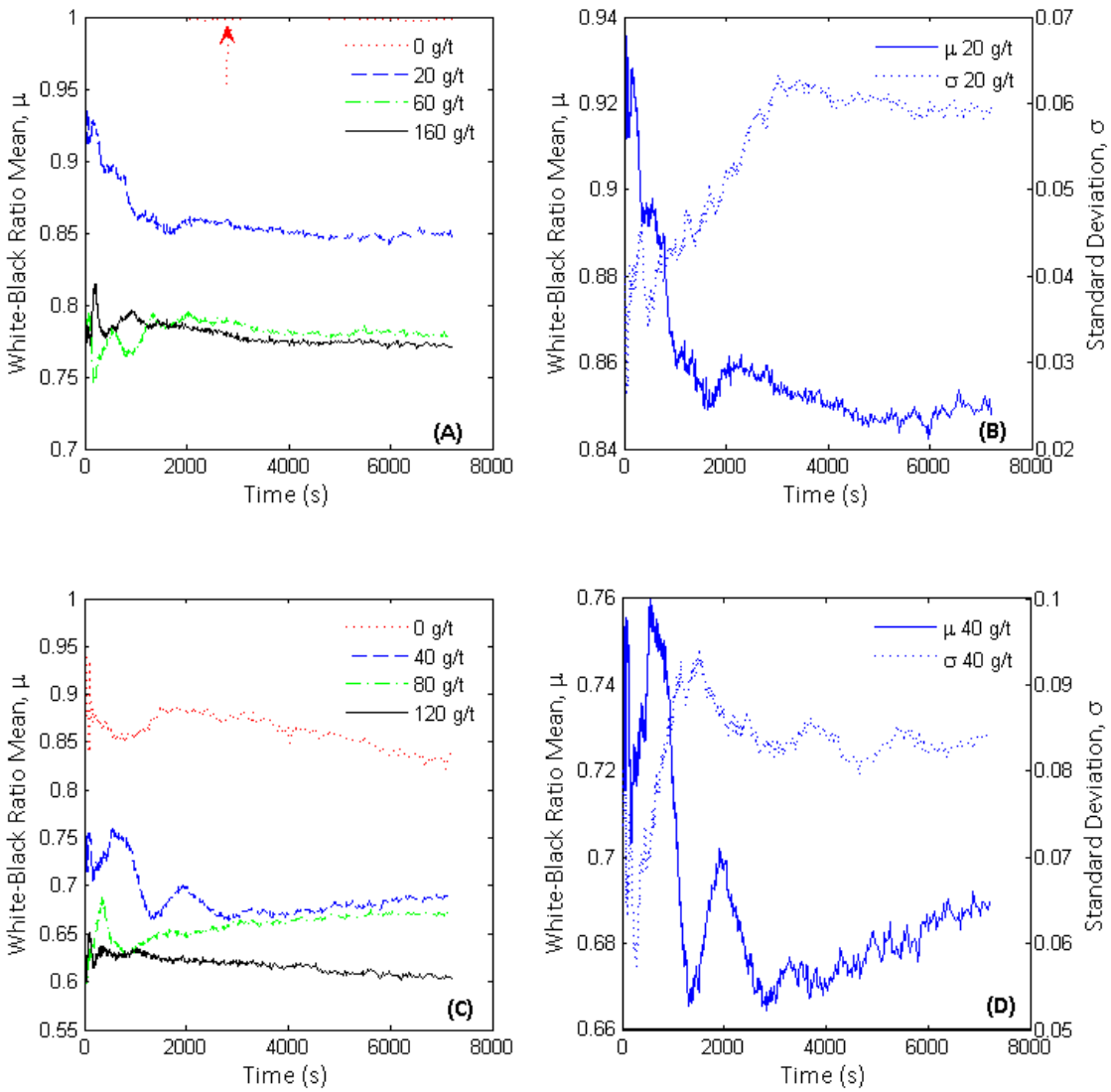

Figure 7.4 White-black distribution ratio parameters for a time series of images taken during batch settling of a kaolin suspension flocculated by varying doses of polyacrylamide in two trials, (A) and (B). The standard deviation of a single sample from each trial is plotted in (C) and (D).

The ratio of white-to-black in the binary images, calculated from the chord ratio distribution or from pixel counting, may be interpreted as an indication of the compactness of the sediment bed. Increased black space in the binary generally indicates more interaggregate void space; while more white space indicates the flocs are more densely packed. In Figure 7.4 (B) and (C), there is no clear trend in the mean value across the two trials. In fact, the size and density distribution of the aggregates as a function of height and time during batch settling is quite complicated and an immediate or direct interpretation of these signals is not expected. For example, later settling flocs may be less dense and have less material above them to cause compaction. This would cause the early decrease in the $p_{\mathrm{w}}(r)$ mean and the later increase.

A second observation is that the field-of-view captures the local flocculation result. The ingress or egress of a particularly large aggregate or collection of small aggregates will impact the $p_{\mathrm{w}}(r)$ values, as it is a measure of local conditions presented to the camera at a given time.

In Figure 7.4 (C) and (D), the mean floc-void ratio decreases while the standard deviation value increases for part of the time series. After a certain point in each experiment, the trend reverses and the standard deviation starts to decrease, but at a slower rate. Such a trend may indicate a tighter packing of flocculated aggregates. The increase in the standard deviation toward the end of the trials may indicate that larger, less dense flocs, which have settled later, are entering the field of view.

7.3 VOID CHORD LENGTH DISTRIBUTIONS

The mean of the exponential void chord distribution, μ_{v}, is plotted as a function of time for two different batch settling trials and is shown in Figure 7.5. In this study, an exponential distribution model was chosen which only has one parameter, the distribution mean. Another distribution such as the Weibull may also be a suitable model that would allow monitoring of the distribution shape, k, and scale, λ, parameters.

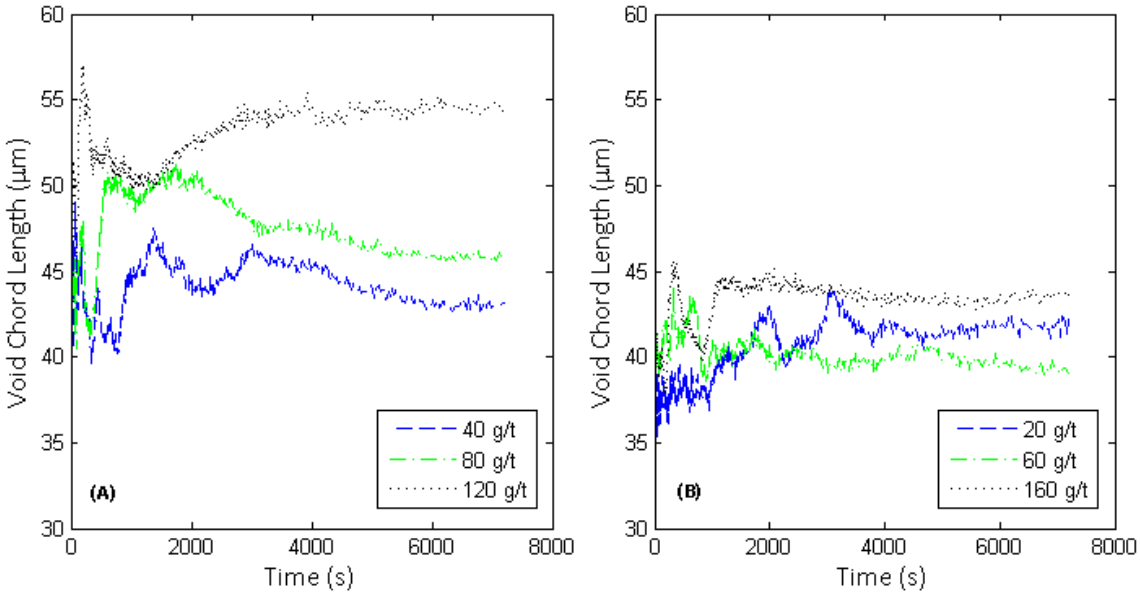

Figure 7.5 Mean of void chord distribution as a function of time measured from images of batch settling of kaolin flocculated by varying dosage of high MW, non-ionic PAM

In Figure 7.5 (A), the samples follow the "expected" flocculation trend. A higher dose of polymer results in larger aggregates and a lower bed density due to a larger amount of void space between particles. Figure 7.5 (B) does not follow the "expected" trend. The 20 g/t sample void distribution mean is above that of the 60 g/t sample. This result does not agree with visual observation or measurement of the final bed height. One cause could be that the field-of-view in camera was not large enough to capture an adequate representation of the sample.

7.4 ROTATION SERIES OF IMAGES

In Figure 7.6, the $p_{\mathrm{w}}(r)$ mean, calculated from 10 images taken from different angles and 5000 line segments, is plotted against applied polymer dosage and final sediment bed height. It was expected that such an approach would allow an improved statistical representation of the material at this specific height. Rather than using a single image, with 500 chords, this approach uses 10 images and 5000 lines to sample $p_{\mathrm{w}}(r)$.

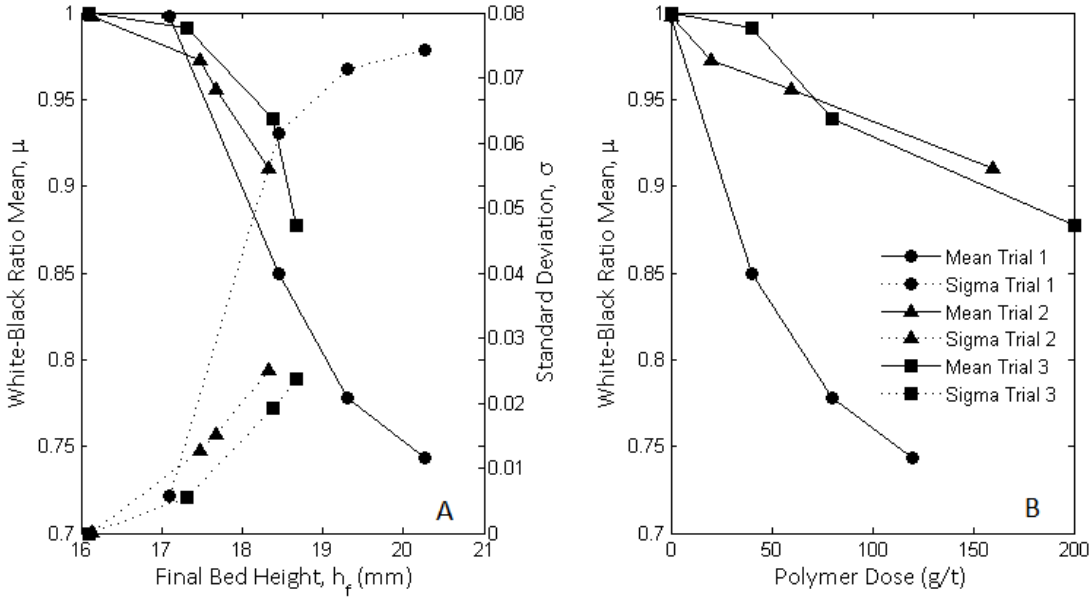

Figure 7.6 White-black ratio distribution mean, μ, and scale parameter, s, as a function of: (A) final bed height; and (B) polymer dosage, at the end of the two-hour batch settling period for three different kaolin flocculation trials.

When the initial solid volume is the same, final sediment bed height can be compared among samples as a relative measure of bed density and flocculation extent. Based on this correlation, the trend in the mean $p_{\mathrm{w}}(r)$ in Figure 7.6 (A) indicates that samples are composed of larger flocs with more interaggregate space when the final bed height is higher. The white-black distribution mean is higher and the standard deviation is lower when the final sediment bed height is lower.

Although the polymer dose applied can be controlled relatively well, flocculation is also dependent on the applied shear and distribution of polymer within the sample. These changes to hydrodynamic conditions may produce different aggregate sizes, flocculation extents, and consequently settling rates [68] [1]. For this reason, the trend in Figure 7.6 (A), with white-black ratio plotted against final bed height, is much clearer than Figure 7.6 (B), where the white-to-black distribution mean is plotted against applied polymer dosage. This correlation between, μ, σ, and final sediment bed height indicate that this method could provide a useful measure of flocculation extent or relative aggregate size if a statistically representative surface area is used to calculate $p_{\mathrm{w}}(r)$.

Plotting the monitored signal value against a sediment property, such as bed height or density, and the data follows a good trend. This indicates that the signal value developed can be used to monitor the result of flocculation and is independent of the hydrodynamic conditions used to generate the aggregates.

7.5 STANDARD DEVIATION ANALYSIS

The white-to-black ratios, shown in Figure 7.6 have a mean that is directly comparable to the value obtained by taking the simple pixel-based black to white ratio, as summarized in Table 7.1.

Table 7.1 Comparison of white-to-black ratio (floc-to-void ratio) from the entire image and from chords

$Trial$	$Dose\ [g/t]$	$Pixel\ WB\ Ratio$	$CLD\ WB\ Ratio\ Mean$	$CLD\ WB\ Ratio\ Sigma$
A	0	0.973	0.974	0.029
A	20	0.861	0.861	0.071
A	60	0.844	0.832	0.078
A	160	0.823	0.812	0.084
B	0	0.983	0.981	0.005
B	40	0.929	0.935	0.028
B	80	0.801	0.796	0.052
B	200	0.732	0.716	0.064

The standard deviation, or sigma, of black-to-white ratio distributions can give some idea of the spatial structure of the aggregated material in the sample. The pixel-based calculation is simply a measurement of the ratio of black-to-white space in the image, and cannot adequately represent the void space in the material, as indicated in Figure 7.7.

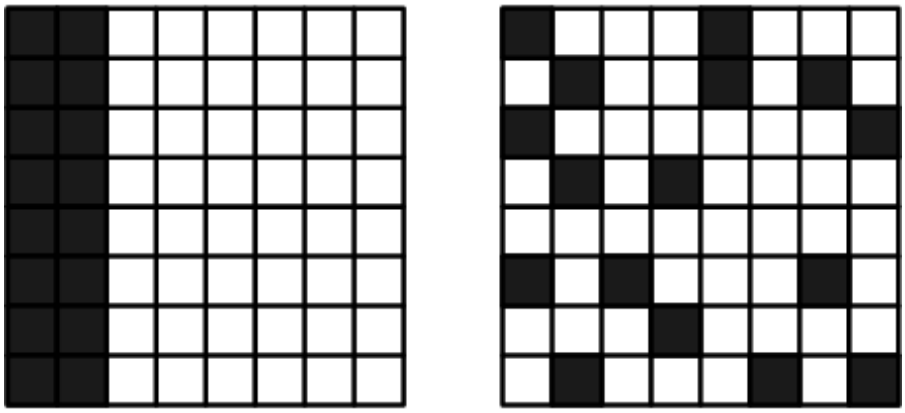

Figure 7.7 Two images with a 25% void space. The white-to-black ratios of these images would both be 0.75, however such a calculation loses information about the spatial arrangement of the phases within the material.

The use of a chord length approach to calculating black to white ratios retains some measure of the material connectivity and spatial arrangement. An increasing white-to-black ratio is an indication of a denser packing of aggregates, as the amount of black, or void space, in the sample decreases. Conversely, a larger amount of void space indicates a looser sediment bed packing.

8 CONCLUSIONS

The primary motivation of this thesis was to develop optical backscattering (OBS) and image analysis methods which can be used to analyse aggregate size and bed density *in situ*, with no disturbance to the material. Throughout this thesis, the relationship between the result of flocculation and signals from OBS and image analysis was developed. Despite the inconsistent flocculation results, the OBS and image analysis signal interpretation methods applied here are independent of the method used to induce flocculation. When the signal values are plotted as a function of a sediment property, such as aggregate size or sediment bed height, a strong correlation between the signal value and sediment property is observed. This means that the optical methods applied here are independent of the hydrodynamic conditions of the experiment, and the measured quantities are only a function of sediment features and properties. The way in which the sediment is produced is of secondary importance.

The correlation between calculated OBS signal values, F_{rms}, F_{mean} and F_{delta}, and the underlying material state were explored through the measurement of OBS from solid spheres and mineral sediments, and modelled with computer simulation. Two types of OBS signal calibration, an aggregate size calibration method and an iterative solid volume profile calibration method, were employed to extract information from optical backscattering measured during batch settling experiments.

The relationship between aggregate size and F_{rms} was developed by measuring and calculating OBS height scans from model spheres. It was found that an increasing F_{rms} value is strongly correlated with increased particle size. An effective diameter, called the 'equivalent scattering diameter', D_F was proposed to relate the scattering from solid spheres to that from flocculated minerals. Direct application of the OBS size calibration method to other flocculated systems may be possible but the impact of refractive index should be considered carefully. Whether or not a diameter calibration curve is available, F_{rms}, F_{mean} and F_{delta}, all show good correlations with

particle size. Each signal value could be used as an indicator of a change in the aggregation state or as an index of flocculation.

An iterative calibration algorithm was used to convert OBS as a function of height and time, $F(h,t)$, to solid volume as a function of height and time, $\phi_s(h,t)$. This enabled the settling surface to be plotted, which possibly contains a wealth of information about the settling behaviour of these flocculated mineral suspensions. Analysis of the calibration function parameters agree with the Mie theory prediction of decreased scattering efficiency with increasing aggregate size. The generally reported trend that, after concentration, particle size has the biggest impact on OBS response was also observed in this thesis. Further comparison of the results is difficult, because the Turbiscan measures % OBS and transmission, but the actual voltage response of the sensor is not known. The application of the solid volume profiles to calculate effective pressure profiles appears to give good results. However, similarity in the calculated and measured values is not necessarily an indication of the accuracy of the measurement. The calibrated $\phi_s(h)$ functions and P_s (h) do not include 'wall' effects, which could have a significant impact the actual pressure profile in the sample vessel.

The *in situ* image analysis carried out for this thesis showed two measures of interaggregate space that can be obtained by applying chord length distributions to images of flocculated minerals. The approach is statistical, based on sampling the probability density functions, but it also retains a physically meaningful representation of the material. Interpretation of changes in the white-to-black ratio is intuitive and comparison with final sediment bed height showed that it can be used as a relative measure of flocculation. However, the significance of changes in the standard deviation of the white-black ratio distributions over time has not been fully explained. The relationship between lighting conditions and corresponding threshold values required should be clarified to develop a more reliable parameter selection method for the image processing algorithm. Another consideration to be made is the relationship between aggregate size and the field of view size necessary to adequately sample the material.

The methods developed in the course of this thesis form a good basis for future research in the area of solid-liquid separation, with a focus on measurement and modelling of material structure and transport properties. In the next section, a research idea based on this thesis is outlined.

RECOMMENDATIONS

Further development of OBS and image analysis techniques developed in this thesis could include installation of OBS measurement and image acquisition equipment on a larger scale batch settling or pilot thickening device. Such an installation would allow a more detailed analysis of batch settling experiments to be carried out as a direct study of gravity separation and as part of a more detailed characterization of the rheological properties of suspensions. It should be emphasized that such an installation would form part of a more comprehensive settling and thickening instrument which could be used in a number of fundamental and applied studies of flocculation, sedimentation, and thickening.

Here is a list of several considerations for a larger scale installation of an OBS height scan instrument:

1. It is necessary to test the methods developed in this thesis further to study the limitations of refractive index and solid volume in the Turbiscan.
2. The $\phi_s(h)$ for a given sample should be verified by an independent measurement, such as computed tomography (CT) scans of the samples.
3. The process to be monitored should be capable of highly reproducible flocculation and settling. This requires careful attention to the hydrodynamic conditions throughout the device, such as feed introduction, flocculant dosing, applied shear, and vessel shape.
4. Auxiliary equipment such as vacuum filtration or compression apparatus would allow complete rheological characterization and extraction of parameters relevant to operation, design and sizing of solid-liquid separation equipment.
5. A 'dynamic' batch settling device, with shear from a rake or paddle, should be considered to be consistent with modern batch settling techniques.
6. Installation of multiple OBS laser-sensor pairs should be considered as this will significantly improve the estimates of $\phi_s(h,\mathrm{t})$, $P_s(h,\mathrm{t})$ and any other parameters derived from the acquired signal.

9 REFERENCES

[1] K. A. Landman and L. R. White, “Solid/liquid separation of flocculated suspensions,” *Adv. Colloid Interface Sci.*, vol. 51, pp. 175–246, 1994.

[2] P. A. Vanrolleghem, J. De Clercq, B. De Clercq, M. Devisscher, D. J. Kinnear, and I. Nopens, “New Measurement Techniques for Secondary Settlers: A Review,” *Water Sci. Technol.*, vol. 53, pp. 419–429, 2006.

[3] F. Concha, “A Century of Research in Sedimentation and Thickening,” *Kona*, vol. 20, no. 20, pp. 38–70, 2002.

[4] M. A. Yukselen and J. Gregory, “The reversibility of floc breakage,” *Int. J. Miner. Process.*, vol. 73, pp. 251–259, 2004.

[5] A. Blanco, E. Fuente, C. Negro, and J. Tijero, “Flocculation Monitoring: Focused Beam Reflectance Measurement as a Measurement Tool,” *Can. J. Chem. Eng.*, vol. 80, no. August, pp. 1–7, 2002.

[6] A. T. Owen, P. D. Fawell, J. D. Swift, D. M. Labbett, F. A. Benn, and J. B. Farrow, “Using turbulent pipe flow to study the factors affecting polymer-bridging flocculation of mineral systems,” *Int. J. Miner. Process.*, vol. 87, no. 3–4, pp. 90–99, Jul. 2008.

[7] Y. Matsui and N. Tambo, “On-ine floc size evaluation by Photometric Dispersion Analyzer,” *Water Supply*, vol. 8, pp. 71–78, 1991.

[8] J. Gregory and D. W. Nelson, “Monitoring of aggregates in flowing suspensions,” *Colloids and Surfaces*, vol. 18, pp. 175–188, 1986.

[9] M. S. Żbik, Y.-F. Song, R. L. Frost, and C.-C. Wang, “Transmission X-ray Microscopy—A New Tool in Clay Mineral Floccules Characterization,” *Minerals*, vol. 2, no. 4, pp. 283–299, Oct. 2012.

[10] J. Du, R. A. Pushkarova, and R. S. C. Smart, “A cryo-SEM study of aggregate and floc structure changes during clay settling and raking processes,” *Int. J. Miner. Process.*, vol. 93, no. 1, pp. 66–72, 2009.

[11] T. N. Hunter, L. Darlison, J. Peakall, and S. Biggs, “Using a multi-frequency acoustic backscatter system as an in situ high concentration dispersion monitor,” *Chem. Eng. Sci.*, vol. 80, pp. 409–418, 2012.

[12] G. J. Kynch, “A theory of sedimentation,” *J. Chem. Soc. Faraday Trans.*, vol. 48, pp. 166–176, 1952.

[13] R. Buscall and L. R. White, “The consolidation of concentrated suspensions,” *J. Chem. Soc. Faraday Trans. 1*, vol. 83, pp. 873–891, 1987.

[14] H. S. Chung and R. Hogg, “Stability criteria for fine-particle dispersions,” *Colloids and Surfaces*, vol. 15, pp. 119–135, Jan. 1985.

[15] C. Rattanakawin and R. Hogg, “Aggregate size distributions in flocculation,” *Colloids Surfaces A Physicochem. Eng. Asp.*, vol. 177, no. 2–3, pp. 87–98, Feb. 2001.

[16] M. S. Nasser and A. E. James, “Effect of polyacrylamide polymers on floc size and rheological behaviour of kaolinite suspensions,” *Colloids Surfaces A Physicochem. Eng. Asp.*, vol. 301, pp. 311–322, 2007.

[17] B. A. Bolto, “Soluble Polymers in Water Purification,” *Prog. Polym. Sci.*, vol. 20, pp. 987–1041, 1995.

[18] L. Nabzar, E. Pefferkorn, and R. Varoqui, “Poiyacrylamide-Sodium Kaolinite Interactions : Flocculation Behavior of Polymer Clay Suspensions,” vol. 102, no. 2, 1984.

[19] M. S. Nasser and A. E. James, “Settling and sediment bed behaviour of kaolinite in aqueous media,” *Sep. Purif. Technol.*, vol. 51, no. December 2005, pp. 10–17, 2006.

[20] S. Bárány, R. Meszaros, L. Marcinova, and J. Skvarla, “Effect of polyelectrolyte mixtures on the electrokinetic potential and kinetics of flocculation of clay mineral particles,” *Colloids Surfaces A Physicochem. Eng. Asp.*, vol. 383, no. 1–3, pp. 48–55, Jun. 2011.

[21] W. P. Talmage and E. B. Fitch, “Determining thickener unit areas,” *J. Ind. Eng. Chem*, vol. 47, pp. 38–41, 1955.

[22] R. Spehar, A. Kiviti-Manor, P. Fawell, S. P. Usher, M. Rudman, and P. J. Scales, “Aggregate densification in the thickening of flocculated suspensions in an un-networked bed,” *Chem. Eng. Sci.*, vol. 122, pp. 585–595, 2015.

[23] R. Bürger and A. Narváez, “Steady-state, control, and capacity calculations for flocculated suspensions in clarifier-thickeners,” *Int. J. Miner. Process.*, vol. 84, pp. 274–298, 2007.

[24] R. G. De Kretser, S. P. Usher, P. J. Scales, D. V. Boger, and K. a. Landman, “Rapid filtration measurement of dewatering design and optimization parameters,” *AIChE J.*, vol. 47, no. 8, pp. 1758–1769, 2001.

[25] G. V. Franks and Y. Zhou, “Relationship between aggregate and sediment bed properties: Influence of inter-particle adhesion,” *Adv. Powder Technol.*, vol. 21, no. 4, pp. 362–373, 2010.

[26] F. Concha, N. N. Rulyov, and J. S. Laskowski, “Settling velocities of particulate systems 18: Solid flux density determination by ultra-flocculation,” *Int. J. Miner. Process.*, vol. 104, pp. 53–57, 2012.

[27] F. Concha, D. Sbarbaro, A. Pereria, J. P. Segovia, and S. Vergara, “On-line instruments for measuring thickening parameters in industrial thickeners,” in *International Mineral Processing Congress*, 2014, pp. 170–188.

[28] B. B. G. van Deventer, S. P. Usher, A. Kumar, M. Rudman, and P. J. Scales, “Aggregate densification and batch settling,” *Chem. Eng. J.*, vol. 171, no. 1, pp. 141–151, 2011.

[29] J. Gregory, “Monitoring particle aggregation processes.,” *Adv. Colloid Interface Sci.*, vol. 147–148, pp. 109–23, 2009.

[30] L. Liang, Y. Peng, J. Tan, and G. Xie, “A review of the modern characterization techniques for flocs in mineral processing,” *Miner. Eng.*, vol. 84, pp. 130–144, 2015.

[31] M. Lunven, P. Gentien, K. Kononen, E. Le Gall, and M. M. Daniélou, “In situ video and diffraction analysis of marine particles,” *Estuar. Coast. Shelf Sci.*, vol. 57, pp. 1127–1137, 2003.

[32] S. J. Peng and R. A. Williams, “Direct measurement of floc breakage in flowing suspensions,” *J. Colloid Interface Sci.*, vol. 166, pp. 321–332, 1994.

[33] O. S. Agimelen, A. Jawor-Baczynska, J. McGinty, C. Tachtatzis, J. Dziewierz, I. Haley, J. Sefcik, and A. J. Mulholland, “Integration of in situ Imaging and Chord Length Distribution Measurements for Estimation of Particle Size and Shape,” 2015.

[34] E. J. W. Wynn, “Relationship between particle-size and chord-length distributions in focused beam reflectance measurement: Stability of direct inversion and weighting,” *Powder Technol.*, vol. 133, pp. 125–133, 2003.

[35] J. Downing, “Twenty-five years with OBS sensors: The good, the bad, and the ugly,” *Cont. Shelf Res.*, vol. 26, no. 17–18, pp. 2299–2318, Nov. 2006.

[36] J. A. C. Bunt, P. Larcombe, and C. F. Jago, “Quantifying the response of optical backscatter devices and transmissometers to variations in suspended particulate matter,” *Cont. Shelf Res.*, vol. 19, no. 9, pp. 1199–1220, Jul. 1999.

[37] R. W. Spinrad and H. Pak, “Volume scattering function of suspended particulate matter at,” vol. 17, no. 7, pp. 1125–1130, 1978.

[38] H. C. Van de Hulst, “Light Scattering by Small Particles,” New York: Dover, 1981, p. 470.

[39] T. F. Sutherland, P. M. Lane, C. L. Amos, and J. Downing, “The calibration of optical backscatter sensors for suspended sediment of varying darkness levels,” *Mar. Geol.*, vol. 162, no. 2–4, pp. 587–597, Jan. 2000.

[40] G. C. Bushell, Y. D. Yan, D. Woodfield, and J. Raper, “On techniques for the measurement of the mass fractal dimension of aggregates,” *Adv. Colloid Interface Sci.*, 2002.

[41] C. Aldrich, C. Marais, B. J. Shean, and J. J. Cilliers, “Online monitoring and control of froth flotation systems with machine vision : A review,” *Int. J. Miner. Process.*, vol. 96, no. 1–4, pp. 1–13, 2010.

[42] G. Bonifazi, S. Serranti, F. Volpe, and R. Zuco, “Characterisation of flotation froth colour and structure by machine vision,” vol. 27, pp. 1111–1117, 2001.

[43] M. Kistner, G. T. Jemwa, and C. Aldrich, “Monitoring of mineral processing systems by using textural image analysis,” *Miner. Eng.*, vol. 52, pp. 169–177, 2013.

[44] M. Hurst, M. Weber-shirk, P. Charles, and L. W. Lion, “Apparatus for Observation and Analysis of Floc Blanket Formation and Performance,” vol. 140, no. January, pp. 11–20, 2014.

[45] A. Keyvani and K. Strom, “A fully-automated image processing technique to improve measurement of suspended particles and flocs by removing out-of-focus objects,” *Comput. Geosci.*, vol. 52, pp. 189–198, 2013.

[46] R. K. Chakraborti, K. H. Gardner, J. F. Atkinson, and J. E. Van Benschoten, “Changes in fractal dimension during aggregation,” *Water Res.*, vol. 37, pp. 873–883, 2003.

[47] J. P. M. Syvitski and E. W. H. Hutton, “Floc : Image Analysis of Marine Suspended Particles,” *Comput. Geosci.*, vol. 23, no. 9, pp. 967–974, 1997.

[48] D. H. Li and J. J. Ganczarczyk, “Stroboscopic determination of settling velocity, size and porosity of activated sludge flocs,” *Water Res.*, vol. 21, no. 3, pp. 257–262, 1987.

[49] F. Maggi, A. J. Manning, and J. C. Winterwerp, “Image separation and geometric characterisation of mud flocs,” *J. Hydrol.*, vol. 326, pp. 325–348, 2006.

[50] D. Nobbs, P. Tang, and J. A. Raper, “The design , construction and commissioning of a low-cost optical particle size analyser specifically for measurement of settling velocities and size of flocs,” *Meas. Sci. Technol.*, vol. 13, pp. 297–302, 2002.

[51] K. Malysa, S. Ng, J. Czarnecki, and J. H. Masliyah, “A method of visualization and characterization of aggregate flow inside a separation vessel, Part 2. Composition of the

bitumen-air aggregates," *Int. J. Miner. Process.*, vol. 55, pp. 189–202, 1999.
[52] C. Oliveira, R. T. Rodrigues, and J. Rubio, "A new technique for characterizing aerated flocs in a flocculation- microbubble flotation system," *Int. J. Miner. Process.*, vol. 96, no. 1–4, pp. 36–44, 2010.
[53] F. Concha, "Amira International P996," 2012.
[54] P. D. Thorne and D. Hurther, "An overview on the use of backscattered sound for measuring suspended particle size and concentration profiles in non-cohesive inorganic sediment transport studies," *Cont. Shelf Res.*, vol. 73, pp. 97–118, 2014.
[55] D. J. W. Wu, "Dynamic online monitoring of fine coal dewatering performance," The University of Queensland, 1999.
[56] O. Mengual, G. Meunier, I. Cayré, K. Puech, and P. Snabre, "TURBISCAN MA 2000: Multiple light scattering measurement for concentrated emulsion and suspension instability analysis," *Talanta*, vol. 50, no. 1999, pp. 445–456, 1999.
[57] S. . Koppal, "Lambertian Reflectance," in *Computer Vision: A Reference Guide*, I. Katsushi, Ed. Boston, MA, 2014, pp. 441–443.
[58] T. Rosendaal, A. Babahin, A. Kuznetsov, A. Nussbaumer, A. Riakiotakis, and A. Montagne, "Blender." Blender Foundation, Amsterdam, 2015.
[59] C. F. Bohren and D. R. Huffman, "Adsorption and Scattering of Light by Small Particles," Wiley-VCH Verlag GmbH, 2007, pp. 82–83.
[60] R. J. Gibbs and E. Wolanski, "The effect of flocs on optical backscattering measurements of suspended material concentration," *Mar. Geol.*, vol. 107, pp. 289–291, 1992.
[61] C. S. Conner and A. M. De Visser, "A laboratory investigation of particle size effects on an optical backscatterance sensor," *Mar. Geol.*, vol. 108, pp. 151–159, 1992.
[62] F. M. Tiller and Z. Khatib, "The theory of sediment volumes of compressible, particulate structures," *J. Colloid Interface Sci.*, vol. 100, no. 1, pp. 55–67, 1984.
[63] S. Torquato, "Chord-length distribution functions for many-body systems," vol. 98, no. April, 1993.
[64] G. E. Mueller, "Numerically packing spheres in cylinders," *Powder Technol.*, vol. 159, pp. 105–110, 2005.
[65] F. A. L. Dulien, *Porous Media. Fluid Transport and Pore Structure.*, 2nd ed. Academic Press Inc., 1992.
[66] R. Hogg and R. Klimpel, "Evaluation of floc structures," *Colloids and Surfaces*, vol. 55, p. 279, 1991.
[67] P. Hill, "Models for effective density and settling velocity of flocs Models pour la densité effective et la vitesse de sédimentation de flocs," *J. Hydraul. Res.*, vol. 44, no. 3, pp. 390–401, 2006.
[68] J. B. Farrow and J. D. Swift, "A new procedure for assessing the performance of flocculants," *Int. J. Miner. Process.*, vol. 46, pp. 263–275, 1996.
[69] S. Atkinson, F. H. Stillinger, and S. Torquato, "Detailed Characterization of Ratterles in Exactly Isostatic, Strictly Jammed Sphere Packings," *Phys. Rev. E - Stat. Nonlinear, Soft Matter Phys.*, vol. 88, no. 062208, 2013.
[70] J. Kilander, S. Blomström, and a. Rasmuson, "Spatial and temporal evolution of floc size

distribution in a stirred square tank investigated using PIV and image analysis," *Chem. Eng. Sci.*, vol. 61, pp. 7651–7667, 2006.

APPENDICES

APPENDIX A. CHORD LENGTH DISTRIBUTION RATIOS

A chord length distribution, (z), is obtained by laying random lines over a binary black and white image and determining where the lines intersect each of two phases, as explained in Section 5.1. The length of a section within a phase is the chord length. After a suitable number of samples, the mean and standard deviation of the chord length distribution is expected to converge on a specific value.

A MATLAB script was written to calculate white-to-black chord length ratio distributions based on measurement of binary images. In Figure A.1, an example of chord length measurement on a binary image of a flocculated kaolin sample is shown.

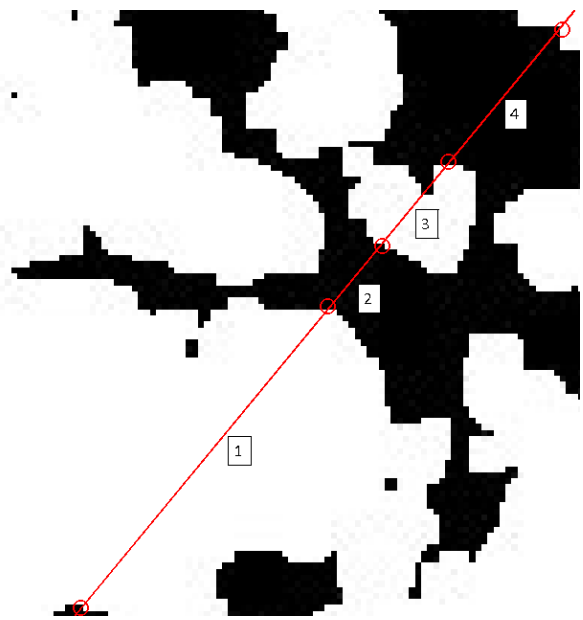

Figure A.1 Chord length measurement on sub-section of a binary image of kaolin flocculated by 100 g/t anionic polyacrylamide.

The ratio of occupied-to-unoccupied space on each line segment is calculated by dividing the number of white pixels by the total pixels. In Figure A.1, a line cast over the image results in line segments intersecting different phases of the material. Line segments 1 and 3 intersect the

aggregated material while segments 2 and 4 intersect void space. The lengths and corresponding white-black ratio can be calculated by using the points of intersection. For example, the line segments in Figure A.1 are defined by the following points in format ([X1,X2],[Y1,Y2]):

$S1$ = ([18,59],[100,50]); $S2$ = ([59,68],[50,40]); $S3$ = ([68,79],[40,26]); $S4$ = ([79,98],[26,4]).

The total line length is 124.99 and the line segment lengths, in pixels, are: $\overline{S1}$ = 64.66, $\overline{S2}$ = 13.45, $\overline{S3}$ = 17.80, $\overline{S4}$ = 29.07. The white-to-black ratio is calculated as the sum of chords intersecting white space, S1 and S3, divided by the total line length. In this example, the ratio is 0.66.

This process is repeated for each line segment overlaid on the image, then for each of 10 images taken from different angles. The resulting distribution of white-to-black ratios are plotted as a frequency histogram and also converted to a probability density function. Representation as a density function allows a better visualization of the white-black ratio probability trends across the samples analysed. The mean and standard deviation of these distributions can be calculated and analysed to observe trends in the sample as a result of increasing dosage of polymer applied or as a function of time during a batch settling experiment.

APPENDIX B. MODELLED CHORD LENGTH DISTRIBUTION RATIOS

METHOD

The physical significance of using white-to-black chord ratios to analyse 2D sections of packed sediment beds is further considered through the use of simulated 2D images of randomly close packed spheres. The sphere coordinates of randomly close packed spheres are imported and horizontal planes are inserted in the structure, as shown in Figure B.1.

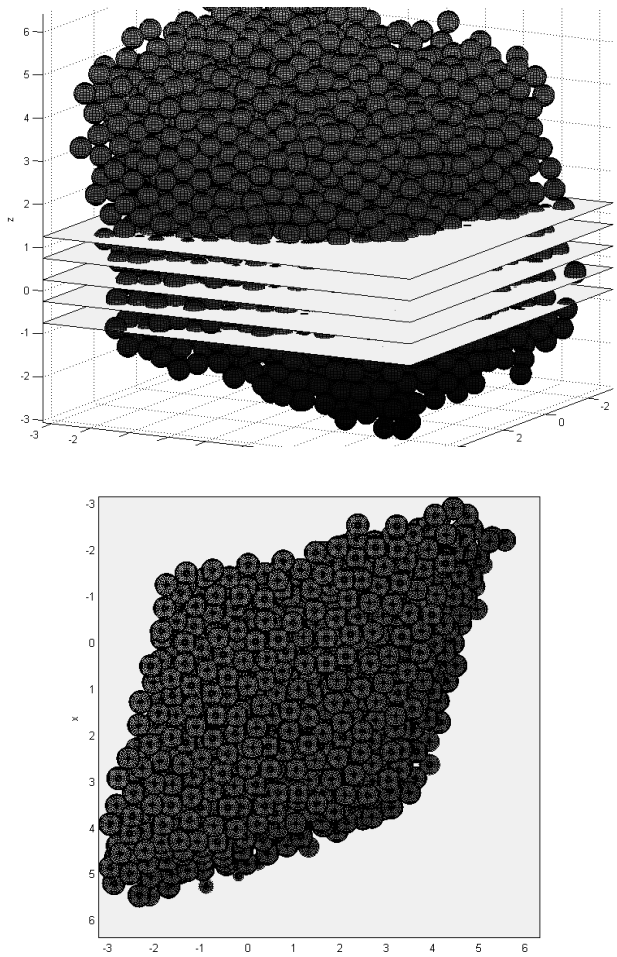

Figure B.1 Orthogonal and top view of a packing structure of 2000 randomly close packed spheres at a 0.6031 packing fraction.

The circle of intersection for each sphere and plane is determined. This allows 2D plots of the intersecting circles on the planes to be generated. A fixed size region of interest is extracted from the centre of the plane and converted to an image file for further processing, as shown in Figure B.2. The ratio of occupied to unoccupied area in each 2D image is examined through the use of chord length distributions. A varying range of sphere sizes are analysed using the chord length distribution approach and the results are used to discuss the trends observed in images of flocculated mineral sediments.

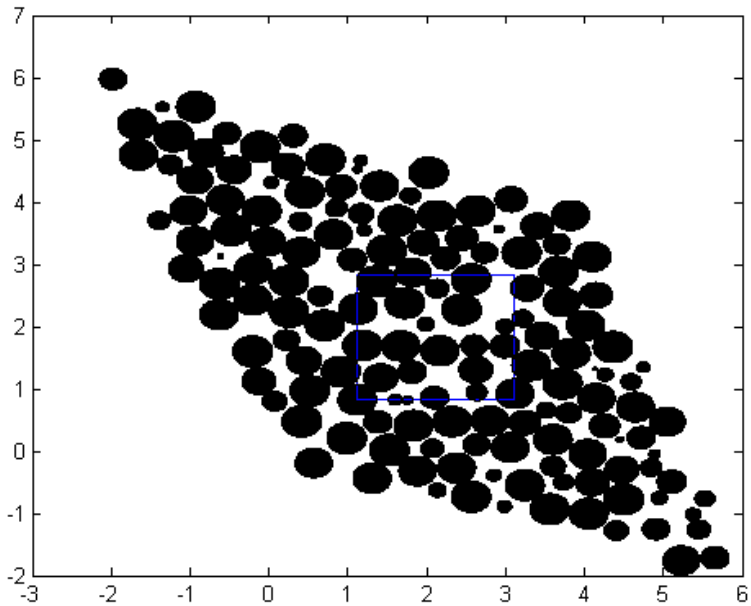

Figure B.2 2D image of the circles of intersection of randomly close packed spheres with a horizontal plane. A region of interest, which is used to generate an image, is indicated by the blue square.

RESULTS

The physical significance of using white-to-black chord ratios to analyse 2D sections of packed sediment beds is further considered through the use of simulated 2D images of randomly close packed spheres. The chord length distribution method described in Section 5.1 is applied to ideal spheres in a randomly close packed arrangement. In Figure B.3, the result of increasing sphere size on the chord length white-black ratio is shown.

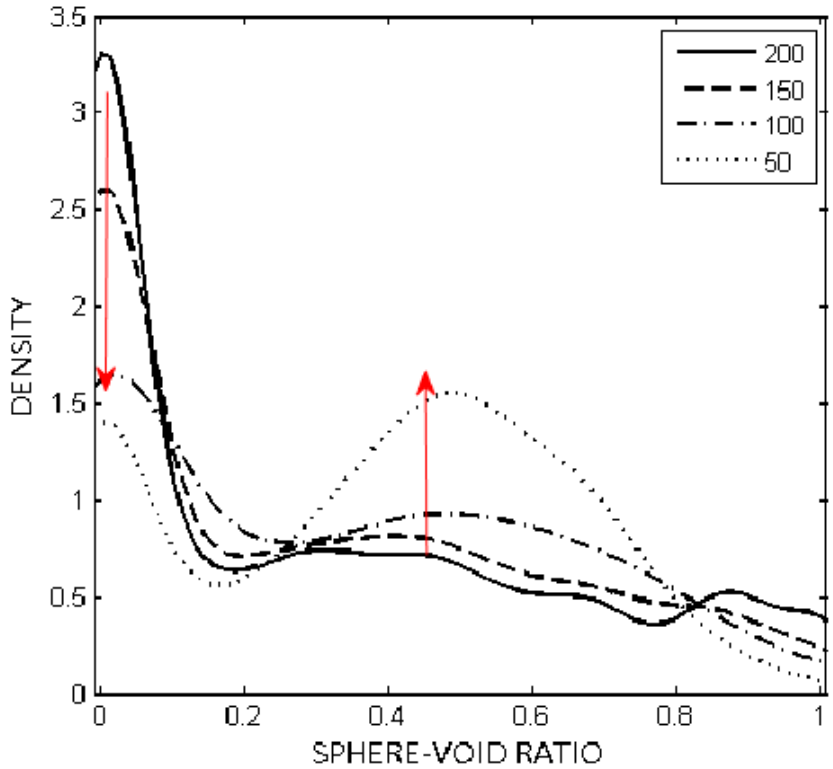

Figure B.3 Sphere-void ratio from chord length distributions of spheres of varying size. Red arrows indicate the trend in low and medium sphere-void ratio as sphere diameter decreases.

For ideal spheres, the distribution of white-to-black line segments is bivariate and does not follow a normal or logistic distribution like segments from images of flocculated aggregates. Nonetheless, a non-parametric fit is applied for visualization purposes in Figure B.3. As indicated with red arrows in Figure B.3, there is a decrease in the low sphere-void ratio peak and an increase in the high sphere-void ratio peak as the sphere size decreases. This indicates a trend toward an increased ratio of occupied space in the 2D images.

APPENDIX C. SOLID PARTICLE BACKSCATTERING DATA

Figure C.1 Grinding media of various sizes in Turbiscan sample cylinders. Samples 'F' and 'G' not shown.

Table C.1 Size data for grinding media in Figure C.1

$Sample$	$Diameter\ [mm]$	D_c/D_s
A	-3.33/ 2.35	8.5
B	-3.33/ 2.35	8.5
C	-3.33/ 2.35	8.5
D	-2.35/ 1.41	14.2
E	-1.41/1.18	16.95
F	-1.18	20
G	-6.7/ 4.76	4.2

Table C.2 Signal values F_{rms} and F_{mean} as a function of diameter for spherical ceramic grinding media

$Diameter\ [mm]$	$F_{\mathrm{rms}}\ [\%]$	$F_{\mathrm{rms}}\ [\%]$
-1.18/1	78.4	3.18
-1.41/1.18	73.1	5.43
-2.35/ 1.41	85.05	5.06
-3.33/ +2.35	73.49	10.19
-6.7/ 4.76	73.59	17.61

Table C.3 Results for height-volume calibration of Turbiscan sample cylinder

$M_{water}[g]$	$V_{water}\ [cm^3]$	$Height\ [mm]$
3.0179	3.03	6.9
5.0163	5.03	10.9
7.1288	7.15	15.14
9.0116	9.04	18.94
10.0136	10.04	20.94
12.0223	12.06	24.98
15.0178	15.06	31.02
17.0463	17.10	35.1
19.0225	19.08	39.06
21.0236	21.09	43.1
23.0047	23.07	47.06
25.0186	25.09	51.02

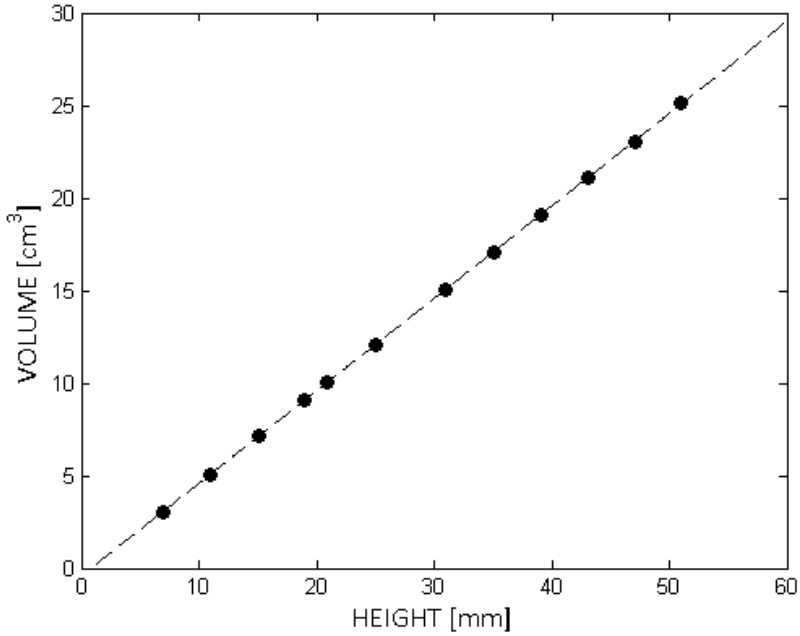

Figure C.2 Volume-height relationship for increasing quantity of water in a Turbiscan sample vial.

The data in Table C.1 and Figure C.2 are fitted with a linear equation, with $R^2 = 1$, a = 0.4993 and b = -0.4173. These parameters are used for the conversion of sediment bed height to solid volume fraction.

Table C.4 Mean radial porosity, ε_m, for cylinder to sphere diameter ratio D_c/D_s .

D_c/D_s	ε_m	D_s [mm]
20.3	0.393	0.99
14.1	0.395	1.42
7.99	0.431	2.50
5.96	0.451	3.36
5.6	0.453	3.57
3.96	0.476	5.05

APPENDIX D. CALCULATED OPTICAL BACKSCATTERING HEIGHT SCANS

Sphere coordinates of spheres packed in an FCC arrangement were generated in MATLAB, then imported to Blender. The sphere coordinates for randomly close packed (RCP) unit cells were obtained from Torquato et. al. [69], then scaled as necessary to get the appropriate sphere diameter in global coordinates and exported to a custom text file. Next, the sphere coordinates of the packing structure are imported to Blender, a 3D modeling software [58], using the ATOMIC BLENDER plugin. The spheres are positioned flush with the XZ plane which acts as a "cuvette wall." A light source and camera are positioned in an arrangement which is physically similar to the Turbiscan. Images of the model are then rendered at 40 μm intervals over the height of the structure. The internal rendering engine of Blender, was used to calculate the images. Further discussion of the algorithms behind the computation of reflectance functions and their subsequent sampling is outside the scope of this thesis. The calculated images are then imported to MATLAB and integrated to get a calculated light flux. The raw counts are arbitrary units, and are sensitive to distance of the light from the spheres, light intensity, image resolution, and many other parameters. In this way, the height series of 2D images become a 1D image, with the integrated light intensity of each image representing a single pixel in the 1D image. To mimic the rotation of the sample vials, used in the measured scans to sample a new section, a simple importance sampling technique is chosen to maximize the expected variation in optical backscattering. A new part of the packing structure is scanned by offsetting the light source and camera in fractional diameter increments.

Refer to D.3, where the measurement 'x-scan' indicates the amount of offset applied in a given OBS height scan. The reported F_{rms} and F_{delta} values are obtained by calculating the OBS height scan at three different positions: 'x_scan' = 0; 'x_scan' = $\frac{1}{3}D_{s;}$ and 'x_scan' = $\frac{2}{3}D_s$; where D_s is the sphere diameter.

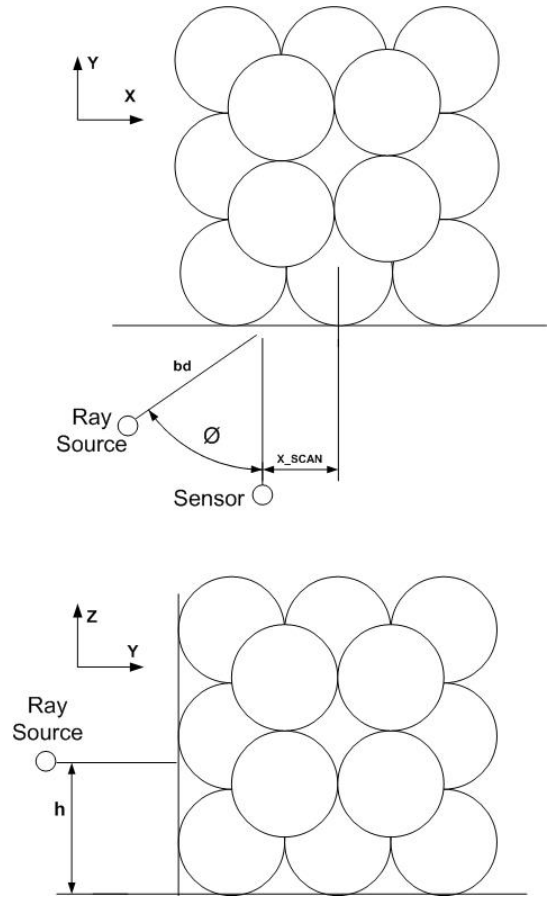

Figure D.3 Schematic of face centred cubic packing structure calculated optical backscattering height scan arrangement.

APPENDIX E. CALCULATED SOLID VOLUME PROFILES

Table E.1 Fit parameters for data modelled with power functions.

Figure	Dataset	R2	RMSE	a	b	c	d
4.12	RMS vs bed height	0.9148	0.0909	-1.56E+01	0.1822	1.56E+01	0.1825
4.13	MEAN vs bed height	0.9075	0.6580	2.14E+05	0.0177	-2.14E+05	0.0177
4.14	SCALED SUM vs bed height	0.9614	0.7455	6.47E+04	0.0454	-6.46E+04	0.0454
4.15	SCALED SUM vs solid volume fraction	0.9652	0.7079	6.44E+05	-11.4300	-6.44E+05	-11.4300

RELATIVE ERROR IN FITTED SOLID VOLUME PROFILES

In most cases, the optimization program found parameters that produced low relative error in the total solid volume value across the entire time series of scans. As shown Figure E.1, several trials produced upward of 15% relative error in the first scan. The solid volume as a function of time is shown Figure E.1 for the two trials with the largest relative error.

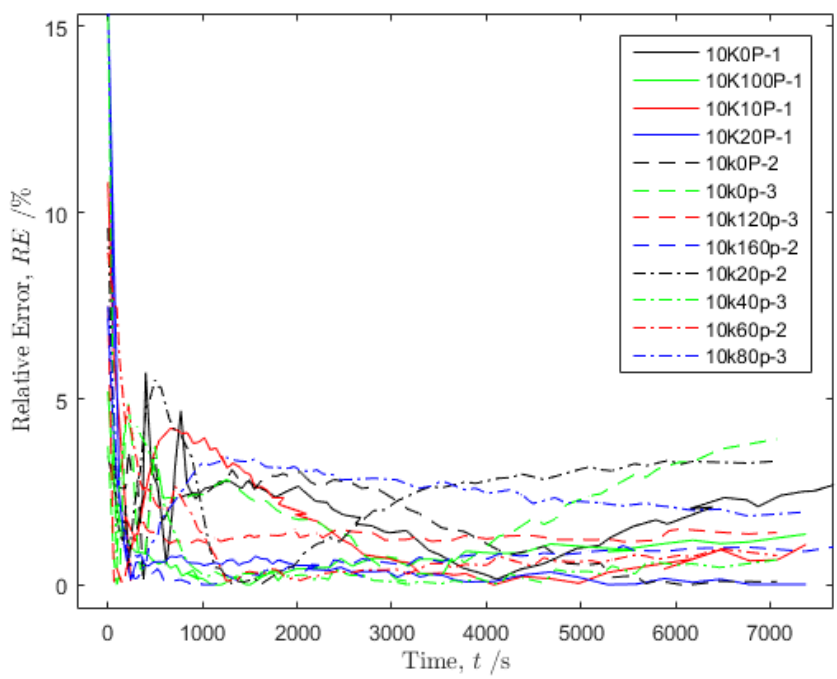

Figure E.1 Relative error as a function of time for total calculated solid volume during batch settling of flocculated kaolin.

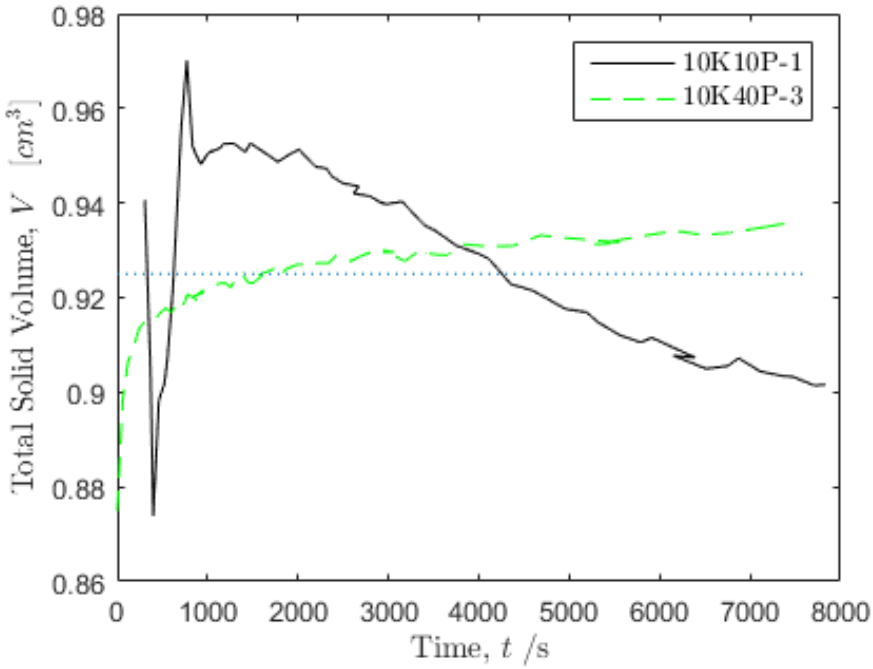

Figure E.2 Total solid volume as a function of time for two batch settling trials of PAM flocculated kaolin. The line at 0.925 cm^3 indicates the approximate total solid volume for all trials.

In the slower settling samples, there is a higher error in the early stages of batch settling whereas the higher dosage of PAM produced more rapid settling and a more consistently low relative error over the course of the batch settling experiment.

APPENDIX F. CALCULATED EFFECTIVE PRESSURE PROFILES

METHOD

To demonstrate an application of the calculated $\phi_s(h,t)$, data, the effective pressure as a function of depth is calculated. Effective pressure $P_s(L)$ can be calculated from the equilibrium condition for the effective pressure gradient continuity equation [62],

$$\frac{\partial P_s}{\partial x} = (\rho_s - \rho) g \phi_s - \frac{\mu(1-\phi_s)}{K}(\mu - \mu_s), \tag{F.1}$$

where $\partial P_s/\partial x$ equals the buoyed weight of the solids, $(\rho_s - \rho) g \phi_s$, minus the upward drag of the liquid, where K is the permeability, and $(\mu - \mu_s)$ is the difference in the relative velocities of the solid and liquid. At equilibrium, the relative velocity term is 0, so the effective pressure as a function of depth becomes,

$$P_s = (\rho_s - \rho) g \int_0^L \phi_s(x) dx \tag{F.2}$$

where L is depth from the top of the sediment. To get an idea of the error in this measurement, the calculated effective pressure at the bottom of the sediment beds is compared to expected effective pressure, based on the known mass of the sample in the sediment bed,

$$P_{\text{tot}} = \frac{m_{\text{k}}(\rho_s - \rho) g}{A_c} \tag{F.3}$$

where A_c is the area of the sample container and m_k is the initial mass of kaolin in the suspension.

RESULTS

The effective pressure as a function of depth, $P_s(h)$, is calculated from the $\phi s(h)$ data obtained in the previous section. $P_s(h)$ is plotted for several samples in Figure F.1 using Equation (F.2). The samples should attain the same effective pressure at the bottom of the sample because they all have the same total solid volume, which is calculated using Equation (F.3). The error in the

maximum effective pressure is directly related to the error in the calibration of the $\phi_s(h)$ function from optical scattering data.

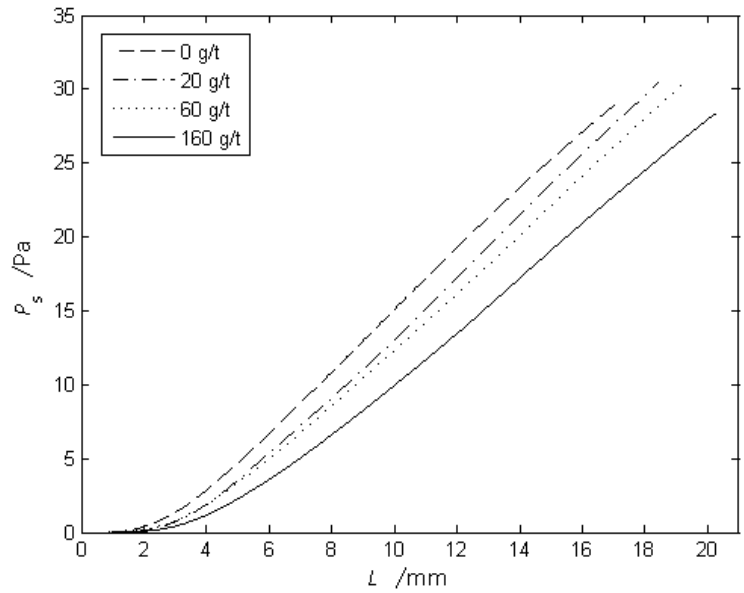

Figure F.1 Effective pressure as a function of depth from final sediment bed height, L, calculated from solid volume height profiles, $\phi_s(h)$, from optical backscattering data.

In Table F.1, the calculated effective pressure at the bottom of the sediment beds is compared to expected effective pressure, based on the known mass of the sample in the sediment bed,

$$P_{\text{tot}} = \frac{m_{\text{k}}(\rho_s - \rho)g}{A} \tag{0.4}$$

where A is the area of the sample container and m_{k} is the initial mass of kaolin in the suspension. The error in solid volume calculations by evaluating the calculated total solid volume from Equation (4.13) is also given.

Table F.1 Effective pressure and calculated total solid volume from optical backscattering calibration data

Polymer Dose [g/t]	Calculated P_s [Pa]	Fitted P_s [Pa]	RE [%]	Calculated V_s [cm^3]	Fitted V_s [cm^3]	RE [%]	+/- 0.95 CI
0	29.45	29.00	1.51	0.925	0.871	5.85	+/- 1.51
20	29.48	30.40	3.15	0.924	0.927	6.18	+/- 4.13
60	29.71	30.47	2.58	0.931	0.924	3.32	+/- 2.16
160	29.53	28.32	4.10	0.925	0.859	8.33	+/- 4.13

APPENDIX G. SEDIMENTATION IMAGE ANALYIS

Sedimentation image analysis was carried out to measure the size of flocs obtained during batch settling experiments. After data acquisition of OBS and *in situ* high resolution images a small amount of flocculated material is removed from the sample cylinder to carry out size analysis with sedimentation image analysis. This method uses a high magnification camera to obtain images of individual flocs as they are freely falling through a cylinder of liquid.

METHOD

A large calibre syringe fitted with a short piece of PTFE is used to carefully remove small amounts of aggregated material from the sample cylinder and to introduce them to a 250 mL graduated cylinder filled with distilled water. Microvideo is recorded at 15 frames per second until 200 images are obtained. The sample is allowed to settle, then another series of 200 images are recorded. This is repeated 4-5 times to obtain a representative sample for further processing. A high frame rate is required to capture a sufficient number of fast moving, 'in-focus' flocs.

The images are processed using a combination of ImageJ and MATLAB with an approach described by Keyvani et. al. [45], as shown in Figure G.1. This approach applies a Gaussian kernel function, which is effectively a high band pass gray scale gradient filter, as the key step in the processing algorithm [49]. A MATLAB script and several functions were written to handle the images, extract information from the text files, calculate parameters, generate distributions, and plot the results. ImageJ is used to carry out background subtraction, thresholding, object identification and measurement; while MATLAB is used to carry out the final elimination of out-of-focus flocs, calculations, data analysis, and plotting functions.

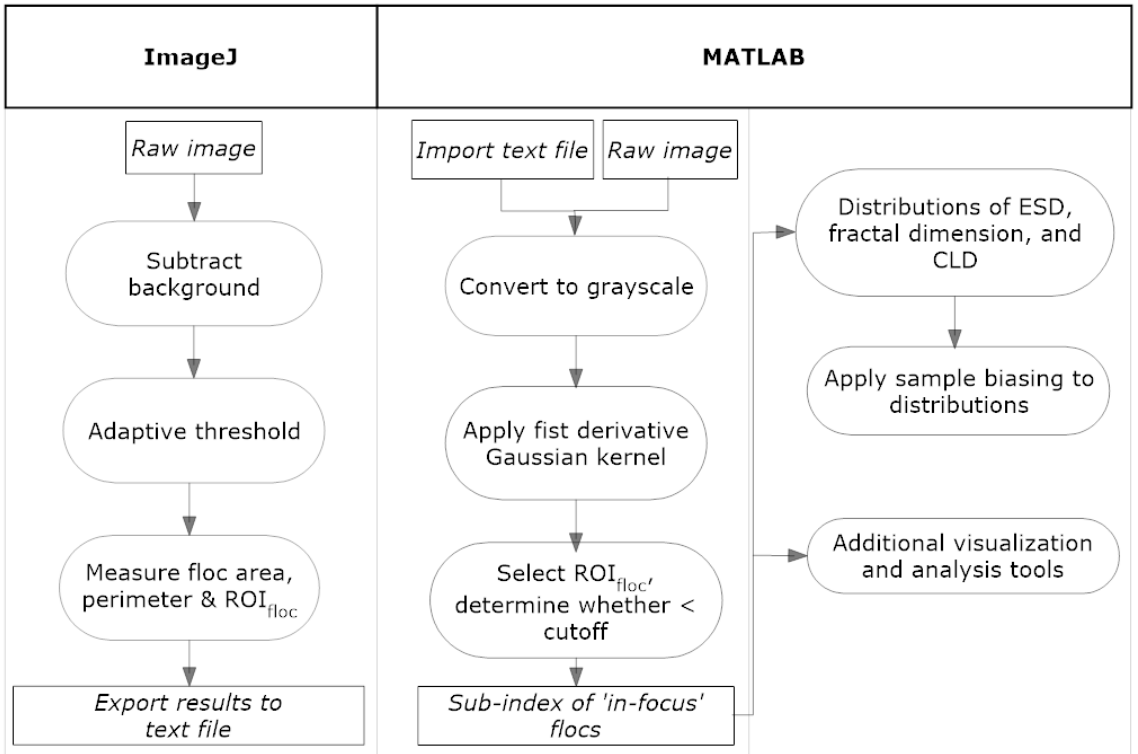

Figure G.1. A Image processing algorithm, adapted to reflect changes in the current study from [45]

The projected equivalent spherical diameter, D_P [70], is then calculated for all 'in-focus' flocs from Equation G.1,

$$D_P = \sqrt{\frac{4A_\mathrm{P}}{\pi}} \tag{G.1}$$

where D_P is the projected area diameter of the aggregate in the ROI and A_P is the area of the aggregate.

RESULTS

This section contains a few details on setting up the experiment and the result of measuring flocculated sediments after batch settling experiments. In this thesis several sedimentation image analysis trials were attempted, but only the final trial produced reasonable results which are reported here.

There are several important factors which influence whether good images of flocs can be obtained with this procedure. Light position and intensity, method and rate of floc introduction, and image acquisition rate are all important. It should be noted that a permanent setup was not used in these experiments, so changes in the optical setup from experiment to experiment may have occurred.

A key step in processing the sedimentation images is to determine whether an identified floc is 'in focus' or not. After IMAGEJ is used to identify all flocs in the images, MATLAB is used to further process the results by applying a Gaussian kernel function. This method essentially examines the sharpness of the floc edge to determine whether they are in focus or not. The two important Gaussian kernel parameters are the gradient threshold and the standard deviation of the gradient. By adjusting the values of these two clarity parameters, a greater or lesser number of flocs will be identified as 'in focus,' as depicted in Figure G.2.

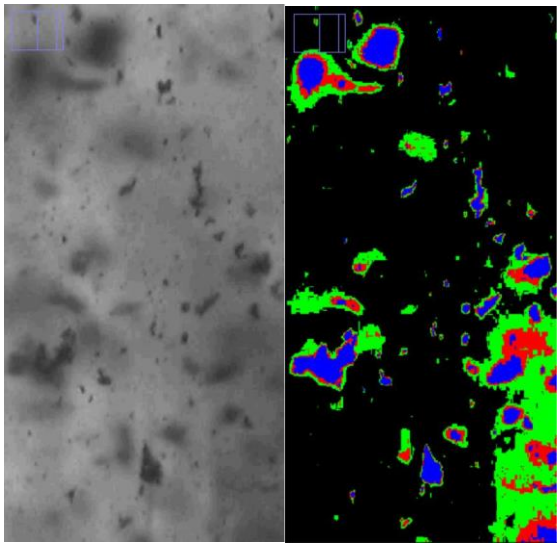

Figure G.2 Single image of PAM-flocculated kaolin (left.) On the right, a depiction of the result of the Gaussian kernel function. Steeper gradients are indicated by narrower bands of green and red around the dark blue centres.

The result of applying the Gaussian kernel, at specific gradient threshold and standard deviation, results in the identification 'in focus' flocs, as shown in Figure G.3. The gradient threshold and standard deviation can be manipulated to filter out 'out-of-focus' flocs, summarized in Table G.1.

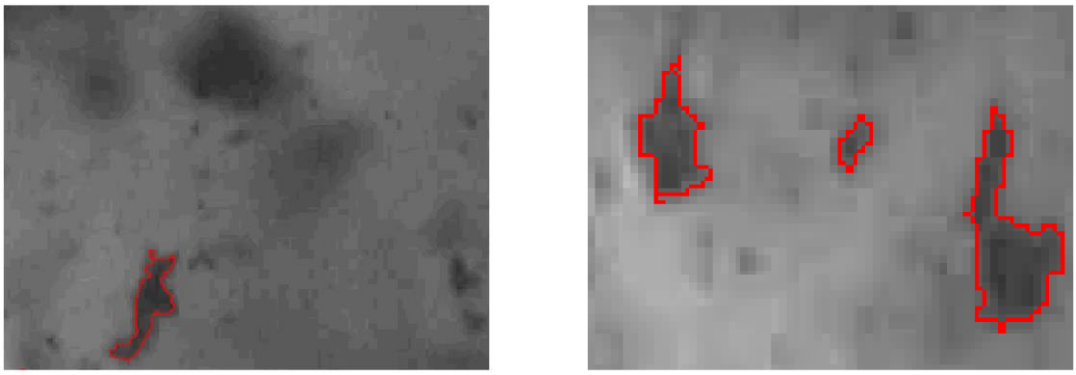

Figure G.3 Examples of PAM-flocculated kaolin image analysis with 'in-focus' flocs labelled. 'Out-of-focus' flocs are present but not analyzed any further. Note brightfield technique shown here, the data set for discussion and analysis was collected using a dark field technique.

The clarity parameter values which produced a sufficient number of in focus flocs for measurement, grayscale minimum = 170 and standard deviation = 1.1, were chosen for analysis and applied to all samples.

Table G.1 Clarity parameters and resulting equivalent spherical diameter, D_s, for 55328 flocs identified in sedimentation image analysis of a 10% w/w kaolin sample flocculated by 160 g/t polyacrylamide.

$Clarity\ parameters$			
$Grayscale\ Minimum$	$Gradient\ SD$	$Flocs\ in\ focus$	$D_s\ [\mu m]$
180	1	270	237.7
170	1	345	242.7
170	0.9	159	227.0
170	1.1	684	259.3

Figure G.4 shows an example distribution of measured equivalent spherical diameters of flocs which result from acquiring images during sedimentation of a 10 % w/w kaolin suspension flocculated by 160 g/t polyacrylamide.

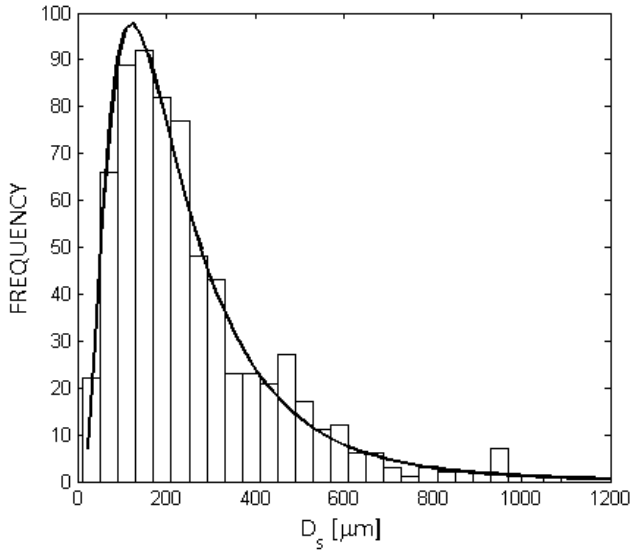

Figure G.4 Lognormal distribution of equivalent spherical diameter values, D_s, of flocs from sedimentation image analysis of a 10 % w/w kaolin sample flocculated with 160 g/t polyacrylamide.

The mean of the lognormal distribution is used to report the equivalent spherical diameter, which is summarized in Table G.2

Table G.2 Results of sedimentation image analysis for kaolin flocculated by non-ionic polyacrylamide

$Dose\ [g/t]$	$Image\ Total$	$Flocs\ total$	$Flocs\ in\ focus$	$D_s\ [\mu m]$
0	1672	167085	14769	103.3
20	2200	210345	25472	134.0
60	1200	88691	9709	224.9
160	2000	55328	684	259.7

The results in Table G.2 indicate an increasing particle size with increasing dose of polyacrylamide applied. This is in agreement with visual observation of high magnification images of the flocculated samples, for example in Figure 6.13.

The two equivalent spherical diameter, D_{A}, distributions in Figure G.5 demonstrate that changes in the gradient cut-off and standard deviation can have a large impact, 10 % here, on the calculated mean equivalent spherical diameter.

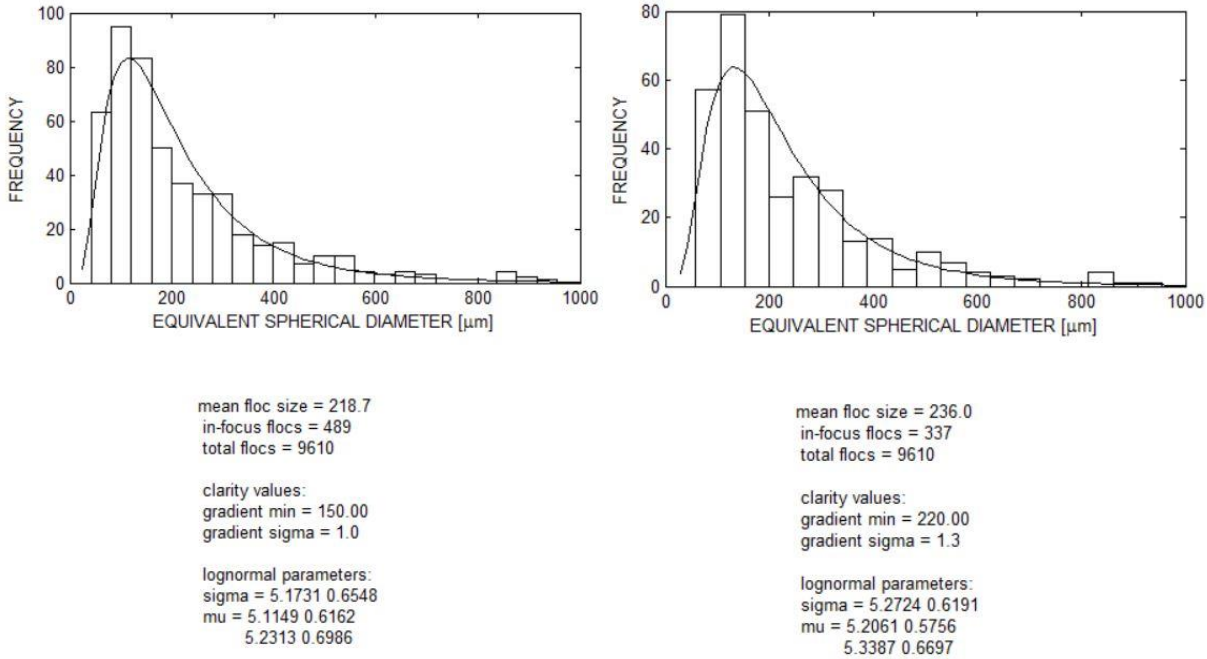

Figure G.5 Equivalent spherical diameter for PAM-flocculated kaolin for two different sets of gradient parameters.

Sedimentation image analysis was applied successfully in one trial. The results are roughly in agreement with those obtained from OBS calibration. However, the samples composed of larger aggregates, from higher PAM dosage or longer conditioning, are likely under-sampled by the photographic setup due to the camera frame rate, maximum 15 FPS, and the lighting setup, low power, non-stroboscopic LED.